REACTOR CORE MATERIALS

A Quarterly Technical Progress Review

Prepared for U. S. ATOMIC ENERGY COMMISSION by BATTELLE MEMORIAL INSTITUTE

4 - JUN 21
Copy ___ 1960

May 1960

● VOLUME 3

● NUMBER 2

TECHNICAL PROGRESS REVIEWS

To meet the needs of industry for concise summaries of current atomic developments, the Atomic Energy Commission is publishing this series, Technical Progress Reviews. Issued quarterly, each of the reviews digests and evaluates the latest findings in a specific area of nuclear technology and science.

The four journals published in this series are:

Nuclear Safety, W. B. Cottrell, editor, R. A. Charpie, advisory editor, and associates, Oak Ridge National Laboratory

Power Reactor Technology, Walter H. Zinn and associates, General Nuclear Engineering Corporation

Reactor Core Materials (covering solid material developments), R. W. Dayton, E. M. Simons, and associates, Battelle Memorial Institute

Reactor Fuel Processing, Stephen Lawroski and associates, Chemical Engineering Division, Argonne National Laboratory

Each journal may be purchased ($2.00 per year for subscription and individual issues $0.55) from the Superintendent of Documents, U. S. Government Printing Office, Washington 25, D. C. See back cover for remittance instructions and foreign postage requirements.

●

Availability of Reports Cited in This Review

Unclassified AEC reports are available for inspection at AEC depository libraries and are sold by the Office of Technical Services, Department of Commerce, Washington 25, D. C.

Unclassified reports issued by other Government agencies or private organizations should be requested from the originator.

Unclassified British and Canadian reports may be inspected at AEC depository libraries. British reports are sold by the British Information Service, 45 Rockefeller Plaza, New York, N. Y.; Canadian reports (AECL series) are sold by the Scientific Document Distribution Office, Atomic Energy of Canada, Ltd., Chalk River, Ontario, Canada.

Classified U. S. and foreign reports identified in this journal as Classified may be purchased by properly cleared Access Permit Holders from the Technical Information Service Extension, U. S. Atomic Energy Commission, P. O. Box 1001, Oak Ridge, Tenn. Such reports may be inspected at classified AEC depository libraries.

REACTOR CORE MATERIALS

A REVIEW OF RECENT DEVELOPMENTS

Prepared for U. S. ATOMIC ENERGY COMMISSION
by BATTELLE MEMORIAL INSTITUTE

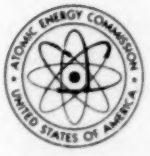

● MAY 1960

● VOLUME 3

● NUMBER 2

foreword

Reactor Core Materials is one of four Technical Progress Reviews, each covering a different area of nuclear technology, prepared under the auspices of the Industrial Information Branch of the U. S. Atomic Energy Commission. *Reactor Core Materials* is written by staff members of Battelle Memorial Institute, who comb the literature as it becomes available and each quarter present the latest significant developments in the form of highlighted reviews. Extensive reference lists are included at the ends of the various sections for the benefit of readers who wish to obtain more detailed data.

R. W. DAYTON
E. M. SIMONS
R. W. ENDEBROCK
Battelle Memorial Institute

contents

ii	Foreword	
1	I	FUEL AND FERTILE MATERIALS
1		Unalloyed Uranium
3		Alpha-phase Uranium Alloys
3		Epsilon-phase Uranium Alloys
3		Gamma-phase Uranium Alloys
4		Dilute Uranium Alloys
4		Plutonium and Its Alloys
5		Thorium and Its Alloys
5		Dispersion Fuel Elements
5		Refractory Fuel and Fertile Materials
7		Basic Studies of Irradiation Effects in Fuel Materials
8		Mechanism of Corrosion of Fuel Alloys
8		Metal-Water Reactions
9		References
12	II	MODERATOR MATERIALS
12		Graphite
13		Beryllium Metal and Alloys
15		Beryllium Compounds
15		Solid Hydrides
17		References
19	III	NUCLEAR POISONS
19		Dispersion Poison Materials
21		Metallic Poison Materials
21		References
22	IV	CLADDING AND STRUCTURAL MATERIALS
22		Corrosion
25		Zirconium-Water Reactions
25		Radiation Effects in Nonfuel Materials
29		Selected Mechanical Properties of Cladding and Structural Materials
31		Selected Metallurgical Aspects of Cladding and Structural Materials
36		References

contents (continued)

39	V	SPECIAL FABRICATION TECHNIQUES
39		Melting, Casting, Heat-treatment, and Hot Working
42		Cladding
47		Welding and Brazing
49		Explosion Forming
51		Nondestructive Testing
52		References

Issued quarterly by the U. S. Atomic Energy Commission. Use of funds for printing this publication approved by the Director of the Bureau of the Budget on November 1, 1957.

REACTOR CORE MATERIALS

FUEL AND FERTILE MATERIALS

During early 1959 the U. S. Atomic Energy Commission (AEC) formed a task force to review the present status of fuel technology and formulate long-range plans.[1,2] Among the items for consideration were (1) properties of materials, (2) fuel-element design, (3) fabrication techniques, (4) materials and fabrication costs, (5) burn-up, and (6) chemical processing. The information was organized into three major areas:

1. Fuel problems of the major reactor types
2. Materials problems
3. Supporting technology

As a result of the group's deliberation and evaluation, the following major conclusions were reached:

1. The major limitation in the use of metallic fuels for civilian power reactors is their irradiation-induced swelling at elevated temperatures.

2. Uranium dioxide is an important fuel for civilian power reactors.

3. Improved data on the properties of UO_2 would provide better utilization of this fuel material.

4. Considerable effort has been expended on the current major manufacturing technique of cold pressing and sintering.

5. Uranium monocarbide has promise as a high-temperature fuel; it has good physical properties, and initial irradiation results are encouraging.

6. Fueled graphite is of considerable interest in gas-cooled reactors.

7. Determination of burn-up is one of the most important factors in the irradiation testing of fuel materials.

8. An essential requirement in the irradiation testing of fuel is uniform and controlled burn-up and temperature.

9. Fast-breeder reactors and plutonium-recycle reactors are necessary to utilize uranium reserves effectively.

10. Recycling of fuels holds economic promise and may become a necessity.

Unalloyed Uranium

Mallinckrodt Chemical Works[3] has determined diffusion coefficients for hydrogen in uranium at beta- and gamma-phase temperatures. For dingot metal in the beta region, diffusion coefficients ranged from 4.8×10^{-5} cm^2/sec at 670°C to 6.0×10^{-5} cm^2/sec at 750°C. For the gamma region, values ranged from 6.4×10^{-5} cm^2/sec at 800°C to 1.5×10^{-4} cm^2/sec at 970°C. The activation energy of diffusion was calculated to be 3.6 and 11.4 kcal/gram-atom in the beta and gamma regions, respectively.

The self-diffusion coefficient of uranium was measured at Argonne[4] at four temperatures in the gamma phase. The data fitted the Arrhenius type equation $D = 2.33 \times 10^{-3} \exp(-28{,}500/RT)$ cm^2/sec and agree well with previously reported results. The value of D_0 is lower than that predicted by Zener's theory, and the activation energy is much less than the value expected from various empirical correlations.

British investigators[5] have determined the rates of oxidation of uranium by CO_2 over the range 500 to 1000°C. The rate increases with temperature from 500 to 780°C, with a sudden marked increase when the metal is near or at the β-γ transition (772°C). At higher temperatures up to 1000°C, the rate decreases with increasing temperature. The reaction generally obeys a linear rate law for the 500 to 800°C range. In the 500 to 725°C range, the activation energy is 26 ± 10 kcal/mole, which is consistent with the hypothesis that oxygen-ion diffusion is the rate-controlling mechanism.

A new method for the preparation of perfect crystals of uranium is reported by the French.[6] It is based on the stretching of imperfect crystals produced by the $\beta \rightarrow \alpha$ phase change, followed by an anneal in the high alpha range. Depending on the orientation of the original imperfect crystal, deformation takes place by slip, twinning, or deformation bands. Annealing gives perfect recrystallization crystals whose orientation is directly related to that of the original crystals. There are some crystallographic characteristics of the deformation mechanism during the course of the recrystallization. For example, the (0 0 1) direction, which is the rotation axis allowing the formation of the deformation bands, is preserved during recrystallization. In the case of deformation by twinning, the recrystallized grains show less clearly marked orientation relations, but the growth of larger crystals is facilitated.

Quench cracking of irradiated uranium was studied by Hanford investigators.[7] Uranium disks $\frac{1}{4}$ in. thick, irradiated to 0.13 at.% burn-up, were heated to 600°C and quenched at a rate estimated to be similar to the cooling rate that can occur in the center of reactor fuel elements. After 10 heating and quenching cycles, internal cracking was observed. The proposed mechanism of crack formation is as follows: During reactor exposure the macroscopic and microscopic stresses are relieved by stress relaxation. Upon reactor shutdown the anisotropic contraction of the uranium crystals causes large microscopic strain incompatibilities, or thermal shock, which can induce cracks in the uranium embrittled by irradiation. The stresses due to thermal gradients are generally small compared with the strains produced by anisotropic crystallographic expansion. Cracks observed in irradiated specimens were random with respect to the macroscopic stress fields, lending support to the above theory.

The thermal conductivity of uranium irradiated to 0.018 and 0.031 at.% burn-up was found[8] to be 18 to 30 per cent lower than that of unirradiated uranium, depending on test temperature. The thermal conductivity vs. temperature curve for the specimen irradiated to 0.031 at.% burn-up was reversible, indicating no recovery at elevated temperatures. A consistent relation between thermal conductivity and electrical conductivity was not apparent in the data.

The unalloyed uranium fuel elements used in the SRE (Sodium Reactor Experiment) contain 2.78 per cent U^{235} and are clad with type 304 stainless-steel jackets. NaK is used as a bond between the fuel and the cladding. Examination of elements removed from the reactor[9] revealed no increase in cladding diameter after an exposure of 850 Mwd/ton calculated maximum burn-up. Some stretching of the cladding was evident at 950 Mwd/ton. Destructive examinations at maximum burn-ups of 65, 105, 390, and 850 Mwd/ton showed progressive irradiation-induced dimensional changes. Maximum changes in diameter of 1.7 per cent, in length of 2.9 per cent, and in density of −2.6 per cent were observed for the highest burn-up. All surface and dimensional characteristics appeared to be directly related to burn-up. Some relation was found between surface roughening and fuel-element surface temperature. Fuel-element cladding examinations indicated no apparent change in ductility after exposure to surface temperatures of about 850°F and to the thermal cycling resulting from repeated start-up and shutdown of the reactor.

The British[10] have carried out metallographic studies of enriched-uranium specimens irradiated at 200 to 800°C to burn-ups ranging from 0.13 to 0.41 at.%. The examination confirmed that swelling of uranium during irradiation at elevated temperatures is due to the formation of cavities in metal, although generally it has not been possible to account for the entire density change in terms of observed porosity. At least part of the discrepancy can be explained by corrosion effects that occurred during irradiation or storage and part by inaccuracies in the porosity assessment.

In specimens showing the greatest swelling, the holes varied in size from 3 mm to less than 1 μ in diameter, the larger ones often being formed by the coalescence of the smaller. The volume increase due to bubbles about 5 μ in diameter was less than that for larger or smaller bubbles. There was no evidence that holes formed at inclusions. In none of the specimens was it possible to relate the porosity to any microstructural feature.

The amount of cracking varied considerably and was not necessarily associated with the existing grain boundaries nor with the inclusions originally present in the metal. It was often associated with the hydrogen-bearing phases seemingly formed during or after irradiation and with carbide inclusions which had been redistributed during the exposure.

Peculiar loop-form inclusions or inclusion-filled cracks were observed in those specimens showing large volume increases and containing quantities of a phase thought to contain hydrogen. There were none of the dendritic inclusions usually found in arc-melted uranium and which were present in the specimens prior to irradiation.

The British[11] have published a list of abstracts covering unclassified atomic-energy project reports and published literature on uranium. In addition, information on uranium, including fatigue properties and the effects of irradiation, creep, and thermal expansion, has been added to the Uranium Data Manual.[12] (M. S. Farkas)

Alpha-phase Uranium Alloys

Nuclear Metals[13] has issued a report dealing with the effects of thermal cycling on integrally coextruded, tubular fuel elements of uranium–2 wt.% zirconium clad with Zircaloy-2. These elements were cycled 200 times between 500 and 100°C with no significant changes in the dimensions, straightness, or ultrasonic bond strength. The cycling was conducted so that, 10 to 15 sec after the tube entered the low-temperature bath, estimated temperature differences of 150 to 280°C were obtained between the midwall and the surface of the tube.

The effects of irradiation on uranium–1.2 wt.% molybdenum powder compacts are reported by Atomics International.[14] The results are presented in Table I-1. The data, showing greater than 20 per cent change in volume with about 0.3 at.% burn-up, are similar to results of irradiation tests performed elsewhere. The data for the uranium–1.2 wt.% molybdenum specimens, which swelled only about 7 per cent in volume at about 0.2 per cent burn-up, are similar to recent results obtained at Argonne.[16]

The Germans[17] have investigated the diffusion behavior in the uranium-zirconium and the uranium-nickel systems. In the former system, the investigation was carried out above the transformation temperature in the solid-solution range of the gamma phase. In the latter system, the investigation was carried out at temperatures below the eutectic temperature of 740°C, at which seven intermetallic compounds occur in very small homogeneous zones.

A bibliography on uranium alloys, with binary phase diagrams and selected data on properties, has been published recently[18] and is of general interest. Also, the effects of alpha-beta thermal cycling on uranium and uranium alloys are reported in a recent journal article.[19]

(M. S. Farkas)

Epsilon-phase Uranium Alloys

Uranium-Zirconium

An annotated summary of the properties and behavior of zirconium-uranium alloys has been published by Battelle.[20] Constitution, transformation kinetics, microstructure, the effect of heat-treatment on microstructure and properties, mechanical and physical properties, corrosion resistance, and irradiation behavior are discussed. (A. A. Bauer)

Gamma-phase Uranium Alloys

Uranium-Molybdenum

Procedures for the fabrication of Zircaloy-2-clad uranium–12 wt.% molybdenum alloy fuel rods by coextrusion are presented in a paper by Goodwin et al.[21]

A patent[22] has been assigned to Westinghouse for gamma-phase uranium-molybdenum-niobium alloys as corrosion-resistant fuels.

Table I-1 DIMENSIONAL CHANGES OF IRRADIATED SPECIMENS[14]

Specimen composition, wt.%	Measured central temp., °F		Calculated surface temp., °F		Burn-up,* total at.%	Maximum increase in diameter, %	Increase in volume,† %
	Range	Av.	Range	Av.			
U–1.2 Mo	830–700	756	655–555	598	0.25	9.9	22
U–1.2 Mo	1050–920	972	825–740	763	0.33	13	31
U–1.2 Mo	1245–905	1017	980–715	799	0.22	7.7	6.9
U–1.2 Mo	1130–990	1052	890–775	827	0.22	9.6	7.3

*Based on chemical analyses of some specimens and heat balance on all specimens.
†Based on density measurements of central sections.

Maximum corrosion resistance to 650°C water was secured by a uranium–9 wt.% molybdenum–1.4 wt.% niobium alloy. (A. A. Bauer)

Dilute Uranium Alloys

Aluminum-Uranium Alloys

Further corroboration of the ability of silicon to suppress the UAl_3-UAl_4 transformation has been reported by Gualandi and Schileo.[23] Results of this work show that, when silicon in amounts up to 3.5 wt.% is added to aluminum–17 wt.% uranium alloys, the UAl_4 is replaced by UAl_3 containing part of the silicon in solid solution. Since both zirconium and tin are also excellent suppressors of the UAl_3-UAl_4 transformation, Battelle[24] has continued to study the effects of these additions on the properties of the binary alloys. Alloys containing additions of up to 3 wt.% of either of these two metals have increased ductility and require less extrusion pressure than the binaries alone.

Tin-bearing ternary alloys of an aluminum–35 wt.% uranium-base material can be air melted with no difficulty into sound pore-free ingots.[25] On the other hand, zirconium-containing alloys have to be air melted twice or vacuum melted to avoid excessive porosity. Alloys containing less than 3.0 wt.% tin revealed well-defined reaction areas in the periphery of the primary compound particles. The extent of this zone is inversely proportional to the tin content of the alloy. The 3.0 wt.% tin alloy showed little or no reaction zone. A study of microstructures indicates that between 2 and 3 wt.% zirconium might be the optimum zirconium addition.

After heat-treatments at 600°C for 8, 24, and 48 hr, the microstructures of the specimens were studied.[26] In all cases the eutectic portion spheroidized in 24 hr. The UAl_3-UAl_4 reaction progressed at a higher rate in the alloys containing tin than in the alloys containing zirconium. In either case the smaller the addition, the faster the reaction. Hot hardness was taken on the binary alloy (aluminum–35 wt.% uranium) and on ternary alloys containing either tin or zirconium in amounts between 0.5 and 3.0 wt.%. In all cases the hardness was maintained to 300°C, not differing greatly from the room-temperature hardness of 58 to 68 DPH. Above 300°C, softening began to occur rapidly.

All the alloys discussed in the preceding paragraph were exposed for 30 days in 200°C water.[27] All alloys exhibited weight gains less than those for 2S aluminum. Weight gains of samples from extrusions or vacuum-melted castings were comparable. There seemed to be little or no difference in corrosion behavior between the tin-containing and the zirconium-containing alloys. Tensile tests were performed at 100, 250, and 400°C on extruded stock. At 100°C the strengths of the various ternaries were not much different from the strength of the binary. The air-melted zirconium-containing alloys exhibited the lowest tensile strengths (17,000 to 17,140 psi), as compared with the strengths of the other alloys (18,000 to 18,900 psi). At 250 and 400°C, any strength differences between the alloys becomes less distinguishable.

Argonne[28] has studied aluminum-uranium alloys containing 2 wt.% nickel and 0.5 wt.% iron. The uranium content varied between 15 and 53 wt.%. All material that could be fabricated was exposed to 290°C water in the wrought condition. The material that could not be worked (53 wt.% uranium alloys) was tested in the cast condition. After a 60-day exposure to 290°C water, the rate of attack of an aluminum–15 wt.% uranium–2.2 wt.% nickel–0.43 wt.% iron alloy was about double that of X-8001 cladding alloy. On the other hand, an aluminum–52.7 wt.% uranium–2.1 wt.% nickel–0.6 wt.% iron alloy exhibited a low rate, 6 mg/(dm^2)(day), which represents a penetration rate slightly lower than that of X-8001 cladding alloy. It can be concluded that the addition of uranium does not reduce the corrosion rate until the UAl_2 composition is exceeded, in which case the resulting free uranium corrodes very rapidly.

Plutonium and Its Alloys

The British[29] have prepared a compilation of plutonium data which includes physical properties, mechanical properties, chemical properties, and phase diagrams. In an investigation to determine the effects of small additions of plutonium to thorium, uranium, and uranium-molybdenum alloys, Critchley and Sinclair[30] found that plutonium increases the hardness and density of thorium. Little effect was noted in the other alloys. Data from the study are shown in Table I-2. The effects of plutonium on thorium can be attributed to solid-solution hardening.

Table I-2 EFFECTS OF PLUTONIUM ADDITIONS ON THE PROPERTIES OF THORIUM, URANIUM, AND URANIUM-MOLYBDENUM ALLOYS[30]

Composition, at.%	Hardness, VPN	Density, g/cm³	Coefficient of expansion, 10^{-6}/°C
Thorium	80	11.50	11.0
Th–5 Pu	96	11.77	
Th–10 Pu	107	11.81	11.6
Uranium	250	19.04	16.1
U–3 Pu	256	18.97	
U–4.5 Pu	284	18.98	
U–6 Pu	264	18.98	15.8
U–20 Mo	316	18.0	13.6
U–20 Mo–4 Pu	304	17.35	15.5
U–28 Mo	350	17.1	
U–28 Mo–4 Pu	349	16.80	

In an investigation[31] of liquid plutonium alloys, a ternary eutectic was found to exist at cerium–12.0 wt.% cobalt–7.0 wt.% plutonium at a temperature of 402°C. The plutonium content of the alloy can be increased to 30 wt.% without raising the melting point above 450°C. Quaternary additions of iron to the alloy resulted in no measurable change in the melting point.

Los Alamos[32] has determined the density, ρ, of liquid plutonium to be equal to $[17.567 - (1.451 \times 10^{-3})T] \pm 0.021$ g/cm³. For a liquid plutonium–7.93 at.% iron alloy, $\rho = [16.888 - (1.369 \times 10^{-3})T] \pm 0.012$ g/cm³, where T is in degrees Centigrade. (V. W. Storhok)

Thorium and Its Alloys

A portion of the thorium-indium constitution diagram has been delineated by Murray.[35] A eutectic exists at about 1160°C and 18 at.% indium between Th_2In and alpha thorium solid solution containing 9 at.% indium. The solubility of indium in alpha thorium decreases to 5 at.% at 1000°C and to 1.7 at.% at 800°C. The compound Th_2In was found to melt at 1170°C and to have a tetragonal structure of the $CuAl_2$ type. The existence of the phase $ThIn_3$ was confirmed.

Frye et al.[36] have obtained the pole figures showing the preferred orientations resulting from cold-reducing thorium 95 per cent in thickness at room temperature. The thorium examined contained 0.14 wt.% oxygen, 90 ppm carbon, 60 ppm nitrogen, 100 ppm iron, and 50 ppm silicon as major impurities. (W. Chubb)

Dispersion Fuel Elements

A process is being developed at Stevens Institute of Technology[37] for fabricating clad dispersion fuel elements by a slip-casting process. Elements, 2 in. wide by 4 in. long with a 0.020-in.-thick fuel core of 75 wt.% stainless steel and 25 wt.% UO_2, were clad with 0.005 in. of stainless steel. It is reported that microstructural examination indicated no fragmentation of the UO_2, fully dense cladding, uniform and fine grains in both the matrix and cladding, and no discontinuity at the cladding-core interface after drastic cold working. Tensile properties of the annealed plate were reported as follows: 55,800 psi ultimate strength, 27,600 psi (0.2 per cent offset) yield stress, and 19.4 per cent elongation at room temperature. Specimens from these plates were successfully cold formed to a 0.125 T bend.

It is reported by Thurber and Beaver[38] that uranium carbides are potential fissile dispersoids for aluminum-base fuel elements in which the isotopic enrichment in U^{235} is limited to 20 per cent. Uranium dicarbide appears to be wholly compatible with aluminum at 600°C. Uranium monocarbide, on the other hand, is chemically active under the same conditions and is converted to the uranium-aluminum intermetallic compounds, UAl_3 and UAl_4. Plate type fuel elements containing dispersions of UC_2 in aluminum can be manufactured using established procedures, with the exception that the cores must be vacuum degassed prior to rolling into fuel plates. Corrosion testing in 60°C water indicates that UC_2-aluminum dispersions will corrode catastrophically if the fuel-bearing section is inadvertently exposed to reactor process water. (D. L. Keller)

Refractory Fuel and Fertile Materials

Fabrication of Ceramic Fuels Other Than Uranium Oxides

Uranium monocarbide continued to receive major attention in studies of the fabrication of nonoxide ceramic fuels. The most popular method of preparing the monocarbide is by arc melting mixtures of uranium metal and carbon (references 22, 26, and 39 to 42). The use of

Table I-3 EFFECT OF CARBON CONTENT AND HEAT-TREATMENT ON THE CORROSION RATE OF URANIUM-CARBON ALLOYS IN VARIOUS MEDIA[25]

Specimen	Carbon content (balance U), wt.%	Corrosion rate in medium shown, mg/(cm²)(hr)				
		As-cast material		Annealed material		
		Water at 60°C	Santowax R at 350°C	Water at 60°C	Santowax R at 350°C	Ethylene glycol at 150°C
38	4.6	414		118	*	0.32
39	5.0	†	6.5			
40	5.7	819		1100	4.5	0.37
41	6.6	28.3	0.20	384	0.31	0.03
42	7.0	139	4.3	70.8	1.6	0.51
43	7.8	80.8		230	0.31	0.48
44	8.5	1623	0.85	918	0.40	2.1
45	9.2	488	0.70	441	2.6	0.55

*Specimen completely disintegrated in 1 week.
†Specimen completely disintegrated in 1 hr.

a consumable uranium electrode in preparing uranium carbides is being investigated at the Nuclear Fuel Research Laboratories.[40] Other methods of preparing the monocarbide which are under study include reduction of UO_2 by carbon,[40,41] reaction of uranium or uranium hydride with methane (references 22, 26, and 40 to 42), and reaction of uranium with carbon by sintering,[43] hot pressing,[44] or induction melting.[41]

Reduction of UO_2 by carbon appears to require exceedingly high reaction temperatures and a pumping system of large capacity.[40] Under these conditions, a mixture of mono- and dicarbide results.[41] Induction melting does not appear to be as satisfactory as arc melting in achieving complete reaction between uranium metal and carbon.[41] In studies of the reaction between uranium metal and alkanes such as methane, it was found that propane reacted more rapidly than methane.[26] (M. J. Snyder)

Properties of Refractory Fuels Other Than Uranium Oxides

The properties of the uranium carbides are being evaluated in various laboratories to determine their physical and chemical behavior when in contact with various metals, liquids, and gases. The literature on the uranium-carbon system is reviewed[45] giving the phase diagram and the structural properties of the three compounds UC, U_2C_3, and UC_2. The compatibility of UC and UC_2 with aluminum at 620°C was investigated. This study showed that UC and aluminum react catastrophically at this temperature, whereas the dicarbide (UC_2) with aluminum appears to be relatively stable. The presence of hydrogen in the UC_2-aluminum system destroys the stability of the dicarbide. The corrosion resistance of uranium carbides, containing from 4.6 to 9.2 wt.% carbon, in water, in Santowax R, and in ethylene glycol as determined at Battelle[25] is given in Table I-3. The irradiation behavior of UC, containing 4.6 and 5 wt.% carbon, in sodium for uranium burn-ups of 0.7 and 1.8 at.% has been evaluated.[45] Although some radial and transverse cracks were observed, there were only small changes in density or diameter. The fission gas released to the capsules could be attributed to recoil from the surface during irradiation. Electron micrographs of UC have been made at Battelle after irradiation at 600 and 1300°C. At the higher temperature the structures appeared to be normal for UC containing straight UC_2 needles. However, at the lower temperature the UC_2 needles in the UC matrix appeared to be warped. Annealing of the radiation damage at the higher temperature was suggested by these studies.

Nowotny et al.[46] have investigated the structure of three complex carbides that contain uranium. The unit-cell dimensions of these orthorhombic carbides are

$UCrC_2$ $a_0 = 5.42_2$, $b_0 = 3.22_5$, and $c_0 = 10.61_5$

$UMoC_2$ $a_0 = 5.61_2$, $b_0 = 3.20_5$, and $c_0 = 10.9_5$

UWC_2 $a_0 = 5.62$, $b_0 = 3.24_5$, and $c_0 = 10.9_5$

Ivanov and Tumbakov[47] reported on the preparation of UBe_{13} and on the result of calorimetric measurements of the heat evolved in the solution of UBe_{13} and of a mixture of uranium and beryllium. The difference, 106.5 ± 8.6 cal/g, is given as the heat of formation for UBe_{13}.

Basic studies at Hanford[48] on plutonium oxides include investigations on the preparation of the suboxide Pu_2O_3 and the thermal expansion of PuO_2. To date, attempts to prepare Pu_2O_3 have been unsuccessful. The thermal-expansion coefficient of a 90 per cent dense sintered PuO_2 body was found to be $15.2 \times 10^{-6}/°C$ over the temperature range 125 to 911°C.

The caking of ThO_2 slurries in an elevated-temperature loop experiment was studied by Draper and Milligan.[49] Pore-size distribution studied by nitrogen and water-vapor absorption measurements indicate a sharp peak in the number of pores about 10 A in size and a large number of pores between 10 and 200 A in size. No polymorphs or impurities could be detected by X-ray- or electron-diffraction examinations. Electron micrographs revealed that ThO_2 particles are aggregates of minute crystals. The edges of the crystals become rounded on heating to 1600°C, suggesting initial stages of sintering. (D. A. Vaughan)

Fabrication of UO_2-containing Ceramics

Olin Mathieson[40] has been developing a process for the fabrication of UO_2 fuel pellets by cold pressing and sintering in nitrogen. Roasting commercial UO_2 powders in air in the temperature range 100 to 140°C prior to pressing was found to increase the sintered density of the ceramic. Densities as high as 99 per cent of theoretical were reported for specimens made from the roasted powder after compacting at 80,000 psi and sintering for 5 hr at 1300°C in nitrogen. The sintered UO_2 was found to be nearly stoichiometric. (H. D. Sheets)

Basic Studies of Irradiation Effects in Fuel Materials

Metallic Fuels

The principal kinds of lattice damage produced in metallic fuels by fission products are discussed both qualitatively and quantitatively in a report from Atomics International.[50] These kinds of damage include interstitial atoms, vacant lattice sites, displacement spikes, and fission-product impurity atoms. Atomistic mechanisms of growth, swelling, and phase transformation are considered. Growth is thought to result from the combined effects of displacement spikes and interstitials and vacancies, whereas swelling results from the agglomeration of the inert-gas fission products. The phase reversal in uranium-molybdenum and uranium-niobium alloys is interpreted as a result of the action of displacement spikes. Bubble formation of gas formed in a transparent plastic by gamma irradiation has been studied.[51] The results are interpreted, and, by analogy, the expected behavior of metal fuels is described.

The development of macrocracks in irradiated uranium due to internal strains caused by the anisotropic thermal expansion of uranium crystals has been determined experimentally and compared for in-reactor and out-of-reactor treatments at Hanford.[8]

Twelve samples of uranium–0.5 at.% chromium alloy irradiated to 0.19 at.% burn-up under various conditions and temperatures were examined by the British.[52] In the range of 525 to 550°C, swelling of specimens occurred primarily by the formation of intergranular cracks. Effective restraint prevented this occurrence. Microscopy suggests that the cracks are formed by strings of small cavities joining together, and it is suggested that the formation and growth of these cavities is markedly influenced by thermal cycling. Cycling through the alpha-to-beta transformation was also studied.

Additional research is in progress at Hanford[34] to determine the mobilities of rare-gas fission products in uranium in order to understand the mechanisms of pore formation. The amount, mode of deposition, and depth of penetration of rare gas into uranium is being studied after electrical glow discharge. Both krypton and xenon are being studied in this manner. (F. A. Rough)

Nonmetallic Fuels

At Oak Ridge[53] the monitoring of the instantaneous release of fission gases from an in-pile experiment is being conducted. From total activity data, it is concluded that the release from a ThO_2-UO_2 sample at 1300°F and higher is by diffusion, recoil release being minor. More detailed analyses of the activity from various materials during in-pile irradiation is planned.

A mathematical analysis has been made[54] of the effects of closed pores upon the release of fission gases from UO_2. If a "no-closed-pore" model is used to obtain diffusion coefficients from short-term experiments and the same model is employed to predict the gas release under power-reactor conditions, the predicted value will be correct for the initial part of the exposure. For longer periods the estimated release would be larger than the actual release. Measurement of the fraction of gas which is trapped in pores during annealing of irradiated UO_2 would provide a parameter that could be used in mathematical treatments of the problem to allow for the effect of sealed pores.

Thin films of aluminum containing 1-μ-diameter UO_2 particles have been irradiated at Hanford[34] up to thermal fluxes of 3.4×10^{19} nvt. As the exposure increases the UO_2 becomes redistributed, presumably by sublimation or its equivalent, and is identified by X-ray diffraction as small crystallites over the face of the aluminum. (F. A. Rough)

Mechanism of Corrosion of Fuel Alloys

Battelle has recently completed a visual study of the corrosion of defected Zircaloy-2-clad fuel-element specimens in high-temperature water.[55] Progress of corrosion was followed by means of time-lapse color motion pictures taken through a windowed autoclave. Core materials were unalloyed uranium and uranjum–2 wt.% zirconium alloy. The water temperature ranged from 200 to 345°C.

The sequence of events associated with corrosion at the drilled defect was the same for all specimens, although the time at which different stages occurred varied. After an induction period, the first evidence of attack was the formation of a blister in the cladding area surrounding the defect. No hydrogen evolution or loss of corrosion product was observed during this early period. (This suggests that hydriding of the uranium may be occurring at this stage of corrosion.) Eventually, a crack appeared at the base of the blister. This was accompanied by the evolution of copious quantities of hydrogen and the expulsion of corrosion product. Catastrophic failure of the specimen occurred soon afterward. The time required for each phase was reduced as the temperature was raised. Diffusion-treated uranium–2 wt.% zirconium cores were most resistant to attack, whereas beta-treated water-quenched natural-uranium cores were least resistant.

Efforts to correlate observed hydrogen evolution with that theoretically available from the corrosion reaction were unsuccessful because of (1) incomplete reaction of the core with the water (unreacted core metal was found in some specimens) and (2) difficulty in maintaining an absolute leaktight seal on the autoclave. A hydride layer was detected on the inner surface of the Zircaloy-2 cladding in these specimens, in contrast to the general permeation by hydrogen which is observed during the corrosion of more corrosion-resistant uranium-alloy cores. The Battelle workers believe that the hydride layer was the result of rapid reaction with the hydrogen produced from the corrosion reaction, plus insufficient time at temperature to allow significant diffusion of hydrogen into the matrix of the Zircaloy-2 cladding. (W. E. Berry)

Metal-Water Reactions

Effort has continued at Argonne[56] on the study of uranium-water reactions. In this study, metal wires are rapidly melted and dispersed in a water-filled cell by a surge current from a bank of condensers. The energy input to the wire indicates reaction temperature; the transient pressure measures reaction rate; the amount of hydrogen generated gives the extent of reaction; and the particle size of the residue indicates the surface area exposed to reaction.

The total extent of reaction for 60-mil uranium wires, as determined from measurements of the total hydrogen liberated, is plotted in Fig. 1. Uranium appears to be considerably more reactive than zirconium at similar temperatures. Both metals show a significant reaction in the region of their melting points.

Results showed also that there was a 5- to 20-msec delay, or induction period, before evolution of hydrogen commenced. In many runs the residue consisted of flakes or chips rather than spherical particles as was the case with zirconium. These latter points will receive additional study.

Harwell[57] has recently reported results of a study of the uranium–water vapor reaction between 160 and 1400°C at 1 atm using a thermogravimetric method. Up to 880°C the reaction

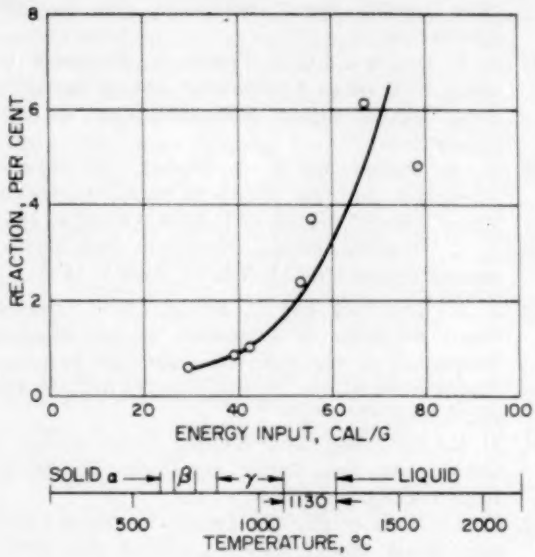

Figure 1—Uranium-water reaction: percentage reaction as a function of energy input and initial temperature.[56]

follows a linear rate law, with maximum rates at approximately 300°C [2.7 mg weight gain/(cm²)(min)] and 750°C [6 mg weight gain/(cm²)(min)]. Above 880°C a parabolic rate law applies for the first 60 to 120 min, after which the rate is constant. The oxide formed in the initial period coalesces and gives protection to the underlying metal. The subsequent rate is as low as that at about 200°C [0.1 mg weight gain/(cm²)(min)].

Experiments with molten uranium at 1200 and 1400°C showed that the rate was initially parabolic, with rates as high as 37 mg weight gain/(cm²)(min). However, the rate decreased with time; and, after about 10 to 20 min, it reached a steady value of 4 to 5 mg weight gain/(cm²)(min).

X-ray diffraction of the reaction product indicated that uranium dioxide (UO_2 to $UO_{2.24}$) was formed over almost the entire temperature range. The only exception to this was one sample, reacted at 300°C, which appeared to be U_3O_8.

Phillips Petroleum[58] reports a series of experiments using an automatically recording thermobalance to measure the rate of weight gain, hence the oxidation rate, of molten-metal samples contained in an alumina crucible suspended from one of the arms of the balance. The crucible was enclosed by a furnace containing water vapor at a pressure of 1 atm. Preliminary measurements of reaction rates have been obtained for aluminum and for an aluminum–21.4 wt.% uranium alloy.

Although experimental difficulties due to the permeability of the alumina crucibles were encountered, preliminary results are reported. These indicate that the reaction rate of pure aluminum (99.99 per cent) with water vapor reaches a maximum of about 0.004 mg weight gain/(cm²)(min) at 1600°F, decreasing both above and below this temperature.

For the aluminum–21.4 wt.% uranium alloy, the reaction rate, to a close approximation, doubles with every 100°F rise over the range 1500 to 1800°F. At 1800°F it is about 0.033 mg weight gain/(cm²)(min); the rate decreases to about 0.007 at 1900°F. Although the assumed order of reaction was not specified, the Arrhenius energy of activation was reported as 46 kcal/mole over the temperature range 1500 to 1800°F. The report does not disclose whether any variation in rate with time was observed.

(A. W. Lemmon, Jr.)

References

1. B. R. Hayward, Fuel Element Technology, *Transactions of the American Nuclear Society*, 2(2): 50–51 (November 1959).
2. Civilian Reactor Fuel Element Review Group, Report on Civilian Reactor Fuel Elements, USAEC Report TID-8505, June 1959.
3. H. W. Myers et al., The Application of Diffusivity Data in Reducing the Hydrogen Content of Gamma-Extruded Uranium Bars, USAEC Report MCW-1439, Dec. 10, 1959.
4. S. J. Rothman et al., Self-diffusion in Gamma Uranium, USAEC Report ANL-5971, July 1959.
5. J. E. Antil and K. A. Peakall, Kinetics of Oxidation of Uranium by Carbon Dioxide, *Journal of the Less-common Metals*, 1: 227–231 (June 1959).
6. D. Calais et al., Influence of the Mode of Plastic Deformation on the Recrystallization of Imperfect Uranium Single Crystals Produced by the $\beta \rightarrow \alpha$ Transformation, *Revue de métallurgie, Memoires Scientifiques*, 46: 261–272 (1959).
7. K. R. Merckx, Cracking of Irradiated Uranium by Rapid Cooling, USAEC Report HW-62447, Oct. 30, 1959.
8. Reactor and Fuels Research and Development Operation Monthly Report for October 1959, USAEC Report HW-62587A, Nov. 15, 1959. (Classified)
9. J. L. Balliff et al., Sodium Reactor Experiment Fuel Irradiation Experience, USAEC Report NAA-SR-3887, Sept. 15, 1959.
10. E. C. Sykes and V. J. Haddrell, Metallographic

Examination of Irradiated Enriched Unalloyed Uranium, British Report AERE-M/R-2735, November 1958.

11. R. W. Clarke, comp., Abstracts of Atomic Energy Project Unclassified Reports and Published Literature on the Actinide Elements (papers dated 1957 noted up to June 1958). Part 3. Uranium, British Report AERE-C/R-2472(Pt. 3), July 1958.
12. E. L. Francis, comp., Uranium Data Manual, British Report IGR-R/R-287, May 20, 1958.
13. R. G. Jenkins, Effects of Thermal Cycling on an Integrally Coextruded Tubular Fuel Element of Uranium–2 Wt.% Zirconium Clad with Zircaloy-2, USAEC Report NMI-4391, Aug. 3, 1959.
14. B. R. Hayward and L. E. Wilkinson, Radiation Behavior of Metallic Fuels for Sodium Graphite Reactors, USAEC Report NAA-SR-3411, Aug. 15, 1959.

16. J. H. Kittel and S. H. Paine, Effects of Irradiation on Powder Compacts of Uranium and Some Uranium-base Alloys, USAEC Report ANL-5664, June 1957.
17. Norbert Müller, Investigation of Diffusion in the Systems Uranium-Zirconium and Uranium-Nickel (in German), *Zeitschrift für Metallkunde*, 50(11): 652–660 (November 1959).
18. H. C. Friedemann and H. H. Hausner, Bibliography on Uranium Alloys with Binary-phase Diagrams and Selected Data on Properties, Report NP-7902, Sylvania-Corning Nuclear Corporation, 1959.

19. B. R. Hayward, Effect of Alpha-Beta Thermal Cycling on Uranium and Its Alloys, *Nucleonics*, 17(8): 74–77 (August 1959).
20. A. A. Bauer (Ed.), An Evaluation of the Properties and Behavior of Zirconium-Uranium Alloys, USAEC Report BMI-1350, Sept. 28, 1959.

21. J. G. Goodwin et al., Fabrication of Zircaloy-2-clad Uranium–12 Wt.% Molybdenum Fuel Rods, *American Institute of Mining and Metallurgical Engineers, Institute of Metals Division, Special Report Series*, 5(7): 69–75 (1958).
22. R. K. McGeary and R. D. Leggett, Alloys and Members Produced Therefrom, U. S. Patent 2,888,343, May 26, 1959.

23. D. Gualandi and G. Schileo, The Influence of Silicon on the Structure of Aluminum-Uranium Alloys for Nuclear Reactors, *Alluminio*, 28(10): 449–455 (October 1959).
24. N. E. Daniel et al., Effects of Ternary Additions on Aluminum–35 Wt.% Uranium Alloys, USAEC Report BMI-1388, Oct. 27, 1959.

25. R. W. Dayton and C. R. Tipton, Jr., Progress Relating to Civilian Applications During October 1959, USAEC Report BMI-1391, Nov. 1, 1959. (Classified)
26. R. W. Dayton and C. R. Tipton, Jr., Progress Relating to Civilian Applications During November 1959, USAEC Report BMI-1398, Dec. 1, 1959. (Classified)
27. R. W. Dayton and C. R. Tipton, Jr., Progress Relating to Civilian Applications During December 1959, USAEC Report BMI-1403, Jan. 1, 1960. (Classified)
28. W. E. Ruther and J. E. Draley, Corrosion of Aluminum-Uranium Alloys in High-temperature Water, USAEC Report ANL-6053, November 1959.
29. E. L. Francis, comp., Plutonium Data Manual, British Report IGR-161(RD/R), June 1, 1959.
30. J. K. Critchley and D. Sinclair, The Effect of Small Additions of Plutonium on the Physical Properties of Thorium, Uranium, and Uranium-Molybdenum Alloys, British Report AERE-M-424, April 1959.
31. J. K. Critchley, Low Melting Point Alloys of Cerium with Iron, Cobalt, and Plutonium, British Report AERE-M-488, July 1959.
32. C. E. Olsen et al., The Density of Liquid Plutonium Metal, USAEC Report LA-2358, May 1959.
33. H. C. Bowen, High-temperature Aqueous Corrosion of Aluminum-Plutonium and Aluminum-Silicon-Plutonium Alloys, USAEC Report HW-61345, July 31, 1959.
34. F. W. Albaugh, Reactor and Fuels Research and Development Operation Monthly Report for November 1959, USAEC Report HW-62899A, Dec. 15, 1959. (Classified)
35. J. R. Murray, Some Observations on Thorium-rich Thorium-Indium Alloys, *Journal of the Less-common Metals*, 1: 314–320 (August 1959).
36. J. H. Frye et al., Metallurgy Division Annual Progress Report for Period Ending September 1, 1959, USAEC Report ORNL-2839, Dec. 16, 1959.
37. Gregory J. Comstock et al., Slip Casting of Nuclear Fuel Elements, USAEC Report AECU-4255, July 17, 1959.
38. W. C. Thurber and R. J. Beaver, Dispersions of Uranium Carbides in Aluminum for Plate-type Fuel Elements Requiring High Uranium Concentrations, *Journal of Nuclear Materials*, 1(3): 226–232 (October 1959).
39. Development and Properties of Uranium Monocarbide Cermets, USAEC Report AECD-4289, Sept. 17, 1956.
40. Nuclear Fuel Research Laboratories Fuel-cycle Development Program, Quarterly Progress Report No. 1 for Period Ending September 30, 1959, USAEC Report NYO-2684, Oct. 19, 1959.
41. J. J. Finley et al., Columbium-clad Uranium Carbide Fuel Element, USAEC Report ORO-222, Nov. 16, 1959.
42. R. W. Dayton and C. R. Tipton, Jr., Progress Relating to Civilian Applications During September 1959, USAEC Report BMI-1381, Oct. 1, 1959.
43. Jack Williams (assigned to UKAEA), Improvements in or Relating to Cermets Comprising Uranium and Uranium Carbide, British Patent 821,287, Oct. 7, 1959.
44. J. Dubuisson et al., Preparation by Calcination

Under a Charge of U-UC Cermets and of Stoichiometric Monocarbide, USAEC Report AEC-tr-3797.

45. W. C. Thurber and R. J. Beaver, Dispersions of Uranium Carbides in Aluminum Plate-type Research Reactor Fuel Elements, USAEC Report ORNL-2618, Nov. 19, 1959.
46. H. Nowotny et al., On the Double Carbides in the U-Cr-C, U-Mo-C, and U-W-C Systems, *Monatshefte für Chemie*, 89(6): 692–700 (1958); USAEC Report AEC-tr-3807.
47. M. I. Ivanov and B. A. Tumbakov, The Heat of Formation of UBe_{13}, *Atomnaya Energiya*, 7(1): 33–36 (1959).
48. F. W. Albaugh, Reactor and Fuels Research and Development Operation Monthly Report for September 1959, USAEC Report HW-62012A, Oct. 15, 1959. (Classified)
49. A. L. Draper and W. D. Milligan, Structure and Surface Chemistry of ThO_2, USAEC Report AECU-4395, Sept. 1, 1959.
50. J. A. Brinkman, Fundamentals of Fission Damage, USAEC Report NAA-SR-4164, Oct. 15, 1959.
51. G. G. Bentle, Gas Bubble Formation in Irradiated Plastics and Reactor Fuels, USAEC Report NAA-SR-3085, Oct. 1, 1959.
52. O. M. Edwards and R. J. P. Cribb, Atomic Energy Research Establishment, Windscale, June 1959. (Private Communication).
53. Gas-cooled Reactor Project Quarterly Progress Report for Period Ending September 30, 1959, USAEC Report ORNL-2835, Dec. 2, 1959.
54. M. W. Rosenthal, The Effect of Closed Porosity on the Accuracy of the Model for Fission-gas Release from UO_2, USAEC Report CF-59-11-24, Nov. 10, 1959.
55. Elmer F. Stephan et al., A Visual Study of the Corrosion of Defected Zircaloy-2-clad Fuel Specimens by Hot Water, USAEC Report BMI-1387, Oct. 19, 1959.
56. Chemical Engineering Division Summary Report for April, May, and June 1959, USAEC Report ANL-6029, September 1959.
57. B. E. Hopkinson, Kinetics of the Uranium-Steam Reaction, *Journal of the Electrochemical Society*, 106(2): 102–106 (February 1959).
58. J. R. Huffman et al., MTR-ETR Technical Branches Quarterly Report for the Period Ending June 30, 1959, USAEC Report IDO-16561, Nov. 10, 1959.

Graphite

Graphite samples (CSF) irradiated at 30°C with accumulated exposures* up to 11,062 Mwd/at were examined at Hanford.[1] After this long exposure the samples continued to show an expansion in the transverse direction at a rate of 0.26 per cent per 1000 Mwd/at. A decrease in the expansion rate was observed at an exposure of 5000 Mwd/at; however, the rate is apparently constant from 5000 to 11,000 Mwd/at. Similar changes in the contraction rates of parallel samples have occurred. The contraction rate between 5000 and 11,000 Mwd/at is 0.08 per cent per 1000 Mwd/at. Maximum changes observed were 5.43 per cent expansion in the transverse direction and 1.26 per cent contraction in the parallel direction.

Results of an experiment[2] to compare the oxidation resistance of pyrolytic graphite with that of CO graphite in flowing air are presented in Table II-1. The superior oxidation resistance of pyrolytic graphite is evident.

Table II-1 OXIDATION RATES OF PYROLYTIC AND CO GRAPHITES[2]

	Oxidation rate, g/g-hr	
Temp., °C	Pyrolytic graphite	CO graphite (needle coke)
450	1.24×10^{-5}	3.5×10^{-4}
500	9.24×10^{-5}	1.8×10^{-3}
550	4.21×10^{-4}	6.0×10^{-3}
600	1.71×10^{-3}	

The mean linear thermal-expansion coefficient parallel to the crystal planes was determined for pyrolytic graphite using a quartz differential dilatometer; Table II-2 gives the results. The extreme anisotropy of this form of graphite is evidenced by the negative coefficient of linear thermal expansion below 375°C. Heretofore, only natural flake or skeletal graphite had shown this property.

Table II-2 COEFFICIENT OF LINEAR THERMAL EXPANSION OF PYROLYTIC GRAPHITE[2]

Temp. range, °C	Linear thermal-expansion coefficient, 10^{-6}/°C
25–125	−0.13
25–275	−0.09
25–375	0.00
25–625	+0.34
25–925	+0.59

Samples[3] of National Carbon Company Continental coke graphite were annealed at 650°C before irradiation at 550°C. Another similar set of samples was irradiated without prior annealing; the exposure was 885 Mwd/at. For the annealed samples the transverse and parallel length changes were +0.008 and −0.004 per cent, respectively. The corresponding values for unannealed samples were +0.024 and +0.001 per cent. These data indicate that prior annealing may appreciably reduce the initial expansion prior to contraction observed at this irradiation temperature. Samples annealed at 2600°C prior to irradiation are being irradiated. Results should indicate whether or not the expansion observed in the 650°C annealed specimens stemmed from insufficient annealing or from growth due to radiation damage.

In laboratory studies at ORNL[4] on SiC-Si coated graphite, developed by Minnesota Mining and Manufacturing Company, small samples showed no ill effects after being heated for periods up to 1000 hr in air. Near-sonic air blasts at 1830°F did not produce erosion damage, and rapid thermal cycling from 1830°F to room temperature did not crack or damage the specimen. The effect upon the coating of an internal pressure, such as might be produced by build-up of fission gas, was studied. A hollow cylindrical graphite tube, closed at one end, was coated on the outside only with the open end

*One Mwd/at is the amount of irradiation received by a sample during the time required for the ton of uranium adjacent to it to generate 1 Mwd of fission energy. This amounts to an exposure of about 3.9×10^{17} nvt thermal, or about 6.5×10^{17} nvt total.

attached to an Inconel tube. The graphite tube was pressurized to 100 psig with helium, and the temperature was brought to 2000°F by means of a heater placed over the lower half of the graphite tube. The system was checked periodically for leaks by closing off the helium supply and observing the pressure. After 1050 hr at 2000°F, the tube was examined and no evidence of damage was found. No detectable leakage of helium had occurred.

Two coated graphite cylinders were irradiated to 6.3×10^{20} nvt at low temperature. The density of the specimens decreased by 2 per cent. Both specimens appeared sound and did not exhibit leaks when placed in hot silicone oil. These specimens were tested for oxidation resistance at 2000°F in air for 186 hr, and no weight changes were observed (±0.0007 g). The samples returned to their original density during the 2000°F oxidation test. (J. Koretzky)

Beryllium Metal and Alloys

Fabrication

An improved method of compacting beryllium powder into elongated forms is claimed.[5] The powdered metal is placed in a thin metal tube capable of a high degree of plastic deformation. The tube is capped, placed in a suitable die, and compressed from the ends. A thickening and shortening of the tube occurs. Afterward, the tube is easily removed from the die, split, and peeled from the compact.

The feasibility of producing bare beryllium extrusions was definitely proved, although much development remains to be done before the process becomes commercial. A 6-ft-long V-shaped channel has been extruded, using glass as the lubricant. The extrusion had the properties shown in Table II-3. An interim specification for beryllium extrusion material was written to provide target property data for the effort. Minimum properties in the longitudinal direction were specified as 60,000 psi ultimate, 35,000 psi yield, 10 per cent elongation, and 10 per cent reduction of area.[6,7]

The Air Force program[8] at Brush Beryllium for the production of large flat sheets of beryllium has progressed into the fourth and final phase. In Phase III, 50 sheets were rolled to 0.060-, 0.040-, and 0.020-in. thicknesses in various lengths; the yield was only 31.7 per cent. These sheets were made from −325 mesh powder of 2.25 wt.% BeO and 0.15 wt.% iron analysis. Although the strength of the sheets was improved, breakage was much higher, and the yield much lower, than would have been expected had the standard −200 mesh QMV powder of 1.25 to 1.75 wt.% BeO content been used. Therefore in Phase IV, which requires the production of sheets 24 in. or more in width by 60 in. long, the standard powder containing 1.5 wt.% BeO is being used. Lamination and insufficient flatness have been the major difficulties encountered in Phase IV. Wide sheets of the Phase III material could be bent over a 2.5*T* radius at 1200°F. At 800°F and lower temperatures the minimum bending radius depended on and varied with the width of the sheets. Annealing the hot-rolled sheets at 1385 to 1400°F for 10 to 15 min only seemed to be the optimum heat-treatment. Roller leveling of hot-rolled beryllium sheet appears feasible.

The joining of beryllium to itself and other metals continues to be a problem. Brittleness makes the joining of structural parts difficult. Brazing, and possibly adhesive bonding, shows

Table II-3 PROPERTIES OF EXTRUDED BERYLLIUM[6]

Specimen*	Direction of grain	Ultimate strength, psi	Yield strength (0.5% offset), psi	Elongation, %		Reduction of area, %	Modulus of elasticity, 10^6 psi
				Dial gauge	Strain gauge		
1	*L*	68,330	54,000	6.6	1.66	1.0	N.D.†
2‡	*L*	45,200	45,200	0.144	N.D.	0.55	43.3
3	*L*	78,400	50,200	7.0	1.61	0.3	43.7
5	*T*	39,500	N.D.	1.0	N.D.	N.D.	46.5
6	*T*	40,600	N.D.	1.0	N.D.	N.D.	N.D.

*Specimen 4 was pulled from the grips; no values were obtained.
†N.D. = not determined.
‡Fractured prematurely.

the most immediate promise.[9] However, welding is required where the ultimate in strength at elevated temperatures becomes necessary.

Studies at Oak Ridge[10] indicated that diffusion bonding is an excellent method of joining beryllium plugs to beryllium tubes. Pressures for bonding were obtained by heating the tubes with the plug inserted inside a molybdenum jig. The smaller thermal expansion of the molybdenum, compared to beryllium, compressed the joint sufficiently to make a bond. Joints brazed with an alloy of 48 wt.% zirconium–48 wt.% titanium–4 wt.% beryllium cracked on cooling because of differences in the thermal expansion of the alloy and beryllium. The report includes a preliminary evaluation of $\frac{3}{4}$-in.-ID beryllium tubing obtained from England.

Meanwhile, The Brush Beryllium Company reports[11] that the fusion welding process for beryllium, with or without filler rods, has been developed so that the problems connected with obtaining crack-free joints appear to be solved. Brush Beryllium workers are starting a new project aimed at the production of welds of improved quality, making use of beryllium wire as the filler material.

A possible method of making pure beryllium electroplates was reported in Britain.[12] A bath of beryllium chloride etherate [2.5*M* $BeCl_2 \cdot 2(C_2H_5)_2O$ in ethyl ether] at 15°C was used, and bright, thin coherent films were obtained. These coatings were spectrographically free of iron, nickel, aluminum, or other metals. The electrolytic refining of beryllium in molten salt baths also was investigated.

Nuclear Metals, Inc.,[13,14] showed that beryllium could be extrusion and roll clad with type 304 stainless steel, "A" nickel, Inconel, or titanium, but only with a silver interlayer in each instance. The clad material had considerable bend ductility, and the cladding protects the beryllium from scratches. Excellent bend ductilities were obtained from narrow strips of beryllium bonded edge-to-edge with aluminum alloys or with silver.

The Martin Company exhibited the first beryllium structure in the world. Sheet was made by Nuclear Metals, with control of both the crystal size and crystal orientation. Some significant degree of biaxial ductility was obtained so that the sheet could be hot formed and riveted.[15]

Examination of beryllium sheet after grinding and milling operations showed that the worked layer was less than 1 mil thick. Grinding produced more twinning than did milling. However, little difference was found in the bend behavior at room temperature, after six different surface treatments, of specimens whose surface roughness varied between 5 and 65 μin.[16]

Detailed procedures for the preparation of metallographic specimens of beryllium are presented in a DMIC publication.[17]

Mechanical Properties

The time behavior of the stress just ahead of, and perpendicular to, the leading edge of a crack in a uniform isotropic elastic beryllium plate was analyzed. It was found that the stress decreases slightly at first and then increases without limit in proportion to $t^{1/2}$, when the time t is large.[16]

The problem of ductility in beryllium was reviewed[18] with special emphasis on the defense by G. C. Ellis of the theory that impurities are the cause of brittleness in beryllium. The problem of ductility in tubes is discussed from the standpoint of texture in relation to reduction during manufacture.

An attempt was made[19] to determine the reproducibility of mechanical properties in a single beryllium sheet by testing about 30 tensile specimens in each of three directions. The sheet was prepared from Pechiney flake by cold compacting, followed by hot press forging and hot rolling. Rolling reduction was 33 per cent in the cross direction, followed by 80 per cent in the longitudinal direction. Specimens were ground to a uniform 0.080-in. thickness and were etched before testing. The mean tensile values were (L) 67,000 psi, (45 deg) 54,000 psi, (T) 49,000 psi, with a scatter of about 33 per cent in each case. The elastic limit in bend testing was significantly higher than the 0.2 per cent offset yield stress in tension, apparently indicating that the elastic limit of beryllium is higher under complex stressing than under simple tension.

Another review[20] of beryllium metallurgy, with particular emphasis on processes used in France, gave the mechanical properties shown in Table II-4 for rolled beryllium sheet. The sheet that evidenced the considerable amount of bidirectional ductility shown in Table II-4 had been vacuum cast from Pechiney flake, reduced to powder, pressed and sintered, extruded, and cross rolled.

Table II-4 MECHANICAL PROPERTIES OF BERYLLIUM SHEET[20]

Sheet thickness		Reduction by rolling, %	Longitudinal		Transverse	
Mm	In.		Stress, psi	Strain, %	Stress, psi	Strain, %
2.2	0.087	6	57,000	5	64,000	6.7
1.5	0.059	8	63,000	8.2	70,000	12
1.0	0.039	12	63,000	6.5	70,000	6

Thermal and Chemical Properties

Data on the heat capacity of beryllium were collected from many sources and presented with an evaluation and selection of the best values, together with an estimate of the effect of impurities on those values, in a recent DMIC publication.[21]

The specific heats of uranium, thorium, beryllium, sodium, and a 44.5 wt.% lead–55 wt.% bismuth alloy were determined by a cooling-heating method and by the absolute method using an electron-radiation calorimeter.[22] The beryllium was 99.80 per cent pure; its thermal conductivity at 20°C was determined as 100 kcal/(mole)(hr)(°C). The values obtained for the specific heat of beryllium in cal/(g)(°C) at various temperatures are shown below. These agree very well with the "recommended" values in the DMIC report referred to above.

Temp., °C	Specific heat, cal/(g)(°C)	Temp., °C	Specific heat,* cal/(g)(°C)
20	0.400	350	0.615
50	0.465†	400	0.635
100	0.496†	450	0.655
		500	0.672

The corrosion resistance of beryllium in 600°F water has been investigated.[23] At best, the metal lasts from 140 to 160 days before accelerated local attack takes place. There was some evidence that quenching beryllium from 1750°F improved its corrosion resistance, but it is not known whether the improvement is sufficient to permit the extended use of beryllium in 600°F water.

*Heat capacities obtained in electron-radiation calorimeter.

†Heat capacities obtained by the relative method.

Twenty-nine papers presented at a two-day symposium held at MIT in September 1958 were published as a single volume.[24] These papers cover the entire field of human poisoning by beryllium—history, pathology, diagnosis, treatment, and prevention—from the standpoint of both the physician and the engineer.

(W. Hodge)

Beryllium Compounds

Investigators at Harwell measured the thermal conductivity of two specimens of hot-pressed BeO, one irradiated in the DIDO to 5×10^{20} nvt at 185°C and the other unirradiated.[25] The specimens were about 1 cm square and about 10 cm long. The irradiated specimen had a pre-irradiation density of 2.72 g/cm^3, and the unirradiated specimen had a density of 2.60 g/cm^3. At a mean specimen temperature of 100°C, the thermal conductivity of the irradiated specimen was 13 per cent lower than that of the unirradiated specimen, corrected for the difference in density. The difference in conductivity appeared to decrease to zero at about 350°C, and thereafter no substantial divergence was observable up to 500°C. (J. Koretzky)

Solid Hydrides

Hydrided zirconium-uranium alloys continue to be the subject of much of the research in this area. However, the properties of both zirconium hydride and yttrium hydride are still being determined. Additional information on the niobium-hydrogen system has been reported.

Table II-5 ELECTRICAL RESISTIVITY AND HALL COEFFICIENTS OF ZIRCONIUM HYDRIDE

Sample	Electrical resistivity (ρ), 10^{-6} ohm-cm				Hall coefficient (R), 10^{-5} cm^3/coulomb		
	300°K	77°K	4.2°K	1.1°K	300°K	77°K	4.2°K
$ZrH_{1.54}$	69.1	49.2	44.5	44.5	−34.8	−37.3	−29.9
$ZrH_{1.64}$	66.6	47.3	43.8	43.8	+42.0	+39.8	+39.8
$ZrH_{1.68}$	54.7	33.2	28.9	28.9	+39.0	+50.4	+48.7

Zirconium Hydride

The Hall coefficient and the electrical resistivity of zirconium hydride have been measured at Atomics International. The values are shown in Table II-5 and are characteristic of metallic behavior.

Diffusion coefficients for hydrogen in delta-phase zirconium hydride between 650 and 850°C have been measured at Battelle.[26] The values obtained by the steady-state and the time-lag methods are in good agreement, as shown in Table II-6. It was concluded that the permeation process is diffusion controlled. The diffusion coefficients were found to be independent of concentration and can be expressed by $D = 6.14 \times 10^{-4} \exp(-45{,}900/RT)$ cm^2/sec.

Table II-6 DIFFUSION COEFFICIENTS FOR HYDROGEN IN ZIRCONIUM HYDRIDE[26]

Temp., °C	Average composition, at.% hydrogen	Diffusion coefficient (D_θ), 10^{-4} cm^2/sec	
		Steady-state	Time-lag
500	65.8	0.15	0.21
600	63.3	1.2	1.1
700	59.8	7.2	7.1
700	60.0	7.2	
700	60.0	7.6	
750	60.0	29	27

Espagno et al.[27,28] have developed a dilatometric technique for studying the zirconium-hydrogen system. Changes in sample length are correlated with the hydrogen content of the specimen and with the eutectic temperature. An abrupt change in the dilatation coefficient is claimed to indicate a phase boundary.

Yttrium Hydride

The methods of fabrication and the properties of yttrium hydride have been reported by General Electric. The lattice constant of the face-centered-cubic structure YH_2 is $a_0 = 5.201$ A. The dissociation pressure of hydrided yttrium of various hydrogen compositions is shown as a function of temperature in Fig. 2.

During irradiation of yttrium hydride specimens in the ETR by Oak Ridge, gamma heating produced a temperature gradient up to 400°F from the surface to the center of a 0.800-in.-diameter cylinder. After 90 hr, including seven thermal cycles between 750 and 1550°F, the specimens were still structurally sound.

The change in density of yttrium hydride with hydrogen content has been determined at Denver Research Institute. Table II-7 gives values for the density and the N_H of yttrium hydride containing more than 1 wt.% hydrogen.

Battelle stress-rupture data on hydrided yttrium having N_H values of 4.8 and 5.4 are shown in Table II-8. The higher ductilities and creep rates at 2000°F, as compared to those at 1800°F, are apparent for the specimens with $N_H = 5.4$.

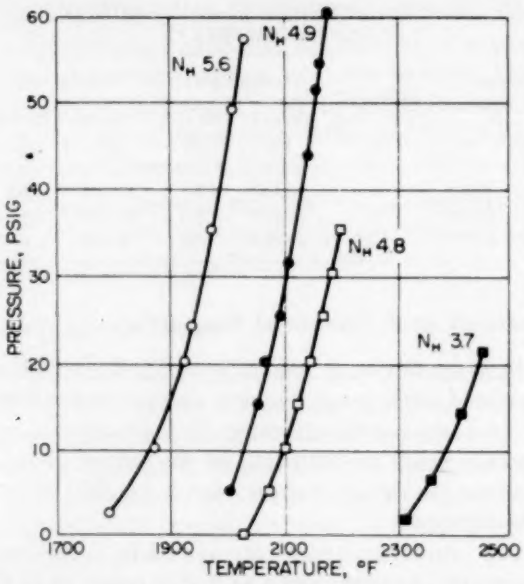

Figure 2—Pressure as a function of temperature at constant volume for hydrided yttrium.

Table II-7 DENSITY AND N_H OF YTTRIUM HYDRIDE AS A FUNCTION OF COMPOSITION

Hydrogen content, wt.%	Density, g/cm^3	N_H
1.08	4.360	2.80
1.26	4.347	3.28
1.44	4.336	3.72
1.59	4.330	4.12
1.82	4.311	4.69
2.19	4.290	5.61

The hydrogen content of yttrium hydride was reduced from 2.11 to 1.92 wt.% by 1000-hr exposure to terphenyls in a dynamic loop at 500°F maximum temperature.

Denver Research Institute found that the hydrogen absorbing capacity of yttrium is only slightly decreased by the presence of 3000 ppm oxygen in the metal and that no serious effect on hydriding was observed with as much as 5000 ppm oxygen.

Niobium Hydride

Metallographic studies of carefully annealed samples of niobium hydride have been reported by Paxton et al.[29] They found evidence that what

Table II-8 RESULTS OF STRESS-RUPTURE TESTS ON HYDRIDED YTTRIUM

Temp., °F	Stress, psi	Rupture time, hr	Total elongation, %	Min. creep rate, %/hr	Atmosphere
		$N_H = 4.8$			
1800	3800	76.6	16.0	0.139	414 mm H_2 346 mm He
2000	2500	4.9	2.0		724 mm H_2 36 mm He
		$N_H = 5.4$			
1800	5600	136.1	5.5	0.028	517 mm H_2 243 mm He
2000	2800	114.9	28.0	0.20	1035 mm H_2
2000	3800	6.1	11.0	2.2	1035 mm H_2

has been proposed to be a miscibility gap in the niobium-hydrogen system, in the temperature range 200 to 300°C, may actually be a martensitic phase transformation.

Alloy Hydrides

LaGrange et al.[30] have studied the zirconium-uranium-hydrogen system in the temperature range 600 to 800°C by hydrogen-dissociation-pressure measurements and high-temperature X-ray-diffraction techniques. The zirconium-uranium alloys investigated contained 1.69, 3.26, 5.05, 15.0, and 54.0 at.% uranium. Isothermal sections of the ternary diagram at 617, 643, 687, and 795°C are presented. No new phases that are not already known to exist in the related binary systems were encountered. The miscibility gap appearing in the body-centered-cubic solid-solution field of the zirconium-uranium diagram expands rapidly with the addition of hydrogen. The solubility of uranium in the face-centered zirconium hydride phase is very limited.

A high-temperature irradiation study of the hydrided zirconium–2 wt.% uranium alloy was conducted by Battelle.[31] Enriched $ZrH_{1.65}$–2 wt.% uranium specimens were irradiated in the MTR. Specially designed capsules were used, which provided a hydrogen atmosphere and allowed center-line temperatures up to 1500°F. The actual temperatures recorded during the exposure period ranged from 900 to 1400°F. Uranium burn-ups of 13 and 25 at.% were achieved. Almost negligible changes in density were produced in the material by the irradiation. Changes of length and diameter were of a degree that could fall within experimental error. Metallographic examination showed no change in microstructure which could be attributed to the effect of irradiation.

Preliminary studies on Zircaloy-4 at Hanford[3] have shown that this alloy picks up molecular hydrogen much more rapidly than does Zircaloy-2. Hydriding was done at 400 to 500°C with both dry and wet hydrogen, and similar results were found in both cases.

(H. H. Krause)

References

1. F. W. Albaugh, Reactor and Fuels Research and Development Operation Monthly Report for October 1959, USAEC Report HW-62587A, Nov. 15, 1959. (Classified)
2. F. W. Albaugh, Reactor and Fuels Research and Development Operation Monthly Report for November 1959, USAEC Report HW-62899A, Dec. 15, 1959. (Classified)
3. F. W. Albaugh, Reactor and Fuels Research and Development Operation Monthly Report for September 1959, USAEC Report HW-62012A, Oct. 15, 1959. (Classified)
4. Solid State Division Annual Progress Report for Period Ending August 31, 1959, USAEC Report ORNL-2829, Dec. 11, 1959.
5. Harold F. Larson, Method of Forming Elongated Compacts, U. S. Patent 2,885,287, May 5, 1959.
6. Program for the Development of Extruded Beryllium Shapes; Interim Engineering Report No. 3 for the Period December 1, 1958 to February 28, 1959, Report NOR-59-227.
7. Program for the Development of Extruded Beryllium Shapes; Interim Engineering Report No. 4 for the Period March 1, 1959 to May 31, 1959, Report NOR-59-353.
8. K. G. Wikle and J. W. Armstrong, Production of Beryllium Sheets Finished Flat to Gauge: Phase III-Phase IV, Progress Report No. 7 for May 1 to July 31, 1959, Report NP-7948, Brush Beryllium Company.
9. Design Tips for Joining Beryllium. Part II. *Aircraft and Missiles Manufacturing*, 2(12): 26–28 (December 1959).
10. Gas-cooled Reactor Project Quarterly Progress Report for Period Ending September 30, 1959, USAEC Report ORNL-2835, Dec. 2, 1959.
11. B. M. MacPherson and W. W. Beaver, Fusion Welding of Beryllium, Progress Report No. 1, May 1 to July 31, 1959, Report NP-7901, Brush Beryllium Company, Aug. 15, 1959.
12. I. A. Menzies and D. L. Hill, Electrolytic Deposition of Beryllium, *Nature*, 183(4664): 816–817 (Mar. 21, 1959).

13. J. Greenspan et al., Beryllium Research and Development in the Area of Composite Materials, Report NMI-9404, Mar. 20, 1959.
14. J. Greenspan et al., Beryllium Research and Development in the Area of Composite Materials, Report NMI-9408, June 23, 1959.
15. Beryllium Structure Made, *Missiles and Rockets*, 5(23): 4 (June 8, 1959).
16. M. Jacobson et al., Beryllium Crack Propagation and Effects of Surface Conditions, Report LMSD-288005, May 20, 1959.
17. R. D. Buchheit et al., Procedures for the Metallographic Preparation of Beryllium, Titanium, and Refractory Metals, Report DMIC-Memo-37, Oct. 26, 1959, Battelle Memorial Institute.
18. Ductility of Beryllium, *The Metal Industry (London)*, 95(11): 224ff (Oct. 23, 1959).
19. N. A. Hill, The Variation of Tensile and Bend Properties in a Beryllium Sheet, British Report AERE-M-482, July 1959 (to be submitted for publication).
20. P. Vachet, Beryllium, British Report IG-IS-59(RD/S), Translation by R. L. Tams, UKAEA, from *Chimie & industrie (Paris)*, 81(1): 64-77 (January 1959).
21. J. W. Holladay, Heat Capacity of Beryllium, Report DMIC-Memo-36, Oct. 19, 1959, Battelle Memorial Institute.
22. E. A. Mit'kina, The True Specific Heats of Uranium, Thorium, and Other Metals (in Russian), *Atomnaya Energiya*, 7: 163–165 (August 1959).
23. Henry Suss, Properties of Beryllium Metal, USAEC Report KAPL-M-HOS-7, Sept. 9, 1959.
24. Beryllium Disease and Its Control, *AMA Archives of Industrial Health*, 19(2): (February 1959).
25. R. C. McGill and J. A. G. Smith, The Thermal Conductivity of Irradiated and Unirradiated Beryllia, British Report AERE-R-3019, July 1959.
26. R. W. Dayton and C. R. Tipton, Jr., Progress Relating to Civilian Applications During November 1959, USAEC Report BMI-1398, Dec. 1, 1959. (Classified)
27. L. Espagno et al., Dilatometric Study of the Zirconium-Hydrogen System, *Comptes rendus*, 247: 1199–1201 (1958).
28. L. Espagno et al., Dilatometric Study of the Zirconium-Hydrogen System Between Ambient Temperature and 550°C, *Comptes rendus*, 247: 2003–2005 (1959).
29. H. W. Paxton et al., Observations on the Niobium-Hydrogen System, *Transactions of the American Institute of Mining, Metallurgical, & Petroleum Engineers*, 215(4): 725–726 (August 1959).
30. L. D. LaGrange et al., A Study of the Zirconium-Hydrogen and Zirconium-Hydrogen-Uranium Systems Between 600° and 800°C, *Journal of Physical Chemistry*, 63(12): 2035–2041 (December 1959).
31. G. E. Lamale et al., High-temperature Irradiation of a Zirconium Hydride–2 Wt.% Uranium Alloy, USAEC Report BMI-1401, Dec. 10, 1959.

Dispersion Poison Materials

Vallecitos[1] has recently published a survey of the physics, metallurgy, and engineering aspects of reactor control materials. The volume contains too much information for a brief résumé; however, it includes a detailed discussion of activities at the major laboratories; a discussion of outstanding problems; a review of applications of various materials, including boron, cadmium, silver, hafnium, and rare earths; recommendations; and many references. The report is unclassified and is available from the Office of Technical Services, Department of Commerce.

Work has also been continued on the control of boron loss in UO_2–stainless steel fuel plates containing a boron burnable poison.[3] Owing to difficulty in analyzing for small quantities of boron in stainless steel, Oak Ridge prepared samples and correlated results between several laboratories which resulted in the development of reliable analytical techniques. Fuel plates containing B_4C (which was used in preparing Army Reactor SM-1 fuel plates) gave an average 22.4 wt.% boron loss. The loss of boron in various matrices during sintering is shown in Table III-1. Because heavy losses occur only when oxygen is available, the following reactions are suggested: (1) $^3/_x MO_x = 2B \rightleftharpoons B_2O_3(liq) + {}^3/_x M$ and (2) $B_2O_3(liq) \rightleftharpoons B_2O_3(gas)$, where reaction 2 is considered to be rate controlling.

Oak Ridge also reports that SrB_6, ZrB_2, B_4C, and BN are not compatible with stainless steel.

At Bettis[4] Zircaloy-2-clad titanium-base dispersions containing enriched boron or enriched titanium diboride were examined as possible control materials. Results of corrosion tests of the nonirradiated dispersions indicated that cladding with a corrosion-resistant material was necessary. Roll bonding Zircaloy-2 cladding to titanium-base dispersions was shown to be feasible through a study of the integrity, corrosion resistance, and bend properties of the clad dispersions. Cladding separation and excessive swelling were noted in the samples of clad titanium-base dispersions containing 5 wt.% enriched boron which were irradiated for long periods. The clad 34 wt.% enriched titanium diboride dispersion irradiated to nearly the same exposures showed no visual evidence of cracking of the cladding or excessive swelling. Metallographic examination after irradiation, which was confined to the 5 wt.% enriched boron dispersion, revealed internal cracking and bond-line damage, the severity of damage increasing with radiation exposure.

Table III-1 AVERAGE BORON SINTERING LOSSES[3] FROM COMPACTS CONTAINING 5 WT.% BORON, BALANCE MATRIX MATERIAL, SINTERED AT 1135°C

Matrix material	Boron loss,* wt.%		
	Vacuum	Argon	Wet helium
Si	2.6	3.4	10.1
SiO_2	12.3	9.1	7.2
Ni	2.6	5.3	9.3
NiO	31.5	8.6	41.5
Cr	1.7	3.0	
Cr_2O_3	2.1	3.3	
Fe	5.1	3.0	

*Sintering environment.

Bettis[5] has also published a study of the extrusion and fabrication characteristics of various titanium-enriched boron dispersions which indicates that hot extrusion of uncompacted powders is a feasible method for producing these materials. Tensile and impact properties of dispersions containing 2.43, 3.4, and 3.8 wt.% B^{10} show a decrease with increasing B^{10} concentration. Irradiation studies of these materials reveal that internal cracking results after thermal-neutron exposure of approximately 4.6×10^{20} nvt and higher. Tensile properties of the dispersions were related directly to the exposure and resulting structure; however, no correlation was found between exposure and impact properties of these materials.

Battelle[6–8] is developing UO_2–stainless steel dispersion fuel plates containing ZrB_2 as a burnable poison. Excellent boron retention is obtained during vacuum sintering. Total boron

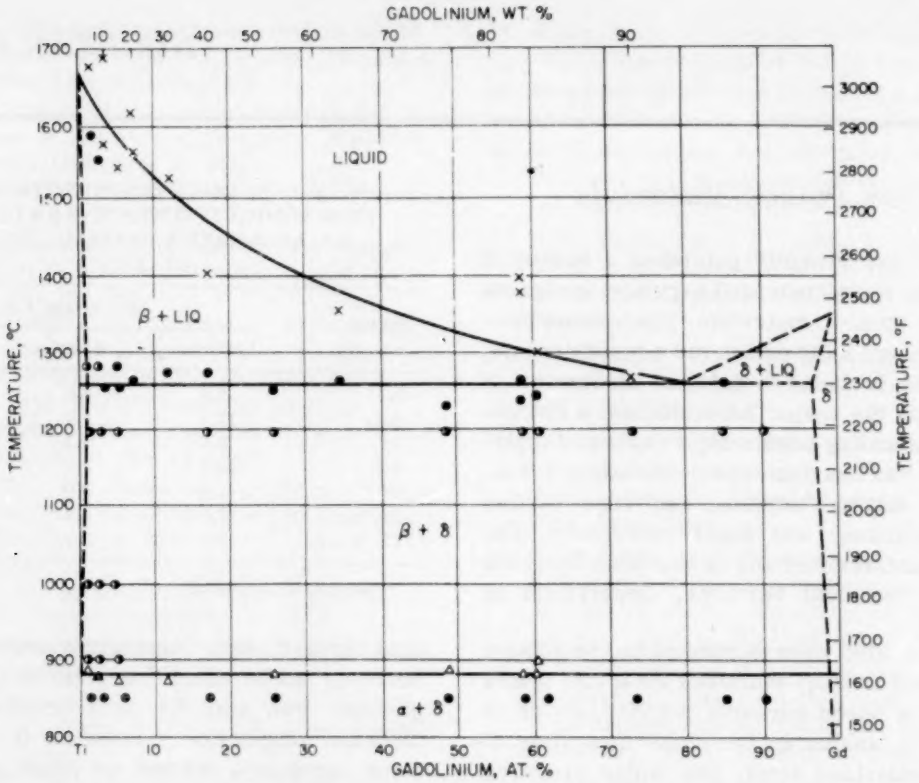

Figure 3—Titanium-gadolinium equilibrium diagram.[10] ×, liquidus (optical). ●, solidus (optical). △, thermal analysis. ◑ and ⊕, two phase (metallographic).

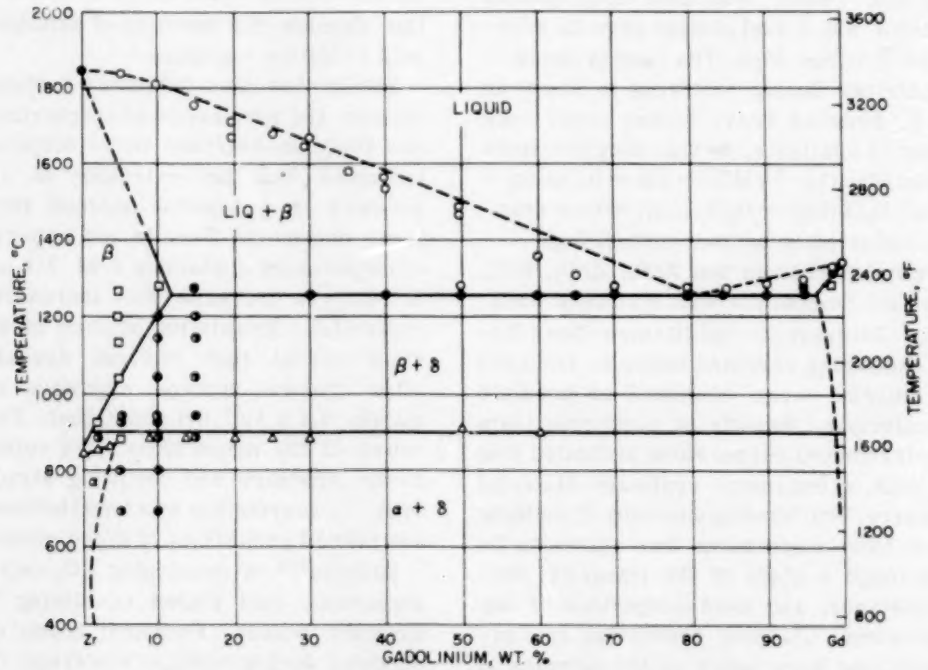

Figure 4—Tentative zirconium-gadolinium phase diagram.[10] ○, liquidus. ●, solidus. △, $\alpha \rightarrow \beta$. □, single phase. ◑, two phase.

loss on fabricated plates is less than 10 wt.%; the last three full-size plates produced had losses of less than 6 per cent. Additional reduction of boron loss appears possible by the use of niobium-coated ZrB_2 particles.

(G. W. Cunningham)

Metallic Poison Materials

Silver-Indium-Cadmium Alloys

A Bettis report[9] reviews the results of an investigation of a silver–15 wt.% indium–5 wt.% cadmium alloy for use as a replacement for hafnium. Conclusions drawn from the review are that the alloy is satisfactory in nuclear and mechanical properties, irradiation stability, and fabricability. Corrosion resistance in high-oxygen water and creep resistance under bending loads are marginal. Electroplated nickel coatings satisfactorily protect the alloy against corrosion. Creep resistance can be improved by coarsening the grain size of cast and wrought material by annealing at 500°C or by fabricating the material by extrusion of prealloyed powders.

Rare-earth Alloys

The titanium-gadolinium phase diagram, as established by the U. S. Bureau of Mines,[10] is shown in Fig. 3. A tentative zirconium-gadolinium diagram is presented in Fig. 4.

(V. W. Storhok)

References

1. Survey of the Physics, Metallurgy, and Engineering Aspects of Reactor Control Materials, USAEC Report GEAP-3183, June 12, 1959.
2. A. B. Townsend, The Preparation of Uranium Diboride, USAEC Report Y-1255, Apr. 10, 1959. (Classified)
3. J. H. Frye et al., Metallurgy Division Annual Progress Report for the Period Ending September 1, 1959, USAEC Report ORNL-2839, Dec. 16, 1959.
4. E. S. Byron et al., Clad Titanium-base Dispersions Containing Boron, *Nuclear Science and Engineering*, 6(5): 361-370 (November 1959).
5. L. B. Prus et al., Enriched Boron-Titanium Dispersions, *Nuclear Science and Engineering*, 6(3): 167-173 (September 1959).
6. R. W. Dayton and C. R. Tipton, Jr., Progress Relating to Civilian Applications During October 1959, USAEC Report BMI-1391(Rev.), Nov. 1, 1959.
7. R. W. Dayton and C. R. Tipton, Jr., Progress Relating to Civilian Applications During November 1959, USAEC Report BMI-1398, Dec. 1, 1959. (Classified)
8. R. W. Dayton and C. R. Tipton, Jr., Progress Relating to Civilian Applications During December 1959, USAEC Report BMI-1403, Jan. 1, 1960.
9. Bettis Technical Review: Reactor Metallurgy, USAEC Report WAPD-BT-15, September 1959.
10. Quarterly Metallurgical Progress Report No. 4 for the Period July 1 to September 30, 1959, USAEC Report USBM-U-647, Sept. 30, 1959.

Corrosion

Niobium

At 550°C all niobium-zirconium alloys investigated at the University of Florida[1] showed parabolic oxidation rates, but at 900°C the reaction rate tended to be linear. At 1090°C the reactions followed the relation $W^n = kt$, with n ranging from 2 (parabolic) for niobium-rich alloys to 3 (cubic) for zirconium-rich alloys.

In work conducted at Thompson Products, Hiltz[2] observed that NbO was formed, in addition to Nb_2O_5, on oxidation of several improved niobium binary alloys for 24 hr at 1000°C. All additions that improved the oxidation behavior fulfilled at least two of the following conditions:

1. An ionic size similar to that of Nb^{+5}
2. A +3 valence state
3. The formation of a second oxide phase during oxidation

Battelle[3-5] is continuing its investigation of hot water and steam corrosion of niobium and niobium alloys. On the basis of cross section, corrosion resistance, and 1200°F mechanical properties, the most attractive alloy is niobium–12 at.% vanadium. Ternary additions of up to 2.5 at.% of titanium, molybdenum, iron, chromium, aluminum, or nickel do not improve the corrosion resistance of this alloy.

The reaction of niobium with 1 atm nitrogen is under further study at Battelle.[4] At 300 to 600°C the reaction follows the logarithmic rate law, whereas at 675 to 1600°C the reaction rate is parabolic. (W. D. Klopp)

Zirconium

The fretting corrosion of Zircaloy-2 in air, oxygen, and high-temperature water has been the subject of considerable study at Bettis.[6] In general, it was found that fretting weight losses between Zircaloy-2 surfaces were significantly less than those obtained for mild-steel surfaces under similar conditions. On the other hand, Zircaloy-2 tested against stainless steel in air or oxygen evinced fretting losses of the order of 10 times those for Zircaloy-to-Zircaloy contacts. This fretting between the Zircaloy–stainless steel couples was considerably less in the water tests. Indications are that the thin oxide films formed on Zircaloy-2 in water help to reduce fretting under light loads and relatively small surface velocities. However, any condition that tends to disrupt this film may greatly increase fretting.

The oxidation kinetics of a series of alloys of zirconium containing 1, 2, and 4 at.% of aluminum, beryllium, carbon, copper, chromium, cobalt, hafnium, iron, lead, molybdenum, nickel, niobium, platinum, silicon, tantalum, tin, titanium, tungsten, uranium, and vanadium have been investigated at Argonne.[7] The initial rates of oxidation of alloys containing those additives which are soluble in alpha zirconium could be interpreted in terms of the Wagner-Hauffe theory of alloy oxidation. For these alloys, it was postulated that the oxidation product consisted of a single phase and that the oxidation number of the additive element in the oxide affects the concentration of anion vacancies, which is directly related to the oxidation rate. This followed since the oxidation proceeded by anion diffusion through vacancies in the oxide lattice. In the case of additives insoluble in alpha zirconium, it was thought that the oxidation produced agglomerates of the alloying metal oxide which tend to remain as a separate oxide phase. For these alloys the Wagner-Hauffe theory did not apply.

It is suggested that the breakaway phenomenon may be predicted by the rule that a breakaway will occur when the ionic radius of the additive element in the oxide differs by 15 per cent or more from the ionic radius of zirconium. This rule was followed by all seven of the alloys that obeyed the Wagner-Hauffe theory. Although the factors causing breakaway are probably different for the insoluble- and soluble-additive systems, the rule also was followed by 10 of the 13 insoluble additives. (W. K. Boyd)

Aluminum

Preliminary out-of-reactor data, obtained at Hanford,[8] indicates that the corrosion rate of the X-8001 aluminum alloy at 300°C in *p*H–4.5 water adjusted with HNO_3 is considerably higher than that in water of similar *p*H adjusted with H_3PO_4. After 642 hr of exposure, the rates were 0.48 and 0.06 mil per month for the HNO_3 and H_3PO_4 water, respectively. On the other hand, corrosion rates of type 304 stainless steel were similar, regardless of whether the *p*H was adjusted with HNO_3 or H_3PO_4. (W. K. Boyd)

Stainless Steels

The behavior of various structural materials including types 304 and 410 stainless steel, low-alloy steels AISI 1020 and 4130, aluminum, and magnesium in an organic-moderated and -cooled reactor has been studied at Atomics International.[9] The test conditions consisted of an eight-month exposure at 600°F in polyphenyl under integrated fluxes of the order of 9×10^{19} nvt thermal and 2.8×10^{20} nvt fast. The corrosion behavior of the stainless steels, low-alloy steels, and aluminum under the above conditions was considered good to excellent. On the other hand, magnesium pitted and is not considered completely satisfactory. No evidence was found of stress-corrosion cracking or accelerated attack of bimetallic couples. (W. K. Boyd)

Corrosion of Iron-base Alloys

A recent Knolls report[10] correlated the results of several tests relating to the behavior of stressed, chromium-plated AISI 410 stainless steel. Under certain high-temperature water environments, AISI 410 is susceptible to stress-corrosion failure, particularly when tempered at temperatures below 1125°F. The results of protection from stress-corrosion failure by chromium plating have been sporadic. In some cases, results have been excellent, with no failure resulting in susceptible material under environments amenable to stress-corrosion failure. Conversely, failures have occurred in plated AISI 410 stainless steel where, normally, the base material would have been resistant. From this, it was concluded that, with an adequate (crack or pore free) coating, protection will be complete. However, in the event of a defective coating, corrosive effects are magnified drastically, resulting in premature failure because of the unfavorable anodic area effect. The coupling of chromium-plated AISI 410 stainless steel to a cobalt-base alloy results in galvanic corrosion that rapidly destroys the chromium plate and the underlying base metal. Because of the apparent inability to control plating processes perfectly, it has been recommended that chromium plating *not* be used on parts that are susceptible to stress corrosion. The complexity of the factors involved suggests that any use of coatings should be explored experimentally to determine the behavior of the coating-base system in the anticipated environment. (E. S. Bartlett)

Oxidation of Nickel-base Alloys

French workers[11] studied the air oxidation of two alloys, Hastelloy X (48 wt.% nickel–21 wt.% chromium–17 wt.% iron–8 wt.% molybdenum–0.25 wt.% titanium) and Nicral D (nominally, 25 wt.% chromium–20 wt.% nickel–1.5 wt.% silicon–balance iron), at 1650 and 2000°F. At 1650°F, both alloys oxidize at about the same rate; but, at 2000°F, Hastelloy X is superior, on the basis of weight-change measurements. Nicral D is oxidized intergranularly at the higher temperature, whereas Hastelloy X does not show this tendency. Internal oxidation was observed in both alloys at 2000°F.

(E. S. Bartlett)

Attack of Magnesium and Aluminum Alloys

A study of the erosion of magnesium–8 wt.% aluminum alloy at Savannah River[12] showed this material to be attacked at the rate of 0.1 in./year in 104°F water flowing at 20 ft/sec. The rate of erosion was several times higher for specimens with lower concentrations of aluminum.

An interesting observation on magnesium rods, clad with Zircaloy-2, in steam environments has been made at Hanford.[13] Two clad magnesium rods, one with a 0.012-in.-diameter defect and the other with a 0.500-in.-diameter defect, were exposed to superheated steam. Corrosion at the smaller defect was very slight after exposure for 24 hr to 660°F steam. The larger defect, when exposed for 20 min to 570°F steam, resulted in a 100-mil metal loss in the magnesium base.

Additional Hanford experiments were designed to study possible spontaneous ignition of clad

Corrosion

Niobium

At 550°C all niobium-zirconium alloys investigated at the University of Florida[1] showed parabolic oxidation rates, but at 900°C the reaction rate tended to be linear. At 1090°C the reactions followed the relation $W^n = kt$, with n ranging from 2 (parabolic) for niobium-rich alloys to 3 (cubic) for zirconium-rich alloys.

In work conducted at Thompson Products, Hiltz[2] observed that NbO was formed, in addition to Nb_2O_5, on oxidation of several improved niobium binary alloys for 24 hr at 1000°C. All additions that improved the oxidation behavior fulfilled at least two of the following conditions:

1. An ionic size similar to that of Nb^{+5}
2. A +3 valence state
3. The formation of a second oxide phase during oxidation

Battelle[3–5] is continuing its investigation of hot water and steam corrosion of niobium and niobium alloys. On the basis of cross section, corrosion resistance, and 1200°F mechanical properties, the most attractive alloy is niobium–12 at.% vanadium. Ternary additions of up to 2.5 at.% of titanium, molybdenum, iron, chromium, aluminum, or nickel do not improve the corrosion resistance of this alloy.

The reaction of niobium with 1 atm nitrogen is under further study at Battelle.[4] At 300 to 600°C the reaction follows the logarithmic rate law, whereas at 675 to 1600°C the reaction rate is parabolic. (W. D. Klopp)

Zirconium

The fretting corrosion of Zircaloy-2 in air, oxygen, and high-temperature water has been the subject of considerable study at Bettis.[6] In general, it was found that fretting weight losses between Zircaloy-2 surfaces were significantly less than those obtained for mild-steel surfaces under similar conditions. On the other hand, Zircaloy-2 tested against stainless steel in air or oxygen evinced fretting losses of the order of 10 times those for Zircaloy-to-Zircaloy contacts. This fretting between the Zircaloy–stainless steel couples was considerably less in the water tests. Indications are that the thin oxide films formed on Zircaloy-2 in water help to reduce fretting under light loads and relatively small surface velocities. However, any condition that tends to disrupt this film may greatly increase fretting.

The oxidation kinetics of a series of alloys of zirconium containing 1, 2, and 4 at.% of aluminum, beryllium, carbon, copper, chromium, cobalt, hafnium, iron, lead, molybdenum, nickel, niobium, platinum, silicon, tantalum, tin, titanium, tungsten, uranium, and vanadium have been investigated at Argonne.[7] The initial rates of oxidation of alloys containing those additives which are soluble in alpha zirconium could be interpreted in terms of the Wagner-Hauffe theory of alloy oxidation. For these alloys, it was postulated that the oxidation product consisted of a single phase and that the oxidation number of the additive element in the oxide affects the concentration of anion vacancies, which is directly related to the oxidation rate. This followed since the oxidation proceeded by anion diffusion through vacancies in the oxide lattice. In the case of additives insoluble in alpha zirconium, it was thought that the oxidation produced agglomerates of the alloying metal oxide which tend to remain as a separate oxide phase. For these alloys the Wagner-Hauffe theory did not apply.

It is suggested that the breakaway phenomenon may be predicted by the rule that a breakaway will occur when the ionic radius of the additive element in the oxide differs by 15 per cent or more from the ionic radius of zirconium. This rule was followed by all seven of the alloys that obeyed the Wagner-Hauffe theory. Although the factors causing breakaway are probably different for the insoluble- and soluble-additive systems, the rule also was followed by 10 of the 13 insoluble additives. (W. K. Boyd)

Aluminum

Preliminary out-of-reactor data, obtained at Hanford,[8] indicates that the corrosion rate of the X-8001 aluminum alloy at 300°C in *p*H–4.5 water adjusted with HNO_3 is considerably higher than that in water of similar *p*H adjusted with H_3PO_4. After 642 hr of exposure, the rates were 0.48 and 0.06 mil per month for the HNO_3 and H_3PO_4 water, respectively. On the other hand, corrosion rates of type 304 stainless steel were similar, regardless of whether the *p*H was adjusted with HNO_3 or H_3PO_4. (W. K. Boyd)

Stainless Steels

The behavior of various structural materials including types 304 and 410 stainless steel, low-alloy steels AISI 1020 and 4130, aluminum, and magnesium in an organic-moderated and -cooled reactor has been studied at Atomics International.[9] The test conditions consisted of an eight-month exposure at 600°F in polyphenyl under integrated fluxes of the order of 9×10^{19} nvt thermal and 2.8×10^{20} nvt fast. The corrosion behavior of the stainless steels, low-alloy steels, and aluminum under the above conditions was considered good to excellent. On the other hand, magnesium pitted and is not considered completely satisfactory. No evidence was found of stress-corrosion cracking or accelerated attack of bimetallic couples. (W. K. Boyd)

Corrosion of Iron-base Alloys

A recent Knolls report[10] correlated the results of several tests relating to the behavior of stressed, chromium-plated AISI 410 stainless steel. Under certain high-temperature water environments, AISI 410 is susceptible to stress-corrosion failure, particularly when tempered at temperatures below 1125°F. The results of protection from stress-corrosion failure by chromium plating have been sporadic. In some cases, results have been excellent, with no failure resulting in susceptible material under environments amenable to stress-corrosion failure. Conversely, failures have occurred in plated AISI 410 stainless steel where, normally, the base material would have been resistant. From this, it was concluded that, with an adequate (crack or pore free) coating, protection will be complete. However, in the event of a defective coating, corrosive effects are magnified drastically, resulting in premature failure because of the unfavorable anodic area effect. The coupling of chromium-plated AISI 410 stainless steel to a cobalt-base alloy results in galvanic corrosion that rapidly destroys the chromium plate and the underlying base metal. Because of the apparent inability to control plating processes perfectly, it has been recommended that chromium plating *not* be used on parts that are susceptible to stress corrosion. The complexity of the factors involved suggests that any use of coatings should be explored experimentally to determine the behavior of the coating-base system in the anticipated environment. (E. S. Bartlett)

Oxidation of Nickel-base Alloys

French workers[11] studied the air oxidation of two alloys, Hastelloy X (48 wt.% nickel–21 wt.% chromium–17 wt.% iron–8 wt.% molybdenum–0.25 wt.% titanium) and Nicral D (nominally, 25 wt.% chromium–20 wt.% nickel–1.5 wt.% silicon–balance iron), at 1650 and 2000°F. At 1650°F, both alloys oxidize at about the same rate; but, at 2000°F, Hastelloy X is superior, on the basis of weight-change measurements. Nicral D is oxidized intergranularly at the higher temperature, whereas Hastelloy X does not show this tendency. Internal oxidation was observed in both alloys at 2000°F.

(E. S. Bartlett)

Attack of Magnesium and Aluminum Alloys

A study of the erosion of magnesium–8 wt.% aluminum alloy at Savannah River[12] showed this material to be attacked at the rate of 0.1 in./year in 104°F water flowing at 20 ft/sec. The rate of erosion was several times higher for specimens with lower concentrations of aluminum.

An interesting observation on magnesium rods, clad with Zircaloy-2, in steam environments has been made at Hanford.[13] Two clad magnesium rods, one with a 0.012-in.-diameter defect and the other with a 0.500-in.-diameter defect, were exposed to superheated steam. Corrosion at the smaller defect was very slight after exposure for 24 hr to 660°F steam. The larger defect, when exposed for 20 min to 570°F steam, resulted in a 100-mil metal loss in the magnesium base.

Additional Hanford experiments were designed to study possible spontaneous ignition of clad

magnesium and aluminum in high-pressure steam. Rods coated with 10 mils of Zircaloy-2 were resistance heated to the point of fusion of the cores in 750°F, 1000-psi steam in an autoclave. Even after complete destruction of the Zircaloy-2 cladding by the molten core, autoignition was not observed with either aluminum or magnesium. At temperatures from 1200 to 1300°F, it was observed that magnesium will destroy the protective quality of a 5- to 10-mil Zircaloy-2 cladding in less than 10 min by interdiffusion of the core and cladding.

(E. S. Bartlett)

Corrosion by Liquid Metals and Fused Salts

Liquid-metal control rods are being considered for the Liquid Metal Fueled Reactor Experiment (LMFRE-I). In the device envisioned, an annular space between two cylinders contains a liquid metal having a high-neutron-absorption cross section and a low melting point. The rise and fall of the liquid level, which is governed by positioning the inner cylinder (actually, a piston), is the feature that establishes reactor control. Basic in the materials problem is the standard requirement that corrosion be avoided; however, there is also the very unusual requirement that the liquid metal cannot wet the contacting surfaces since adhering metal on these surfaces would affect the control characteristics.

In another 1000-hr tilting-furnace corrosion-test series under LMFRE auspices, it was found[14] that three special-purpose materials, molybdenum–0.5 wt.% titanium, tantalum, and beryllium, were unattacked by 975°F peak-temperature bismuth containing 1150 ppm uranium, 350 ppm magnesium, and 175 ppm zirconium; this is the reference composition for the LMFRE circulating fuel. For these particular experiments the container capsules were fabricated of Croloy-2¼.

The previous quarterly review in this series [*Reactor Core Materials*, 3(1): 35 (February 1960)] reported that an Inconel pumping loop had been operated at Oak Ridge under the Molten Salt Reactor Program for over one year with a 53 mole % NaF–46 mole % BeF_2–1 mole % UF_4 salt mixture; attack in the system, which ran between the temperature limits 1300 to 1100°F, ranged from 18 to 38 mils. According to information included in a recent progress report from Oak Ridge,[15] it is now suspected that contamination contributed to this extensive attack. This report also presents data for two INOR-8 systems comparable with the above Inconel system. In one of these INOR systems, no attack was visible anywhere in the system. The other INOR-8 system featured graphite rods in contact with the salt and was operated primarily to provide data pertinent to the INOR 8–graphite–salt system. In this case, light surface roughening and pitting occurred; however, no evidence of carburization could be found by metallographic inspections.

The Molten Salt Reactor Program studies of graphite in contact with molten salts were prompted by the advantage gained if an unclad graphite moderator could be employed. The studies include compatibility tests such as the above, as well as permeability and carburization-effect studies. Diffusion coefficients derived from experimental data indicate that a 50-mil-wall INOR-8 tube would have to be exposed for approximately 20 years in a 1200°F graphite-sodium carburizing medium before the carbon content at the wall midpoint would reach 0.2 wt.%. Although this degree of carburization would be detrimental to room-temperature properties of the material, there is reason to believe that there would be no serious property deterioration in the 1250°F range of prime interest. Graphite permeability studies showed that most of the grades tested (at 1300°F, 100 hr, and 150 psig overpressure) failed to meet the specification that the bulk volume be permeated less than 0.5 per cent. One grade, GT-123, satisfied the requirement, exhibiting a permeability of 0.13 per cent in contact with a salt having the composition 67 mole % LiF–18.5 mole % BeF_2–14 mole % ThF_4–0.5 mole % UF_4.

In a compilation[16] of phase diagrams and associated information obtained over the years from research at ORNL and other laboratories, a large fraction is devoted to alkali metal–alkali metal halide and fluoride systems (sodium, potassium, rubidium, and cesium), hydroxide systems (mixtures of NaOH, LiOH, KOH, $Ba(OH)_2$ and $Sr(OH)_2$, and RbOH), and fused-salt systems (fluorides and chlorides). In the latter group, there are 88 individual systems, involving, for the most part, mixtures that have been prominent in fused-salt-reactor development programs. Fluorides such as NaF, LiF, KF, RbF, BeF_2, ZrF_4, UF_4, and ThF_4 ap-

pear as constituents in a majority of the systems described. (J. H. Stang)

Zirconium-Water Reactions

At Argonne[17,18] the experimental program to determine rates of reaction of molten zirconium with water is continuing. The experimental method involves the rapid melting and dispersion of zirconium wires in a water or steam environment by a surge current from a bank of condensers.

In this work a system of equations has been developed to describe the process whereby hot spherical particles simultaneously react, undergo self-heating, and eventually cool to room temperature. The reaction at the surface was assumed to follow the parabolic rate law, previously found by Battelle to apply approximately.

An analog computer was used to solve the equations, and the solutions were compared with specific experimental results. Various values (constant for each simulated run) of the convective heat-transfer coefficient, surface emissivity, and reaction activation energy were checked to determine the "best" values. A convective heat-transfer coefficient of 92 Btu/(hr)(sq ft)(°F) and a surface emissivity of 1.00 were found to be consistent with the experimental data. The heat-transfer coefficient is also consistent with standard correlations.

Although the results with regard to activation energy are inconclusive (see Fig. 5), a minimum value of 28 kcal/mole is considered appropriate. However, the tentative rate constants are approximately twice those previously reported by Battelle, as shown in Table IV-1.

(A. W. Lemmon, Jr.)

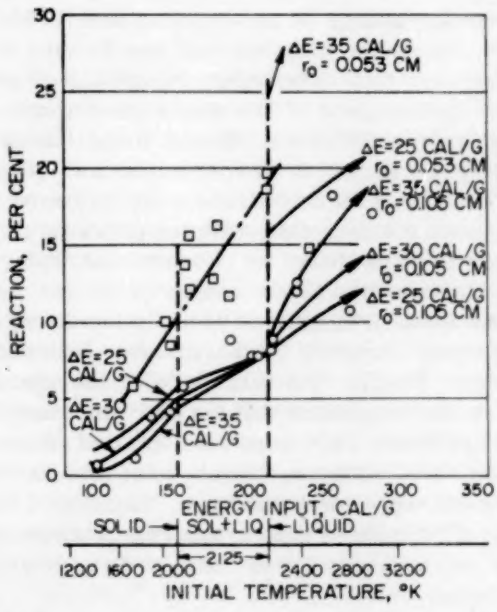

Figure 5 — Comparison of computed and experimental results for zirconium-water reaction by condenser-discharge method.[18] Experimental: ○, 60-mil wire; □— - — , 30-mil wire. Computed: ——.

Table IV-1 COMPARISON OF REACTION RATE CONSTANTS[17]

E, kcal/mole	Parabolic rate constant, $g^2/(cm^4)(sec)$
35	0.00029
30	0.00033
25	0.00035
34*	0.00015*

*Experimental results previously reported by Battelle.

Radiation Effects in Nonfuel Materials

Basic Studies

Small-angle X-ray scattering (SAS) has been used for the investigation of local inhomogeneities in the electron density of a solid on a scale large in comparison with the average interatomic distances, as in studies of the size of submicroscopic particles and the clustering of atoms in solid solution. When applied, however, to fluctuations of lesser amplitude, such as defects in deformed or irradiated pure metals, the results are ambiguous because of the phenomenon of double Bragg reflection (DBR). The present status of SAS was summarized in a conference[19–28] in which a number of authors demonstrated, with remarkable agreement, the existence of DBR and the conditions by which it may mask the weak SAS. These papers will not be reviewed individually; it is only important to note here that SAS can be used for the study of fine-scale lattice imperfections only under special conditions where parasitic DBR can be eliminated. Thus in polycrystalline or very distorted single-crystal specimens the detection of very weak SAS is uncertain. This uncertainty is borne out in the previously reported SAS experiments of Atkinson et al.[28] on neutron-irradiated

copper. Another possibility is the elimination of the primary Bragg reflection by the use of radiation of wavelength greater than the Bragg "cutoff" wavelength of the specimen; this can be accomplished by the method of cold-neutron scattering. Atkinson[23] described such measurements on deformed aluminum and copper, in which small but apparently significant SAS was found, equivalent to a dislocation density of the order of 10^{10} to 10^{11} per square centimeter, consistent with the values obtained by other methods.

Corbett and Walker[29] presented data on the energy dependence of recovery in electron-irradiated high-purity copper, using resistance measurements. The shifts in population of the recovery stages I_A-I_E were measured as a function of bombarding electron energy. The total fraction of recovery in the first three substages increased with decreasing energy at the expense of the higher temperature substages. These data were interpreted as additional confirmation of the proposed model, previously reported, in which I_A, I_B, and I_C represent close-pair recovery and I_D and I_E are due to free diffusion of radiation-induced interstitials. Thus at lower incident energies the interstitials are simply not knocked as far into the lattice.

Sosin and Brinkman[30] have studied the kinetics of recovery of cold-worked nickel and nickel irradiated with 1.25-Mev electrons at 90°K using resistivity measurements at liquid-helium temperature. They report the occurrence of recovery stages near 100°C (Stage III) and 270°C (Stage IV) by a diffusion process following cold work; the defect sinks are believed to be dislocations. Following irradiation, Stage III obeyed a second-order chemical-rate equation; but Stage IV was nearly absent. The activation energy for Stage III was found to be about 1.05 ev for both irradiation and cold work, and it was concluded that the defect migrating in Stage III is an interstitial, and in Stage IV, a vacancy.

Tucker and Webb,[31] using studies of electrical resistivity in electron-irradiated aluminum–2 at.% copper alloy at −60°C, showed that mobile irradiation defects can enhance the low-temperature clustering of copper atoms. This "cold-hardening" process is of interest because it proceeds with an activation energy of 0.5 ev, whereas the activation energy for diffusion of copper in aluminum is 1.4 ev. Since electron irradiation introduces point defects (interstitials and vacancies) which are mobile in the temperature range −80 to −40°C, the present results are consistent with the vacancy mechanism of enhanced diffusion of copper in the alloy.

Hanford[32] reported data on lattice expansion, X-ray line breadth, and hardness of commercial molybdenum irradiated at 35°C with fast-neutron exposures up to 1.2×10^{20} nvt. The curve of lattice constant vs. exposure maximized near 5×10^{19} nvt and showed a net decrease from the preirradiated value at 1.2×10^{20}. Both the line breadth and hardness increased, the latter approaching a limiting value. The results were interpreted as follows: interstitials are mobile at 35°C and, in initial stages, are trapped by impurity atoms (whose concentration is high in commercial molybdenum) and, to a lesser extent, are annihilated at vacancy sites. For exposures above 10^{19} nvt the trapped interstitials are sites for growth of interstitial clusters, causing an increase in hardness and line breadth but a decrease in lattice constant.

Bettis[33] reported measurement of fission-fragment recoil range in zirconium (containing 492 ppm U^{235}), obtaining the values 10.1 and 8.15 μ, respectively, for heavy ($M \approx 138$) and light ($M \approx 96$) masses.

Annealing kinetics of irradiated aluminum and copper exposed to fast neutrons below 50°K are reported by Oak Ridge.[34] The present work was undertaken to explain the apparent anomaly in earlier finding of an annealing peak at 30 to 50°K, in which only one-half the defects annealed out; this observation is difficult to explain on the basis of the single mechanism of close-pair annihilation. Blewitt found that annealing occurred at temperatures as low as 7.2°K and that the activation energy for recovery increased monotonically with temperature. The discrete steps found by Corbett and Walker[6] for electron-irradiated copper were not apparent here. It is difficult to apply the theory of close-pair recovery (with a discrete activation energy). Finally, the magnitude of the energy led to the conclusion that the activation energy is a spectrum. Data were also obtained on zinc, silver, and platinum, which were similar to those for copper and aluminum. The stored energy of irradiated copper was redetermined as 0.19 cal/mole for 4×10^{17} nvt, confirming earlier data.

Also described are resistivity studies[34] of a series of fast-neutron-irradiated alloys exposed at 40°C: (1) copper–15 at.% aluminum, a terminal solid-solution alloy; (2) nickel–15 at.%

beryllium, a substitutional precipitation alloy; and (3) nickel–28 at.% copper, a continuous solid-solution alloy. In the first alloy, a decrease in resistance with irradiation was found, as previously reported, but with an accompanying decrease in specific volume. This suggests that irradiation tends to eliminate a metastable condition in the alloy. In the second alloy, no significant change in resistivity, hardness, or Curie temperature occurred during aging of alloys, nor was re-solution observed. However, irradiation prior to aging enhanced the initial precipitation, probably due to increased nucleation. For the third alloy, irradiation produced an increase in Curie temperature and a decrease in resistivity consistent with removal of copper from solid solution, and evidence of enhanced diffusion approaching the equilibrium state of segregation of copper.

Oak Ridge[15] attempted to investigate the mechanism of the effect of radiation on the gaseous oxidation of niobium (380 to 450°C for 1 to 6 hr at $\sim 10^{12}$ nv) and zirconium (450 to 500°C for 2 hr). Electron and light microscopical studies revealed no differences between irradiated and control samples in the time to initiate blister cracks, in the blister density, and in the rate of film growth. However, calculations indicate that a flux of 10^{15} to 10^{16} nv would be needed to change the oxidation rate significantly as a result of an increase in defect concentration.

The ionization produced in diamond by passage of fast electrons was investigated by Kennedy,[35] who found the mean energy per ion pair to be 20 ev, independent of the energy of the primary electron. This value is higher than a previously accepted value (10 ev). A theory is proposed, involving degradation of the primary energy by interaction with valence electrons of the crystal, in which the mean energy per ion depends not only on the width of the forbidden gap (about 5.6 ev from the optical absorption limit) but also on the position of the maximum in the density of states curve within the valence band (about 10 ev below top of band); adding 2 ev for the mean value of secondary-electron energy, the mean energy is about 18 ev, in good agreement with the observation.

Gilman,[36] by microscopical examination of etched lithium fluoride crystals subjected to short stress pulses, has presented evidence that various heterogeneities can induce nucleation of dislocations: (1) cleavage steps, (2) dislocation loops, (3) glide bands, (4) inclusions, and (5) radiation-induced precipitates. From these observations it is concluded that relatively little dislocation multiplication results from classical Frank-Read sources; instead, multiplication occurs during motion of a prior dislocation through a crystal.

Howard and Smoluchowski[37] have considered the mechanism of formation of interstitials in alkali halides by ionizing radiation; specifically, halogen-ion interstitials, for whose presence experimental evidence was recently obtained. The Varley mechanism of production of multiply-ionized halogen ions was evaluated from the point of view of lifetime, activation energy of motion among interstitial sites, and stability.

A theoretical paper on focusing collisions in a displacement spike in a face-centered-cubic lattice was given by Leibfried,[38] in an attempt to explain the experimentally found long range of the cascade from the primary knock-on. He used the model of Silsbee, with results showing that the range should be determined by focusing collisions without interstitial transport rather than by crowdion collisions.

A review of the effects of irradiation on metals is given by Seitz.[39] Piercy[40] has presented results of the effect of fast-neutron irradiation of superpurity aluminum-magnesium alloys (0.001 to 2.8 wt.% magnesium) on the tensile properties. Recovery of the elastic limit of superpurity aluminum occurred in two steps: (1) near 120°C, with an activation energy of 0.9 ev and (2) at 160°C, requiring 1.7 ev; for the alloys, only one stage was observed at 200°C, with an activation energy of 2.4 ev. These results are interpreted as being due to agglomeration of magnesium-vacancy pairs forming stacking faults.

Nickel foil, fast-neutron irradiated to an integrated flux of 10^{19}, was deformed about 2 per cent and examined by transmission in the electron microscope.[41] The photographs showed tangles of dislocations and loops, interpreted as being the result of interaction of dislocations with irradiation-produced vacancy clusters.

Wittels and Sherrill[42] show, on the basis of X-ray-diffraction data, that, contrary to their earlier results, monoclinic ZrO_2 is stable under fast-neutron bombardment. The observed change to cubic ZrO_2, previously reported, is due to a fission-fragment spike mechanism from fissile impurities. (C. M. Schwartz)

Effects of Irradiation on Mechanical Properties

The effect of neutron irradiation on the Charpy V-notch impact properties of steels is being investigated at Oak Ridge.[34] Eight steels (ASTM A-200 T, A-212 B, A-285 A, A-301 B, A-302 B, Swedish 2112, Corriloy T-1, and high-purity iron–0.18 carbon) were irradiated at doses up to 1×10^{20} neutrons(>1 Mev)/cm^2 at temperatures of 175 to 330°F. All these steels showed similar rises in impact transition temperature and decreases in ductile-energy absorption. Figure 6 indicates that the transition-temperature increase is highly dependent on the logarithm of the dose, provided it is above about 10^{18} neutrons(>1 Mev)/cm^2. The results, with two exceptions, fall in a narrow scatter band. Item 60 represents the Corriloy T-1 high-strength steel, and item 111 represents the vacuum-melted high-purity iron-carbon alloy. At 7×10^{18} neutrons(>1 Mev)/cm^2 the latter showed a smaller increase in transition temperature than did the commercial steels. Therefore, it appears that metal purity has a considerable effect on the response to irradiation and that there is hope of improving properties of irradiated steels by control of alloy composition. The shift in transition temperature for many of the steels measured by subsize Izod impact tests is somewhat different from the Charpy data of Fig. 6. Subsize Izod data indicate a slightly greater increase at about 2×10^{18} and a smaller increase as 1×10^{20} neutrons (>1 Mev)/cm^2. The decrease in shape is attributed to the large geometry differences between the two types of specimens. A plot similar to Fig. 6 is obtained for the drop in energy absorption above the transition temperature as a function of the dose.

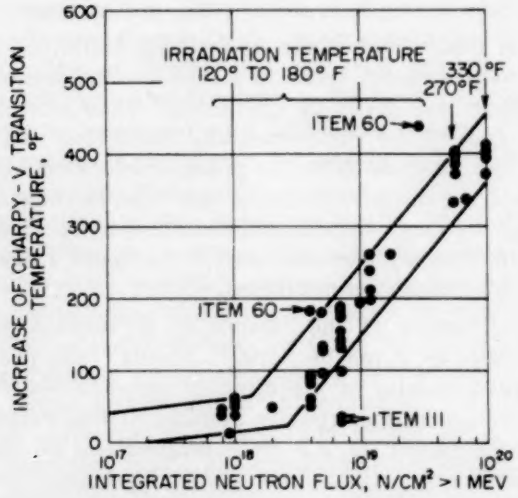

Figure 6—Effect of fast-neutron irradiation on Charpy-V impact transition temperatures of several steels.[34]

Work at Bettis[43] indicates that the Charpy V-notch transition temperatures of various steels may be raised by as much as 200°F by irradiations of 2 to 4×10^{18} neutrons(>0.4 ev)/cm^2 at temperatures of 400 to 650°F. The results are listed in Table IV-2. It appears that for a given flux the higher irradiation temperature results in less damage.

The effect of neutron irradiation on the mechanical properties of Zircaloy-2 has been investigated further. Du Pont[44] showed that the tensile strength, yield strength, and hardness were increased; the ductility was decreased; and the elastic modulus was unchanged after a dose of 2.7×10^{20} fast neutrons/cm^2 at a temperature under 100°C. (B. C. Allen)

Table IV-2 EFFECT OF IRRADIATION ON IMPACT PROPERTIES OF VARIOUS STEELS[43]

Steel	Integrated flux, 10^{18} neutrons(> 0.4 ev)/cm^2	Irradiation temp., °F	Change in Charpy V-notch transition temp., °F
HY-65	2	500	+200
HY-65	3	650	0
AISI 410, hardened and tempered	3	400	+75
AISI 410 with 0.13 carbon, annealed	3	600–650	+40
AISI 410 with 0.06 carbon, annealed	3	600–650	−50
AISI 410 centrifugally cast, annealed	3	650	+10
A-212	4	500	+100
A-302	2	500	+50
A-302	4	650	+50

Selected Mechanical Properties of Cladding and Structural Materials

Zirconium and Zirconium Alloys

The creep properties of reactor-grade zirconium have been determined by Japanese investigators[45] in 1000-hr creep tests at temperatures from 250 to 500°C. Stress levels investigated include 11,400, 17,100, 22,800, and 28,500 psi. All tests were conducted in an argon atmosphere. The creep rates obtained were from 8×10^{-5}%/hr to 34%/hr, depending on the stress and temperature employed.

Studies have also been made in Japan[46] of the effect of aluminum, tin, and molybdenum additions to zirconium. The influence of the alloying elements was evaluated on the basis of hot-hardness tests. Binary alloys were prepared by nonconsumable-electrode arc melting in an argon furnace, and the hot hardness was investigated. It was found that about 3.0 wt.% tin or 4.0 wt.% molybdenum is needed to improve the strength of zirconium at elevated temperatures. A 2.0 wt.% aluminum addition hardens zirconium more than do the other addition elements investigated. For temperatures less than 400°C, molybdenum is the best strengthener, whereas, for temperatures greater than 600°C, aluminum is the most effective strengthener. Heat-treatment of these alloys has influenced hot-hardness values as follows: Alloys harden less when quenched from high alpha temperatures than when slow cooled from the same temperature; however, they harden more when quenched from the beta temperature than when slow cooled. The hot-hardness of slow-cooled alloys decreases with increasing temperature; but, when the zirconium-molybdenum alloys are quenched from 900°C, they exhibit abnormal hardness values between 300 and 400°C. It appears that these abnormal hardnesses are related to precipitation of the ω in the β phase, as reported by H. A. Robinson et al.

(F. R. Shober)

Zircaloy-2

A summary of the results of work done at Hanford with respect to the effects of hydrogen on the tensile properties of Zircaloy-2 is presented[47] for the temperature range from room temperature to 400°C. Hydrogen levels covered are from 10 to 5000 ppm. The ultimate tensile strength, 0.2 per cent offset yield strength, total elongation, reduction of area, and proportional limit were determined as functions of test temperature.

The ultimate strength was influenced only slightly by additions of hydrogen up to 1000 ppm. Additions greater than 2000 ppm decreased the ultimate strength at room temperature but increased the high-temperature strength. The yield strength at room temperature was depressed by hydrogen concentrations less than 2000 ppm. Increasing the hydrogen concentration depressed the reduction-of-area values at all temperatures investigated, but it was more effective at lower temperatures. There was a complete loss of ductility at room temperature and 100°C for material containing 5000 ppm hydrogen. At 300 and 400°C there appeared to be no loss of ductility as measured by total elongation. It also appeared that changes in properties with temperature were more pronounced for Zircaloy-2 having hydrogen concentrations of 2000 ppm or greater.

A pressure-test evaluation of Zircaloy-2 tubing was made by Bettis[48] prior to the construction of the first PWR blanket. Test conditions included normal hydraulic loading, dynamic hydraulic loading, cyclic (fatigue) loading, and creep loading. Evaluations were made as a function of fuel clearance, wall thickness, fabrication processes, crack-arrestor dimensions, and heat-treatment. The burst strengths were influenced significantly but not greatly by the fabrication process, rate of loading, and the presence of notches. Crack arrestors were not successful, and hydraulic shock resulting from failure was not serious. Fractures, in some instances, were extensive enough to allow whole fuel compacts to fall out of the rod and to allow the lips of the fracture to contact adjacent rods. The results were helpful in establishing specifications for dimensional tolerances, cold-work requirements, and processing schedules.

Hydrostatic pressure tests were conducted at Hanford[49] on Zircaloy-2 tubing to obtain design data for the NPR (New Production Reactor) and the PRTR (Plutonium Recycle Test Reactor). It was found that Zircaloy-2 tubes have a higher ultimate strength than was predicted on the basis of tensile data from Zircaloy-2 strip. Zircaloy-2 tubing in the fully annealed and in the as-extruded, 5 to 17.8 per cent cold-worked, condition fails in a ductile manner at 300°C

when internal pressure is applied. Examination of failures indicated a shear mode of fracture.

In studies[50,51] of the strength and deflection characteristics of simulated square Zircaloy-2 oxide fuel compartments, base-annealed Zircaloy-2 diaphragms 0.02 to 0.025 in. thick were loaded with argon gas pressure, and the center deflection was measured. Three types of data were obtained: (1) the cladding pressure-deflection characteristics in the elastic range and the pressure required to rupture a compartment, (2) the cladding creep at various pressure loadings at both room and reactor-operating temperature, and (3) the volume-deflection characteristics of the deformed cladding dome during plastic straining.

The extent to which increasing amounts of cold work improve the creep properties of Zircaloy-2 and the effects of recovery which occurs at test temperatures are being determined at Hanford[13] for 15, 25, and 45 per cent cold-worked Zircaloy-2. The 25 and 45 per cent cold-worked materials, being tested at 400°C at 13,000 and 18,000 psi, respectively, show no indication of third-stage creep after 3000 hr.

Similar studies are being performed at Battelle[3-5] on Zircaloy-2 sheet in both the annealed and cold-worked conditions (15 per cent) at temperatures of 290, 345, and 400°C. Tests are being conducted in vacuum for as long as 15,000 hr. Results from tests on annealed material show that very little creep occurs at 290 and 345°C, even at loads approaching the short-time rupture strength. A substantial strain is evident on loading (approximately 4 per cent), followed by a period of constant creep rate, 0.0001%/hr. At 400°C the creep deformation becomes significant. Cold-worked Zircaloy-2 exhibits considerably improved creep properties over those of the annealed material at all temperatures. For equivalent stresses the average creep rate of the cold-worked Zircaloy-2 is about one-tenth that of annealed material at 290, 345, and 400°C. More creep deformation is apparent for Zircaloy-2 tested under cyclic temperature conditions than that for material at equivalent stresses in isothermal tests. The effect is more pronounced at 345°C and appears to be stress dependent at this temperature. The effect of a 750°F steam atmosphere on the creep properties of annealed Zircaloy-2 is also being investigated.

Knolls workers[52] have reviewed the creep data for Zircaloy-2 and have expressed its behavior at temperatures from 800 to 1200°F in mathematical form. The equations take into account recovery and strain hardening, and otherwise conform to known behavior characteristics. They have been developed for use in machine calculations of swelling of dispersion fuels, relating temperature, fission-gas pressure, and relaxation characteristics of the matrix alloy.

(F. R. Shober)

Niobium

As part of an evaluation of selected niobium-base alloys for service in pressurized-water reactors,[3,4] Battelle workers measured the strengths of several alloys at 1200 and 1500°F. The tensile ductilities of alloys containing large ternary additions of vanadium and zirconium or titanium and chromium are quite low. Ternary alloys of lower alloy content show appreciable ductility and moderate strength at 1500°F. Of the binary alloys tested at 1500°F, the best combination of strength and ductility was obtained in the 1.6 at.% vanadium alloy.

On the basis of experimental data on ultimate tensile strength, yield strength, elongation, and hardness for cast, forged, and recrystallized niobium, the Russians[53] found that all properties except elongation increase with oxygen content. The tensile properties of high-purity niobium were determined by the British[54] over the temperature range −196 to 240°C. Yield points were observed at all temperatures. The temperature dependence of the yield stress was similar to that of other body-centered-cubic metals, and the niobium was ductile to −196°C. Results of some experiments on strain aging suggest that oxygen is responsible for the observed yielding and for the return of yield point on aging.

(F. R. Shober)

Stainless Steel and Other Alloys

The yield strengths of types 304, 304L, 316, and 317 seamless stainless-steel tubing were determined by Bettis[55,56] at various temperatures. The results are shown graphically in Fig. 7. The collapse properties of the tubing showed that 12-in. tubes tend to collapse more readily than 6-in. tubes. It would appear that the long-term collapse tests, 24 hr or greater, are more significant than the short-time tests for evaluating collapse strength of tubing. Seven type 347 seamless stainless-steel tubes, brazed for 4 hr at 1875°F, were run 168 hr at 2500 psi

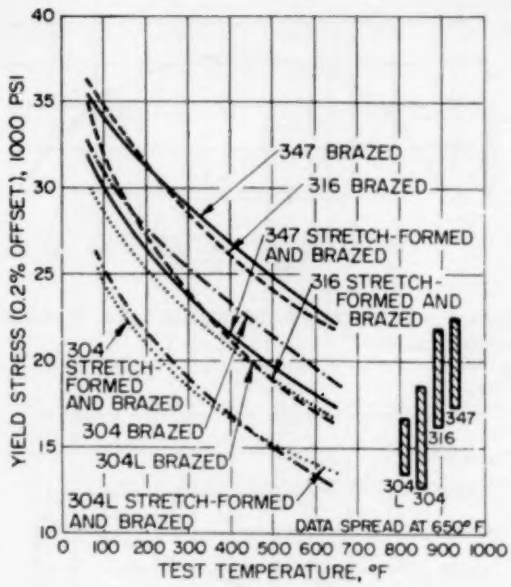

Figure 7 — Yield strengths of several austenitic stainless steels.[55]

and 668°F without collapse. The effect of phosphorus in the brazing alloy (nickel – 9 wt.% phosphorus) on the ductility of stainless-steel tubing was also investigated. The most severely affected tube still had about 15.7 per cent elongation, as compared with approximately 35 per cent for control specimens. The tests indicate that the phosphorus diffusion lowers the ductility of stainless steels.

The Charpy-V mid-energy transition temperatures of a series of iron-chromium alloys, containing up to 24.3 wt.% chromium, and of three series of iron-chromium-aluminum alloys, containing up to 25 wt.% chromium and 6 wt.% aluminum, have been determined at the Naval Research Laboratory[57] for several conditions of mechanical working and heat-treatment. The fracture mode below the transition temperature was invariably transgranular. Transition temperatures of the iron-chromium alloys decreased with increasing chromium content when the alloys had been quenched from 1650°F and increased with increasing chromium content when the alloys were slowly cooled from 1650°F. The effects are not readily explained by the known embrittling mechanisms: 885°F embrittlement and sigma-phase embrittlement. Alloys containing about 0.5 wt.% aluminum had significantly lower transition temperatures than corresponding alloys without aluminum. Alloys containing about 5 wt.% aluminum had higher transition temperatures than those without aluminum. Manganese contents of up to 12.8 wt.% appeared to have no beneficial effect on transition temperatures of the iron-chromium-aluminum alloys, whereas titanium additions up to 1.92 wt.% raised the transition temperature.

At Lewis Research Center[58] the tensile properties of commercial tungsten at 2500 to 4400°F have been measured. Test specimens were prepared from ½-in.-diameter swaged rod. Although a decrease in ductility was noted for specimens tested above 2500°F, an appreciable amount of ductility still existed up to 4400°F. The ultimate tensile strengths at 3500, 4075, and 4400°F are 10,600, 6500, and 4400 psi, respectively. (F. R. Shober)

Selected Metallurgical Aspects of Cladding and Structural Materials

Aluminum-Silicon System

The Naval Research Laboratory,[59] working with the aluminum-silicon system, reports that aluminum and silicon form a simple eutectic (577.2°C, 12.7 wt.% silicon); however, this eutectic structure is abnormal. These investigations reveal that the dendritic form of primary alpha phase is unaltered by changes in growth condition; however, the usual complex idiomorphic form of the silicon phase was transformed to the dendritic form when growth occurred in a supersaturated liquid. Eutectic silicon plates, which have been observed to grow from primary silicon particles, dominate the eutectic transformation and, by branching, restrict the growth of the eutectic alpha phase. This mode of solidification produces fine eutectic colonies in this abnormal eutectic structure. (J. A. DeMastry)

Iron-Chromium Alloys

Russian investigators[60] have performed electroconductivity, hardness, and microscopic analyses of the triangle sections of chromium-iron, manganese-nickel alloy system. They have established phase diagrams showing the distribution of alpha, alpha + gamma, gamma, and sigma-phase areas in the iron angle of the cross section. (J. A. DeMastry)

Niobium Alloys

Oak Ridge reports[15] on the results of a study of twinning and cleavage in niobium single crystals that were cut from ingots of electron-beam-melted niobium. At −196°C deformation twins were produced by both impact loading and slow compression. The twin plane is of the {1 1 2} family, and the twin direction is of the ⟨1 1 $\bar{1}$⟩ family. Only {1 0 0} cleavage occurs at −196°C. It is indicated that relief of stresses at the tips of twins in niobium takes place by slip rather than by kinking or crack formation.

The United Kingdom[61] has published computed values of internal energy, constant-volume specific heat, and linear expansion coefficient for niobium in the range from 60 to 1200°K, as shown in Table IV-3. (J. A. DeMastry)

Table IV-3 SOME THERMAL PROPERTIES[61] OF NIOBIUM IN THE RANGE 60 TO 1200°K

Temp., °K	$E = \int_0^T C_v\,dT$, cal/mole	Specific heat at constant volume (C_v), cal/(mole)(°K)	Linear thermal-expansion coefficient, 10^{-6}/°K
60	59.586	2.82	3.216
100	208.96	4.43	5.075
200	721.00	5.51	6.418
300	1287.00	5.57	6.823
400	1866.40	5.84	7.061
500	2452.50	5.68	7.250
600	3042.60	5.90	7.420
700	3633.00	5.92	7.594
800	4224.80	5.93	7.764
900	4818.60	5.93	7.923
1000	5413.00	5.93	8.089
1100	6007.10	5.94	8.275
1200	6600.00	5.94	8.449

Vanadium-Chromium System

Ames[62] reports that the vanadium-chromium alloy system consists of a series of complete solid solutions. A minimum was noted in the solidus at 70 wt.% chromium and 1750°C, and no intermediate phases were found at the temperatures investigated. Figure 8 is a plot of the hardness of vanadium-chromium alloys.

(J. A. DeMastry)

Yttrium

General Electric has presented phase diagrams for the systems yttrium-chromium, yttrium-iron, and yttrium-nickel. These are shown in Figs. 9 to 11, respectively.

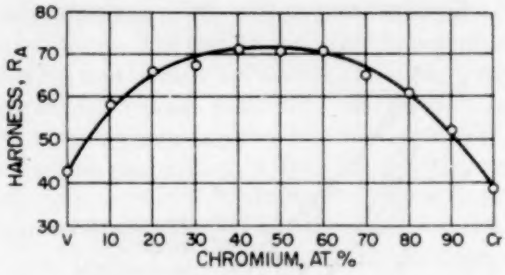

Figure 8—Hardness vs. composition for vanadium-chromium alloys.[62]

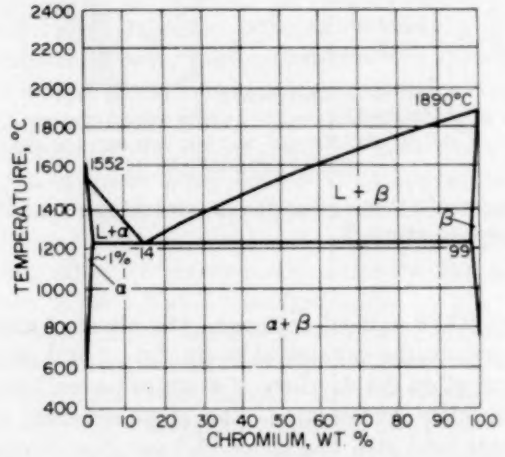

Figure 9—Phase diagram for the binary system yttrium-chromium as determined by Denver Research Institute.

The solid solubility of yttrium in iron–20 to 40 wt.% chromium alloys was found by Battelle workers[63] to be extremely small. Maximum solubility occurs near the solidus temperature, 1320°C, and is approximately 0.12 wt.% yttrium. However, yttrium solubility decreases rapidly with decreasing temperature, and at 600°C the solubility is below 0.05 wt.% yttrium. In general, it is apparent that yttrium solubility increases slightly with chromium content, all other factors being constant.

The presence of YFe_5 was established, and a eutectic between YFe_5 and iron was noted at 1257°C. An intermetallic compound, believed to be YFe_4, was found.

The constitution of iron–20 to 40 wt.% chromium-yttrium alloys containing less than 6 wt.% yttrium was studied between 1250 and

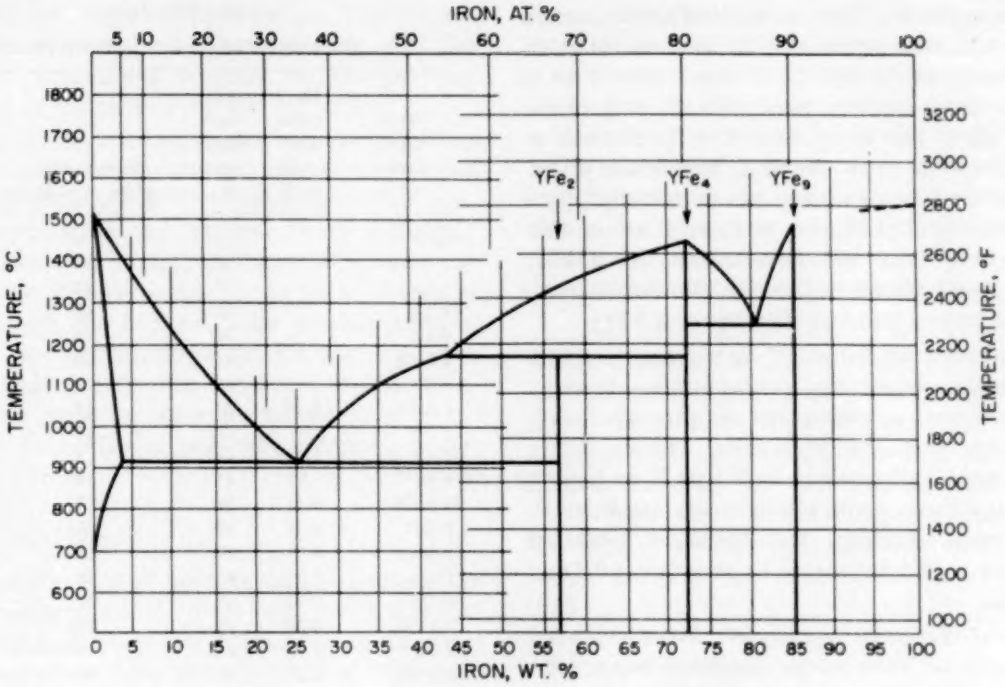

Figure 10 — Tentative phase relations, yttrium-iron system.

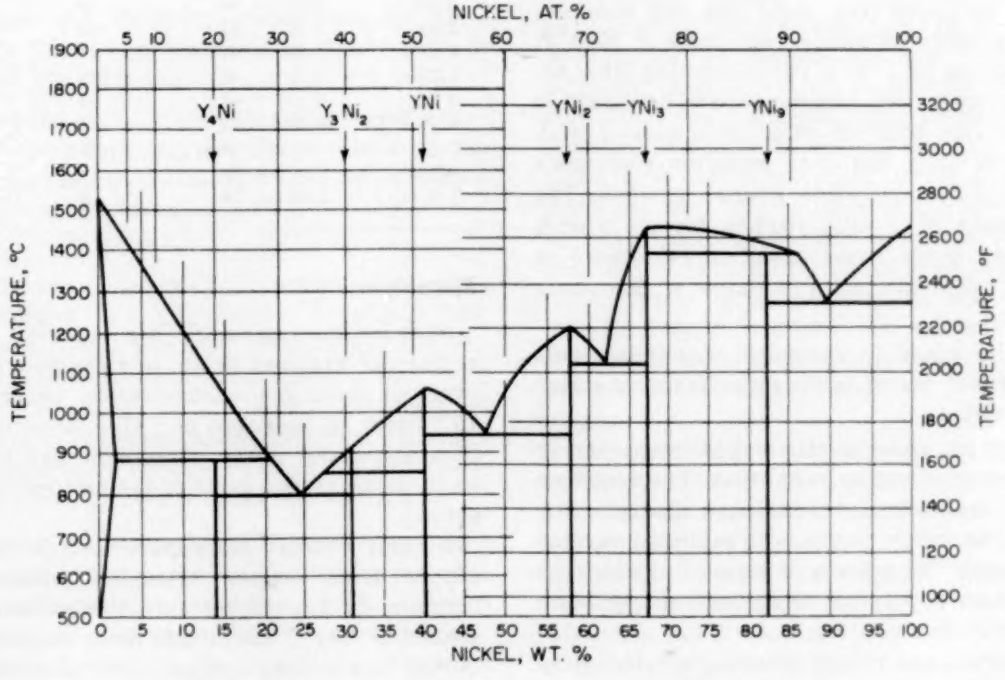

Figure 11 — Tentative phase relations, yttrium-nickel system.

600°C. It was found that, when the solubility limit is exceeded, YFe_5 is formed and occurs in conjunction with alpha iron-chromium. At about 900°C and above 815°C, if more than 6 wt.% yttrium is present in the iron–35 wt.% chromium alloy and more than 3 wt.% yttrium is present in the iron–40 wt.% chromium alloy, YFe_4 forms to give a three-phase field of alpha + YFe_5 + YFe_4. The upper yttrium limit of this phase field was not determined. At 815°C, sigma phase forms in the iron-chromium system and comes into equilibrium with YFe_5.

Other work at Battelle[64] was concerned with the solubility of yttrium and the lanthanide rare-earth elements in chromium and chromium–10, –25, –50, and –75 wt.% iron. The solubility limits were estimated to be 0.1 wt.% or less in the base alloy at room temperature and 2300°F. Dysprosium, erbium, and holmium exhibited solubility limits estimated to be between 0.1 and 0.3 wt.%.

General Electric personnel[65] have reported work done on rare-earth additions to ferrous and nonferrous alloys. They state that, although there is only slight solubility of the rare earths in the iron-chromium system, the rare earths have large effects on iron-chromium alloys. These effects are probably due to scavenging effects on impurities. AISI type 446 stainless steel has good oxidation resistance at 2000°F. The addition of 1 wt.% yttrium to this alloy allows the operating temperature to be raised to 2500°F. The iron–25 wt.% chromium–5 wt.% aluminum alloy has good oxidation resistance at 2300°F but becomes coarse grained. The substitution of 1 wt.% yttrium for the 5 wt.% aluminum gives equal oxidation resistance at 2300°F, and the alloy retains a fine-grain structure.

Yttrium added to austenitic stainless steels has no effect except in the high chromium stainless steels.

Chromium absorbs nitrogen at temperatures above red heat and is embrittled. The additions of rare earths limit the nitrogen absorption by forming an oxide that is not readily penetrated by nitrogen. The effects of rare-earth additions on nitrogen absorption in chromium are shown in Table IV-4.

Approximately 1 wt.% addition of yttrium to vanadium allows production of ingots that are readily fabricable. The yttrium acts as a scavenger for oxygen. (J. A. DeMastry)

Table IV-4 EFFECT OF RARE-EARTH ADDITIONS[65] TO CHROMIUM

(Data Were Taken At 2300°F for 100 Hr)

Rare earth added, wt.%	Rare earth analyzed, wt.%	As-cast hardness, R_A	Weight gain, mg/(sq in.)(100 hr)	N_2 absorption, ppm
Unalloyed Cr	0	39	185	16,500
1 La		37	22	2,400
2 La		35	55	1,820
4 La		36	88	1,850
0.5 Ce		42	30	220
2 Ce		36	30	170
0.5 Pr	0.03	39	15	650
1 Pr		39	15	
2 Pr	1.71	42	8	30
4 Pr		41	38	
0.5 Nd	0.11	38	15	1,170
2 Nd	0.75	40	8	280
1 Sm	0.01	42	22	1,170
2 Sm	0.02	41	20	1,040
5 Sm	0.02	42	22	1,112
0.5 Gd	0.50	38	15	430
2 Gd	1.85	41	8	230
0.5 Dy	0.11	41	66	1,090
1 Dy		40	37	
2 Dy	0.75	41	15	1,170
4 Dy		40	8	
6 Dy	1.95	42	22	1,480
1 Ho	0.45	40	24	580
2 Ho	1.26	40	15	150
0.5 Er	0.03	41	30	1,250
2 Er	1.22	42	12	300
5 Er	3.38	41	8	60
1 Tm	0.12	40	140	850
2 Tm	0.16	42	90	1,990
2 Yb	0.03	43	45	900
1 Lu		39	9	900
0.5 Y		39	15	110
1 Y	0.66	39	8	160

Zirconium

Atomics International[66] has reported that, if a thermal gradient exists in zirconium and the over-all hydrogen concentration exceeds 4×10^{-4} atom of hydrogen per atom of zirconium, then a weaker phase zirconium hydride will form at the cooler parts of the zirconium component.

Nuclear Metals[67] has experienced diffusion of copper from copper extrusion jackets into Zircaloy-2. The jacket extrusion billets were soaked at 800°C for 30 min prior to extrusion. During this soaking a copper-zirconium interaction layer about $^2/_3$ mil thick was formed. Copper had diffused inward from this layer, and successive layers of metal were etched away to de-

termine the depth of penetration. The copper content decreased with each etching until the original Zircaloy-2 content of 33 ppm was reached at 4½ mils below the surface.

Hanford[8] is working on the recovery kinetics of zirconium. Analyses of data revealed that there is considerable softening before recrystallization begins and that this "work softening" is at least a three-step process. When recrystallization finally begins, it is by a nucleation and growth mechanism. This microstructural change is accompanied by further softening and is characterized by a variable activation energy. An equation to express the rate of recovery in terms of per cent recovery at any time is given. (J. A. DeMastry)

Zirconium Alloys

The differences[68] in free energy between the body-centered-cubic (bcc) and the hexagonal close-packed (hcp) modifications of titanium and zirconium have been calculated between 0 and 2000°K by using existing thermodynamic data. These results have been employed to investigate the energetics of the bcc ⇌ hcp reaction in the titanium-zirconium system and in a series of titanium-base alloy systems. It is found that the chemical driving force for martensitic bcc ⇌ hcp reactions in these systems is about 50 cal/mole.

Oak Ridge[15] reports on the aging transformation of zirconium-niobium alloys. The work was performed on zirconium-niobium single crystals aged at temperatures to 600°C. The results obtained are shown below.

Phase Transitions. (1) Successive aging of an as-quenched 15 wt.% niobium crystal at 250, 400, and 500°C partially transformed the retained body-centered-cubic beta phase to a metastable omega lattice, which then reverted to virtually the as-quenched condition. (2) Critical temperature for reversion of this alloy composition was located between 400 and 500°C.

Results of Examination of Room-temperature Diffraction Patterns at Various Stages of These Aging Treatments (400, 500, 600°C). (1) A crystal aged 360 hr at 400°C showed only diffractions of the four omega lattice orientations obtainable from an original beta grain and those of a niobium-enriched residual beta lattice. (2) An as-quenched crystal, aged a total of 96 hr at 500°C, passed through two distinct transition stages. The first, an omega formation, occurred in the first hour of aging. The second stage was a discontinuous precipitation of hexagonal alpha and niobium-rich beta phases from a beta matrix. (3) A crystal aged 524 hr at 600°C gave diffractions characteristic of a continuous, oriented precipitate of the hexagonal alpha phase from a beta matrix. (4) The most significant effect of in-pile irradiation to 10^{21} nvt at 85°C is to accelerate the formation of omega.

Aging of Beta-quenched 25 and 33 Wt.% Niobium Crystals at 325 and 425°C. (1) Omega precipitation in the 25 wt.% alloy, first observed after 168 hr at 250°C, proceeds at 325°C with a gradual niobium enrichment of the residual beta phase. Re-aging at 425°C produces a partial reversion, which is not complete after 20 hr. (2) Omega precipitation in the 33 wt.% niobium alloy is first observed after aging 48 hr at 325°C. (J. A. DeMastry)

Diffusion Studies

Results concerning research on the absorption of noncollimated radiation in the experimental measurement of diffusion by tracer technique were reported by Princeton University.[69] In addition, results of investigation of oxides and the effect of pores and cracks on the kinetics of oxidation, as well as the role of defects in oxide and sulfide crystals on conductivity, diffusion, and scale growth, were presented. The variation of self-diffusivity in the Curie point of alpha iron was determined at 980 to 1167°K, using the Fe^{55} tracer. Data on the iron-nickel-oxygen equilibria and the course of oxidation reaction of iron-nickel alloys are given, in addition to data on the metal sulfide equilibria for PbS-Pb, WS_2-W, and Rh_8S_7-Rh systems. A brief account of work in progress is also included, along with references, equipment diagrams, and graphs.

A paper written by the French[70] deals with different methods in use at present for studying both general self-diffusion and intergranular self-diffusion with the use of radioactive isotopes. The various absorption methods for studying general self-diffusion are examined, each one being illustrated by a specific example. The more limited methods for studying intergranular self-diffusion are also included.

The self-diffusion coefficient of niobium was measured at Sylvania Electric[71] over the temperature range 1535 to 2120°C, using the radio-

active isotope Nb^{95} as the tracer. The data for the temperature dependence of the self-diffusion coefficient are best fitted by the equation $D = (12.4 \pm 0.2) \exp[(-105{,}000 \pm 3000)/RT]$ cm²/sec.

The diffusion rates of aluminum, magnesium, silicon, and zirconium, alloyed as single additives in nickel, were measured at the Bell Telephone Laboratories[72] at temperatures between 800 and 970°C. The method consisted of measuring the weight gain caused by surface oxidation of the additive in a wet-hydrogen ambient. The surface oxides were identified by electron diffraction. The composite volume and grain-boundary diffusion coefficients are given by

$$D_{Al \rightarrow Ni} = 1.1 \exp(-59{,}500/RT)$$

$$D_{Mg \rightarrow Ni} = 2.3 \times 10^{-5} \exp(-31{,}300/RT)$$

$$D_{Si \rightarrow Ni} = 10.6 \exp(-64{,}800/RT)$$

$$D_{Zr \rightarrow Ni} = 1 \times 10^{-5} \exp(-26{,}700/RT)$$

Photomicrographs indicated considerable grain-boundary diffusion, particularly in magnesium-nickel and zirconium-nickel.

The results of an investigation of the diffusion of silicon in tantalum, titanium, iron, and molybdenum are reported by the Russians.[73] An equation describing the relative change in weight of samples at a given temperature and saturation time is derived. The results of measurements of layer thicknesses, phase layers, and microhardness are tabulated. The activation energy and constants for the change of the diffusion coefficient with temperature are also tabulated.

Work on the determination of Fe^{55} and Fe^{59} diffusion rates in copper and silver is continuing at the University of Illinois.[74] Difficulty in specimen preparation after radiochemical isotope separation is a major problem. Coefficients are presented for diffusion in silver at 793 to 945°C. The effects of pressure on the mobility of quenched vacancies in gold were studied by measuring the relative rates of excess resistivity annealing at two or more temperatures. Measurements of the effects of pressure on stress relaxation in the oxygen-vanadium system were made, and data on relaxation time as a function of pressure in vanadium are tabulated. Construction of equipment and preliminary measurements, at atmospheric pressure, on the effect of pressure on ionic conductivity in pure and doped alkali halides are reported. Preliminary measurements of anelastic relaxation in silver-zinc were obtained in an investigation of the effect of plastic deformation on diffusion. Iron oxidation structures are reported for single-crystal whiskers; correlation of oxidation nuclei with dislocation structure is difficult, and a study is being directed toward oxidation while the crystal is under stress. Oxidation at grain boundaries was studied, as well as hydrogen reduction of the oxide. (M. A. Gedwill, Jr.)

References

1. O. Zmeskal and M. L. Brey, Study of the Films Formed on Zirconium-Niobium Alloys in Oxygen Atmospheres, USAEC Report ORO-204, June 1959.
2. R. H. Hiltz, "Some X-ray Observations on the Oxidation Characteristics of Binary Niobium Alloys," Proceedings of the Seventh Annual Conference on Industrial Applications of X-ray Analysis, University of Denver, Denver (1959).
3. R. W. Dayton and C. R. Tipton, Jr., Progress Relating to Civilian Applications During September 1959, USAEC Report BMI-1381, Oct. 1, 1959.
4. R. W. Dayton and C. R. Tipton, Jr., Progress Relating to Civilian Applications During October 1959, USAEC Report BMI-1391, Nov. 1, 1959. (Classified)
5. R. W. Dayton and C. R. Tipton, Jr., Progress Relating to Civilian Applications During November 1959, USAEC Report BMI-1398, Dec. 1, 1959. (Classified)
6. Bettis Technical Review: Reactor Metallurgy, USAEC Report WAPD-BT-15, September 1959.
7. H. A. Porte et al., Oxidation of Zirconium and Zirconium Alloys, USAEC Report ANL-6046, September 1959.
8. F. W. Albaugh, Reactor and Fuels Research and Development Operation Monthly Report for November 1959, USAEC Report HW-62899A, Dec. 15, 1959. (Classified)
9. N. J. Gioseffi and H. E. Kline, Behavior of Structural Materials Exposed to an Organic-moderated Reactor Environment, USAEC Report NAA-SR-2570, Oct. 1, 1959.
10. Henry Suss, Chromium Electroplates for Corrosion Protection of Stressed AISI 410 in High-temperature High-purity Water, USAEC Report KAPL-M-HOS-8, Sept. 4, 1959.
11. J. Sannier et al., Oxidation of Two Refractory Alloys at 900 and 1100°C, *Journal of Nuclear Materials*, 1(3): 213–225 (October 1959).
12. A. H. Peters, Erosion of Magnesium, USAEC Report DP-377, June 1959.
13. F. W. Albaugh, Reactor and Fuels Research and Development Operation Monthly Report for September 1959, USAEC Report HW-62012A, Oct. 15, 1959. (Classified)
14. J. W. Seifert, Liquid Metal Fuel Reactor Experiment; Corrosion Resistance of Mo–0.5 Wt.%

Titanium Alloy, Tantalum, and Beryllium in Liquid Bismuth, USAEC Report BAW-1067, May 14, 1959.
15. Metallurgy Division Annual Progress Report for Period Ending September 1, 1959, USAEC Report ORNL-2839, Dec. 16, 1959.
16. R. E. Thoma (Ed.), Phase Diagrams of Nuclear Reactor Materials, USAEC Report ORNL-2548, Nov. 20, 1959.
17. Chemical Engineering Division Summary Report for April, May, and June 1959, USAEC Report ANL-6029, September 1959.
18. Chemical Engineering Division Summary Report for July, August, and September 1959, USAEC Report ANL-6068, 1959.
19. A. Guinier, Small-angle Scattering Meeting: Summarizing Remarks, *Journal of Applied Physics*, 30(5): 601 (May 1959).
20. R. H. Neynaber et al., On the Mechanism of the Small-angle X-ray Scattering from Cold-worked Metals, *Journal of Applied Physics*, 30(5): 656 (May 1959).
21. A. Guinier and E. Guyon, Internal Double Reflection in a Perfect Crystal, *Journal of Applied Physics*, 30(5): 622 (May 1959).
22. Alfred K. Seeger, Small-angle Scattering from Dislocations in Deformed Single Crystals, *Journal of Applied Physics*, 30(5): 629 (May 1959).
23. H. H. Atkinson, Small-angle Scattering of X-rays and Neutrons from Deformed Metals, *Journal of Applied Physics*, 30(5): 637 (May 1959).
24. K. Thomas and A. Franks, Study of X-ray Scattering from Fatigued Metals, *Journal of Applied Physics*, 30(5): 649 (May 1959).
25. W. H. Robinson and R. Smoluchowski, Small-angle Scattering of X-rays by Plastically Deformed Single Crystals, *Journal of Applied Physics*, 30(5): 617 (May 1959).
26. H. Fricke and V. Gerold, Experiments on Double Bragg Reflections in Deformed and Undeformed Metal Foils, *Journal of Applied Physics*, 30(5): 661 (May 1959).
27. R. E. Smallman and K. H. Westmacott, Structure of Quenched and Irradiated Metals, *Journal of Applied Physics*, 30(5): 603 (May 1959).
28. H. H. Atkinson et al., Small-angle Scattering of X-rays from Neutron-irradiated Copper, *Journal of Applied Physics*, 30(5): 646 (May 1959).
29. J. W. Corbett and R. M. Walker, Energy Dependence of Recovery in Irradiated Copper, *The Physical Review*, 115(1): 67 (July 1, 1959).
30. A. Sosin and J. A. Brinkman, Electrical Resistivity Recovery in Cold-worked Electron-irradiated Nickel, *Acta Metallurgica*, 7(7): 481 (July 1959).
31. C. W. Tucker, Jr., and M. B. Webb, Electron Irradiation of Aluminum-Copper Alloys, *Acta Metallurgica*, 7(3): 187 (March 1959).
32. D. L. Gray and W. V. Cummings, Jr., An X-ray Diffraction Study of Irradiated Molybdenum, USAEC Report HW-60907, July 1, 1959.
33. E. R. Smith and P. W. Frank, Recoil Range of Fission Fragments in Zirconium, USAEC Report WAPD-TM-198, November 1959.
34. Solid State Division Annual Progress Report for Period Ending August 31, 1959, USAEC Report ORNL-2829, Dec. 11, 1959.
35. P. J. Kennedy, Ionization Effects Produced in Diamonds Subjected to Monoenergetic Beta-ray Bombardment, *Proceedings of the Royal Society (London)*, A253(1272): 37 (November 1959).
36. J. J. Gilman, Dislocation Sources in Crystals, *Journal of Applied Physics*, 30(10): 1584–1594 (October 1959).
37. R. E. Howard and R. Smoluchowski, Formation of Interstitials in Alkali Halides by Ionizing Radiation, *The Physical Review*, 116(2): 314 (Oct. 15, 1959).
38. G. Leibfried, Correlated Collisions in a Displacement Spike, *Journal of Applied Physics*, 30(9): 1388 (September 1959).
39. F. Seitz, The Effects of Irradiation upon Metals, *Transactions of the American Institute of Mining, Metallurgical, and Petroleum Engineers*, 215: 354–367 (June 1959).
40. G. R. Piercy, Irradiation Effects in Super Purity Aluminum Magnesium Alloys, Canadian Report CRMet-821 (AECL-810), April 1959.
41. H. G. F. Wilsdorf, Nature of Radiation Damage in Nickel, *Physical Review Letters*, 3(4): 172–173 (Aug. 15, 1959).
42. M. C. Wittels and F. A. Sherrill, Fission Fragment Damage in Zirconia, *Physical Review Letters*, 3(4): 176–177 (Aug. 15, 1959).
43. Materials Department Technical Progress Report for the Period June 26 to September 25, 1959, USAEC Report WAPD-MRK-3. (Classified)
44. L. Isakoff, comp., Heavy-water-moderated Power Reactors Progress Report for August 1959, USAEC Report DP-415, October 1959.
45. Hideharu Ohara, Creep of Zirconium, *Nippon Kinzoku Gakkai-Shi*, 22: 250–253 (May 1958).
46. Effect of Aluminum, Tin, and Molybdenum on the Hot Hardness of Zirconium, *Nippon Kinzoku Gakkai-Shi*, 22: 367–370 (July 1958).
47. H. H. Burton, Hydrogen Effects on Zircaloy-2 Tensile Properties, USAEC Report HW-61077, July 10, 1959.
48. L. F. Cochrun, Pressure Testing of Zircaloy Tubing, USAEC Report WAPD-216, October 1959.
49. V. E. Kahle, Interim Report on the Hydrostatic Destructive Testing of Zircaloy-2 Pressure Tubing, USAEC Report HW-61272(Rev.), Oct. 15, 1959.
50. E. A. Davis, Creep and Deflection Tests on Zircaloy-2 Diaphragms, Report NP-7788, Westinghouse Electric Corporation, Dec. 30, 1958.
51. Review and Evaluation of "Creep and Deflection Tests on Zircaloy Diaphragms," USAEC Report WAPD-PWR-(RD2)-369, May 1959.
52. J. D. Lubahn, The Creep Behavior of Zircaloy-2, USAEC Report KAPL-M-JDL-1, June 12, 1959.
53. G. V. Zakharova et al., Use and Properties of Niobium, *Tsvetnye Metally*, 1: 73-79 (1959).

54. B. F. Dyson et al., The Tensile Properties of High-purity Niobium at Low Temperatures, *Journal of the Institute of Metals*, 87: 340–342 (June 1959).
55. H. E. Walchli, Quarterly Progress Report for the Period January 1 to March 31, 1959, USAEC Report YAEC-125, May 15, 1959.
56. H. E. Walchli, Quarterly Progress Report for the Period April 1 to June 30, 1959, USAEC Report YAEC-161, Aug. 15, 1959.
57. J. E. Srawley, Charpy-V Transition Temperatures of Ferritic Iron Alloys. Part II. Iron-Chromium and Iron-Chromium-Aluminum, Report NRL-5367, Aug. 24, 1959.
58. Paul F. Sikora and Robert W. Hall, High-temperature Tensile Properties of Wrought Sintered Tungsten, Report NASA-TN-D-79, September 1959.
59. R. A. Meussner, The Structure of Aluminum-Silicon Alloys, Report NRL-5341, May 19, 1959.
60. I. I. Kornilon and L. E. Kantnovich, Investigation of Fe-Cr and Ni-Mn Quadrupole System, *Izvestiya Akademii Nauk SSSR, Otdelenie Khimicheskikh Nauk*, 6: 963–970 (June 1959).
61. On the Coefficients of Linear Thermal Expansion of Pure Niobium Between 60 and 1200°K, British Report IGR-TM/D-073, February 1958.
62. O. N. Carlson and A. L. Eustice, Vanadium-Chromium Alloy System, USAEC Report IS-47, November 1959.
63. M. S. Farkas and A. A. Bauer, The Solid Solubility and Constitution of Yttrium in Iron–20 to 40 Wt% Chromium Alloys, USAEC Report BMI-1386, Oct. 20, 1959.
64. S. G. Epstein et al., Solubility Limits of Yttrium and the Lanthanide Rare-earth Elements in Chromium and Chromium-Iron Alloys, USAEC Report BMI-1376, Sept. 1, 1959.
65. J. F. Collins et al., Applications of Rare Earths to Ferrous and Nonferrous Alloys, USAEC Report AECU-4424, Nov. 2, 1959.
66. G. G. Libowitz, Effect of a Thermal Gradient on the Hydrogen Distribution in a Metal; Application to the Sodium Reactor Experiment, USAEC Report NAA-SR-4194, Dec. 1, 1959.
67. S. Isserow et al., Progress Report to E. I. du Pont de Nemours & Company for the Period April 1 to April 30, 1959, USAEC Report NMI-4393, Aug. 14, 1959.
68. L. Kaufman, The Lattice Stability of Metals Titanium and Zirconium, *Acta Metallurgica*, 7(8): 575–578 (August 1959).
69. The Oxidation of Metals and Alloys: Final Report for the Period September 1, 1953 to December 31, 1958, U. S. Air Force Report AFOSR-TR-59-43, James Forrestal Research Center.
70. C. Leymonie and P. LaCombe, Methods of Studying Self-diffusion in Metals by Means of Radioisotopes, *International Journal of Applied Radiation and Isotopes*, 5: 175–196 (May 1959).
71. R. Resnick et al., The Self-diffusion of Niobium. III. Final Progress Report for July 1, 1958 to January 1, 1959, USAEC Report SEP-252, Mar. 30, 1959.
72. H. W. Allison and H. Samelson, Diffusion of Aluminum, Magnesium, Silicon, and Zirconium in Nickel, *Journal of Applied Physics*, 30: 1419–1424 (September 1959).
73. G. V. Samsonov and M. S. Koval'Chenko, An Investigation of the Diffusion of Silicon in Certain Transitional Metals (in Russian), *Inzhenerno-Fizicheskiĭ Zhurnal, Akademii Nauk Belorusskoĭ SSR*, No. 3, 62–67 (March 1959).
74. David Lazarus, Diffusion in Metals: Progress Report and Publication List, USAEC Report AECU-4186, June 1, 1959.

Melting, Casting, Heat-Treatment, and Hot Working

National Lead of Ohio (NLO), operator of the AEC's Feed Materials Production Center, has recently completed a large plant-scale investigation of the effects of mold heating on vacuum-induction-melted ingot quality. It was noted that both process yields (per cent of fabricated slug weight to uranium charge weight) and good slug to total slug yields were increased, and the carbon and nitrogen contents were decreased. However, the importance and effectiveness of mold heating in realizing these improvements depended upon the remelt cycle used (length of time cycle, power input, and induction-coil position).[1] Incidentally, this same mold heating has reduced the ingot mold life because of the failure of the MgO mold wash. Subsequently, a successful development of techniques to flame spray magnesium zirconate ($MgZrO_3$) onto the interior surface of the ingot molds was concluded. Under heated-mold conditions, flame-sprayed molds had $2\frac{1}{2}$ times the life of molds coated with magnesia wash.[2]

A study of the factors affecting the soundness of NLO uranium ingots was made by Battelle.[3] In a two-year study recently concluded and reported, a mathematical model that describes the heat flow during solidification was devised and solved utilizing a digital computer. Contributing to the studies were experiments that described accurately the temperatures at various locations within the solidifying ingot and other experiments that described the time of gap formation at the mold-metal interface. Analysis of the results of the mathematical model indicated (experimentally confirmed in the case of superheat) that variations in pour time, superheat, mold preheat, and outer-mold-wall emissivity had little effect on the formation of center-line voids for the size of mold and casting being used. The use of the mathematical model for a more complete evaluation of the existing casting parameters and the application of the analytical technique to other materials and casting processes are envisioned.

In the continuing quest for metal quality improvement, NLO has been studying the consumable-electrode vacuum arc melting of uranium and has evaluated the fuel slugs fabricated from the ingots produced.[1,2] Vacuum-induction-melted reactor-grade uranium ingots were arc melted and recast to ingots $8\frac{1}{2}$ and $13\frac{1}{2}$ in. in diameter. Various fabrication procedures (rolling or alpha extrusion to 7 in. in diameter and extrusion or rolling to final rod fuel diameter) were used to reduce the ingots to fuel-slug rod stock which was then evaluated in terms of metal quality and process yields. The results were clouded by variations introduced by the undetermined starting metal quality, different ingot diameters, fabrication difficulties, and expediencies in the specific melting practices. However, arc-melted ingots, $8\frac{1}{2}$ in. in diameter, rolled to rod form, were of excellent quality, and slug yields were sufficiently high to justify the conclusion that the arc-melting technique could be used with no increase in slug cost.

Nuclear Metals has applied an old art in a fresh approach to the fabrication of round, hollow fuel slugs.[4] In this case a small-diameter central hole was formed in place in a Zircaloy-clad unalloyed fuel slug by melting and centrifuging. Two advantages were sought for the product and the technique:

1. The placement of a void at the center of a fuel element to accommodate fission gases formed during irradiation
2. The use of the technique to effect the removal of fission gases in nondestructive fuel-element reprocessing

From the test results, it was concluded that:

1. The centrifuging method is feasible and practical for holes $\frac{1}{16}$ to $\frac{1}{32}$ in. in diameter.
2. An axial hole in the end cap does not permit the escape of molten metal from the rotating slug. These results would require checking

if large amounts of fission gases were being released.

3. With Zircaloy as the cladding the reprocessing step could be repeated a number of times since its solution is slow at the temperature proposed. However, accelerated attack of the Zircaloy end caps was noted and would have to be corrected before repeated melting would be possible.

4. With appropriate bearing support the method could be used for long rods.

5. The creation of the hole from the volume created by stretching the cladding requires further study. The method as developed depends upon "built-in" voids near slug ends.

6. Centrifugal force can be used to rid uranium of inclusions present in the liquid by their rejection to the center axis where they can be removed physically.

Bettis also reported[5] on the results of studies of the properties of skull type arc-melted and cast Zircaloy-2 shapes. In these studies the properties of cast extension brackets were found to compare favorably with the properties of wrought and welded extension brackets. Close dimensional control was attained in that internal square-wall dimensions were held to within 0.005 in. in 11 of 12 castings. Surface finishes of approximately 250 μin. rms were measured. The welding, corrosion, and strength properties of the cast shapes were satisfactory when compared with reactor-grade Zircaloy-2 wrought material. The grain size of the castings was about ASTM No. 1, and the grain structure was transformed beta with the usual amount of grain-boundary precipitate.

The importance of melting practices in the preparation of nickel- and iron-base high-temperature alloys has been cited recently by a number of investigators. In particular, the effect of impurities introduced with the charge, the reaction of alloying additions with the crucible, the type of crucible used, and the melting method were all found to be important in the properties of specific alloys.

Decker et al.[6,7] at the University of Michigan have studied variations caused by various melting practices in the hot workability and creep-rupture properties of the 55 wt.% nickel–20 wt.% chromium–15 wt.% cobalt–4 wt.% molybdenum–3 wt.% titanium–2 wt.% aluminum alloy. Most important in this work was the observation that the pickup of boron and zirconium by the alloy, resulting from reaction with the crucible during vacuum melting, improved the hot fabricability and creep-rupture properties. The species of impurity picked up by the alloy depended upon the type of crucible used, e.g., boron was picked up from magnesia crucibles found to contain boron compounds, and zirconium was found in alloys melted in zirconia crucibles. No improvement in properties of alloys melted in alumina was noted, and no pickup of boron or zirconium was detected.

In deliberate additions the level of boron and zirconium was found to be more important than the method of melting (vacuum arc, vacuum induction, or air induction), which explains some of the variance of results that has been reported in the literature on vacuum-melted materials. In fact, it was necessary to have small quantities of either boron or zirconium in the alloy before it exhibited properties thought to be characteristic.

Vacuum melting did improve the fabrication qualities, as manifested by improved surface and reduced edge cracking, and gave more uniform properties within heats. Creep rupture was slightly improved at low boron and zirconium contents in vacuum melts; but, at high levels of boron and zirconium, air heats were better.

As would be expected, the method of melting also affected inclusion and impurity content, which in turn affected workability and creep-rupture properties. The opportunity for impurities to separate also varied with melting method, being greater for the vacuum-melted material.

Structurally the role of zirconium, boron, and zirconium combined with boron in improving creep-rupture properties was to retard deterioration of the structure at grain boundaries. Optimum properties were realized by deliberate, simultaneous additions of both boron and zirconium, suggesting beneficial interaction effects. Excessive amounts were detrimental.

The importance of melting practices was also cited by General Electric[8] and Battelle.[9] In the preparation of iron-base alloys containing yttrium by vacuum-induction melting at Battelle, the tendency of this alloy addition to react with the crucible and with impurities in the charge was most pronounced. Reaction with alumina crucibles was sufficient to limit the recovery of the yttrium addition to about 50 per cent at temperatures in the 2900 to

3000°F range. Additions of sulfur as FeS and oxygen as FeO lowered the yttrium recovery. However, neither these nor other additions (carbon, up to 0.08 wt.%; manganese, 0.25 wt.%; and palladium, 1.0 wt.%) had significant effects on the fabrication (forging and rolling at 2000°F) of 1-lb ingots. The excellent fabrication qualities of the master alloy, containing 2 wt.% yttrium and made from high-purity material to which all impurity additions were made, suggest that other parameters, such as structure, ingot size, and combinations of impurities, may cause the troubles observed in production-size ingots.

The effect of melting methods on the qualities of refractory metals and materials has been the subject of studies by Mallory-Sharon.[10–13] In melting beryllium, a duplex melting cycle (vacuum-arc melting followed by electron-beam melting) was used. It was found that the double melting reduced cracking and improved soundness and that the electron-beam melting method affected the ductility of the extruded and annealed sheet produced from the ingots. Longer melt holding times improved ductility, but it was still low by normal standards. Chromium content was reduced by electron-beam melting, but the improvement in ductility is not attributed to this specific impurity. Titanium carbide and zirconium diboride were both melted by the electron-beam method, but with little success because of titanium and boron losses attributed to their vapor pressures. Boron was also melted by electron beam, but it was still very brittle.

Nuclear Metals has been conducting work over the past years relating to the extrusion of bare, large (2 to 3 in. in diameter, ¼ in. in wall thickness) uranium tubes. Their conclusions[14] are as follows:

1. Satisfactory results are obtained in high-alpha (1100 to 1200°F) extrusion, whereas gamma extrusion gives poor dimensional tolerances.

2. To obtain acceptable surfaces on extruded tubes, a fine-grain structure should be present in the starting stock. This grain refinement can be obtained in a number of ways: alpha working by hammer forging, press forging, or preextrusion; or a triple beta-quench heat-treatment.

3. Coating of the uranium is required to reduce oxidation losses and to facilitate separation from extrusion dies. Of the materials tested, molten salts cause surface gouges; iron, 30 to 40 mils thick, causes striated surfaces; electroplated copper, suitably applied to an 8- to 10-mil thickness, gives satisfactory results.

4. Postextrusion heat-treatment is required to obtain random orientation. High-alpha extruded tubes have pronounced (1 1 0) texture.

5. Although the as-extruded tubes have dimensional tolerances near specification, beta treating results in detrimental dimensional changes.

6. Tube reducing can be used to form extruded tubes to very close dimensional tolerances. However, on subsequent beta treatment, the detrimental dimensional changes are no less than those observed for as-extruded tubes.

7. A satisfactory structure can be obtained by a beta treatment consisting of heating vertically in a salt bath, followed by an air quench.

A promising lower-temperature (700°F) reduction by extrusion of small-diameter heavier-wall tubes was accomplished at Bridgeport Brass Company.[15] The as-extruded tubes had tolerances very near those desired. Metallographic and X-ray diffraction examinations showed that the resulting structure was typically cold worked with a pronounced orientation. This orientation was completely removed by a single beta heat-treatment.

The fabrication of heavy-walled uranium tubes on an Assel Mill (three work rolls impinge on a hollow billet containing a mandrel as it moves through the mill) was successfully demonstrated by NLO at the Westinghouse Electric Corporation fabrication site at Bloomfield, N. J.[2] Hollow billets in the as-cast, beta-treated, and machined condition and in the as-extruded condition were subjected to reductions in area of from 44 to 63 per cent at temperatures of 950 to 1200°F. In almost all cases the eccentricity of the starting pieces was reduced; and, in some cases, it was reduced by two-thirds. No cracks were visible after the initial reductions; inside surfaces were good, although the outside surfaces were of poor quality due to slippage of the mill and consequent local heating. Metallographic examinations revealed that some sections of the tubes had recrystallized.

It has been noted that the rapid quenching of uranium from the beta phase causes a preferred orientation in the resulting structure, the degree of preferred orientation varying with the thermal gradients present during the beta-to-alpha

transformation.[16] Two heat-treatment studies have been in progress at NLO and Bridgeport Brass to study this phenomenon further.[17,18]

The NLO study involved quenching media with varying cooling rates. Of particular interest was the use of oils with cooling rates intermediate between those of water and molten tin. Information from the limited program indicates that oil is a promising quenching medium.

Bridgeport Brass has been engaged in a program of broader scope in that it sought to provide standard uranium macro and microstructure data from which the uranium heating history could be determined. Jominy end-quench tests were used since they provide a variety of cooling rates through the end quenching. Although this specific end quench was not used for hardenability studies, it was very useful in obtaining a large amount of data from a small amount of material. Although the results fell short of the stated objective, they provided the basis for the following clarifying conclusions.

1. The identification of phases and the interpretation of phase transformation remain difficult, even with metallographic standards as guides.
2. Macrostructures provide a favorable guide to the origin of the quenched phase and the degree of quenching.
3. Grain sizes provide some indication of the cooling conditions employed.
4. Twinning concentrations in grain boundaries are not conclusive in determining the origin of the quenched phase or the degree of quenching.
5. Subgrains are more prevalent in beta-treated uranium than in gamma-treated uranium.
6. Hardness profiles are of little assistance in interpretation of heat-treatment conditions.

(E. L. Foster)

Cladding

Cladding by Rolling, Swaging, and Stretch Forming

The fabrication of fuel elements by roll bonding, swaging, and stretch forming is being investigated in an attempt to produce better fuel systems more economically. A marked decrease in the emphasis on cladding by roll bonding can be observed, with the shift in emphasis to UO_2 and high-strength fuels.

An investigation has been initiated at Oak Ridge[19] to evaluate rotary swaging as a technique for producing dense UO_2 rods intimately clad with stainless steel. This process consists merely of pouring the UO_2 powder into a tube that is end capped and swaged to the desired reduction in cross-sectional area. The process, if feasible, would greatly decrease the cost involved in the conventional fabrication of this type of element by cold pressing and sintering of UO_2 pellets which have to be carefully sized to fit into a stainless-steel sheath.

Emphasis has been placed on a parametric study to determine the effects of the type of UO_2, total reduction, swaging temperature, and particle size on the swaged density of UO_2 in type 304 stainless-steel tubing. High-fired, fused and ground, and ceramic oxides were swaged to determine which materials would swage to the highest density. It was found that fused and ground UO_2 cold swages to the highest density, 91 per cent of theoretical, at a reduction in area of approximately 55 per cent. Rod-milled high-fired UO_2 swages to 85 per cent of theoretical density at a similar reduction. Ceramic grades of UO_2, used for making cold-pressed and sintered pellets, swage to densities less than 75 per cent of theoretical under similar conditions and are considered unsuitable for use in swaged fuel rods. It was determined that the swageable grades of UO_2 are characterized by high-tapped bulk density and low surface area.

Examination of swaged UO_2 fuel elements revealed that hot-swaged powders decrease in total surface area with increasing total reductions, indicating that actual bonding occurs between particles. Oxides that are cold swaged exhibit increased total surface area with increased total reductions. This suggests that particle fragmentation and densification of a purely mechanical nature occur.

Cladding-thickness variations in rods swaged to moderate reductions are only of the order of 5 per cent; however, hot swaging and cold swaging to reductions in excess of 70 per cent may produce wall-thickness variations of as great as 14 per cent.

Initial experiments on swaging of tubular fuel elements at the Savannah River Laboratory[20] in a two-die swager were unsuccessful. Several

difficulties were encountered in cladding UO_2 with stainless steel in the two-die swager. These included wrinkling of the inner sheath, sticking of the mandrel in the tube, and ellipticity of the fabricated element. A series of tests conducted at the Fenn Company indicated, however, that a four-die swager was more favorable for the fabrication of tubular-shaped elements than was a two-die swager. The four-die swager is currently being used to compact UO_2 by cold swaging. Zircaloy-clad elements containing fused oxide will be prepared in this manner. This type of oxide had exhibited the best cold-compaction properties in an earlier study.

The Zircaloy-clad natural-UO_2 fuel elements to be produced at Savannah River Laboratory by cold swaging will be suitable for use in the Du Pont design of a D_2O-cooled and -moderated power reactor.[21] This is based on recent studies in which fused UO_2 was clad with stainless steel by swaging, with a resultant UO_2 density of 92 per cent, with stainless-steel sheaths of 0.020, 0.014, and 0.007 in. in thickness. Similar results were obtained with a Zircaloy sheath 0.022 in. thick. The maximum density was obtained with area reductions of 40 to 50 per cent. Further reductions produced thinning of the Zircaloy sheath with no increase in density. Hot-swaged Mallinckrodt UO_2 at 650°C produced densities of 80 per cent, and similar UO_2 was cold swaged to a density of 70 to 75 per cent.

Hanford[22] has successfully produced a large-scale Zircaloy-clad UO_2 fuel element by swaging. This element, 9 ft in length and 0.570 in. in diameter, was clad with 0.030 in. of Zircaloy. The final swaged density was 87 per cent of theoretical.

The concept of a swaged UO_2 fuel element that is reinforced with metallic fibers promises to offer an element with improved thermal conductivity and mechanical-strength properties. The Martin Company[23] is currently producing fuel-element specimens of this type for thermal-conductivity measurements.

Westinghouse[24] has been investigating the fabrication of stainless-steel-clad sintered UO_2 fuel rods, 90 in. in length, by swaging, stretch forming, and compartmenting by stretch forming. In the first instance, UO_2 pellets are loaded into a tube, and the clearance between the tube and fuel is reduced to 0 to 2 mils by cold swaging. Granular pellet fracture resulted from the cold swaging of the fuel rods; consequently, this process was not felt to be as feasible as stretch forming. Stretch forming reduced pellet fragmentation; however, some cracks were observed in the oxide during the slight necking down of the tubing during stretch forming. To better understand this process, studies of work-hardening characteristics and of spring-back properties and flow properties of stainless steel were made. A combination of vertical and horizontal stretch forming of the cladding produced the most desirable results. It was determined that assembly tolerances were critical in preventing large discrepancies in gap uniformity between the pellets. If the stretch-formed fuel element is heated while supported vertically, the fuel pellets shift toward the bottom end, and the fuel-element spacing obtained by stretch forming is lost; consequently, this process would not be desirable for fuel elements positioned in this manner.

Compartmented stretch forming of this type of fuel element was attempted by inserting a stainless-steel disk between every 8-in. stack of pellets. This spacing was further controlled by applying pressure to position firmly the fuel pellets during the stretching of the cladding. Results obtained during this study revealed that nonuniform spacing of compartments would be obtained in stretch forming full-length Yankee type fuel rods. In addition, this problem with spacing would result in excessively high scrap losses of the rejected fuel rods. (E. S. Hodge)

Pressure Bonding

A process involving the use of gas pressure at elevated temperatures is being utilized for the bonding and joining of reactor components and for the densification of ceramic, cermet, and dispersion fuels. This same process has been identified by several names such as gas-pressure bonding, isostatic bonding, pneumastatic bonding, and hydrostatic bonding. The components to be bonded are fabricated to desired final dimensions and are either welded to form a gastight assembly or sealed in a gastight metallic envelope. The process is dependent on differential gas pressure to bring the components into intimate contact. Bonding is usually accomplished above the recrystallization temperature of the metallic components, at a temperature at which the metal is plastic and extensive diffusion can occur.

The factors that affect the pressure-bonding process are being investigated by Battelle.[25–27]

For this study the process has been arbitrarily divided into three basic steps, namely, (1) formation of the bond interface by forcing the mating surfaces into intimate contact, (2) removal of excess voids or vacancies from the bond interface, and (3) growth of grains across the bond interface. The initial studies have been concerned with the solid-phase bonding of OFHC copper. An attempt is being made to isolate each step of the bonding cycle and to determine the mechanism and kinetics of the process.

Uranium slugs have been clad with Zircaloy-2 at 1550°F utilizing a helium-gas pressure of 10,000 psi. Examination of the bonded fuel elements by Hanford[28] has revealed complete bonding between the Zircaloy-2 cladding and uranium and the Zircaloy-2 end plugs, with the exception of minute localized spots exhibiting surface contamination. The Zircaloy-2 cladding had flowed into all defected areas.

Hot-die pressing and gas-pressure bonding have been evaluated by Atomics International[29] for the preparation of the OMR flat-plate fuel plates. The fuel plates consist of a low-enrichment uranium-alloy fuel plate clad with finned aluminum. The gas-pressure-bonding process was found to be best. Bonding was achieved with a gas pressure of 8000 to 10,000 psi at 850 to 1000°F for a period of 10 min.

Sylvania-Corning[30] is investigating the use of the gas-pressure-bonding process for the simultaneous densification and cladding of UO_2 fuel elements. The best results have been obtained with a mixture of ceramic and fused UO_2 powder. Relatively high cold-pressed densities were obtained; and, upon subsequent pressure bonding, additional densification was obtained with a minimum amount of cladding distortion. An investigation has been made to obtain comparable results with one grade of UO_2 in an attempt to simplify the process. Several process variables were investigated; however, in all tests the pressure-bonded density was lower than was achieved with the oxide mixture.

Battelle[25-27] is also investigating the use of the gas-pressure-bonding process for simultaneous densification and cladding of ceramic, cermet, and dispersion fuels with the prime objective of reducing fabrication costs. The cold compaction and densification of seven commercial grades of oxide have been investigated. The oxide has been utilized in the as-received condition to maintain low process costs. In order to minimize cladding distortion during pressure bonding, an attempt is being made to obtain maximum cold-pressed densities. Variables such as particle size, use of binder, blending of oxide types, and stoichiometry are being investigated. Tamp-packed densities up to 70 per cent and cold-pressed densities up to 87 per cent of theoretical have been obtained. Pressure bonding has been conducted at 2100°F at 10,000 psi. As-bonded densities have ranged from 84 to 97 per cent of theoretical. The studies include flat-plate, tubular, rod, and corrugated fuel-element designs.

The solid-phase bonding of niobium and molybdenum is being investigated.[25-27] A satisfactory bonding process has been developed for niobium. It includes surface treatment with a nitric acid solution, followed by bonding at 2100°F at 10,000 psi for 3 hr. A fuel assembly consisting of three niobium-clad compartmented fuel plates was bonded from piece components in one operation. Inserts of UO_2-Al_2O_3 were used to form the channels; and, after bonding, these inserts were leached with acid. Examination and testing of the assembly revealed good bonding with grain growth across the interface. Self-bonding of molybdenum has been accomplished at 2300°F at 10,000 psi for 3 hr. The bonded molybdenum is brittle in all directions except the rolling direction, which retains a portion of the fibrous structure.

A process utilizing gas-pressure bonding has been developed by Battelle[27] for the fabrication of Zircaloy-clad flat-plate compartmented UO_2 fuel plates. The process is now being extended to the bonding of larger specimens measuring 0.10 by 4.0 by 48 in. Initial evaluation of these specimens reveals good bond integrity with no intercompartmental leakage. (S. J. Paprocki)

Diffusion Bonding

Hanford investigators[31] have completed a detailed metallurgical examination of various pressure-bonded Zircaloy-2-clad uranium tubular fuel elements. The investigation has revealed the mechanism of compound formation along the bonding interface. Since the samples were held at 845°C for 4 hr at 10,000 psi, the diffusion zone was much thicker than a normal coextruded bond. Reaction appeared to begin by uranium diffusion across the interface forming an epsilon phase with the zirconium. Si-

multaneously, diffusion progressed into the uranium, forming a delta phase, followed by a eutectoid formation of alpha-plus-delta phase. Pressure bonding of an as-cast bonded sample caused an increase in the epsilon-plus-delta, delta, and a threefold increase in the alpha-plus-delta phases that extended into the uranium.

Metallurgically bonded specimens of Zircaloy-2-clad nickel-iron alloy, with and without an evaporated layer of zirconium–4 wt.% beryllium alloy or nickel metal on the bonding surfaces of the nickel-iron pellets, were fabricated and hot upset at 1730°F at Bettis.[32] Diffusion heat-treatments of 10 and 40 min were performed in a salt pot on some of the specimens after pressing. In general, thick diffusion zones formed in the specimens, especially those which were heat-treated. Bend testing indicated a low strength, with brittle fracture through the diffusion layer of all the specimens. However, photomicrographs showed no evidence of any residual evaporated metal.

Ten promising diffuser elements were used in experiments[33] aimed at joining Zircaloy-2 components by the "eutectic-diffusion" bonding technique. Copper, nickel, nickel-phosphorus, manganese, and silicon appeared most favorable for this purpose.

The eutectic-diffusion bonding process for ceramic plate type elements for the PWR Core 2 blanket was described in detail in earlier *Reactor Core Materials* reviews.

Substitution of pyrolytic carbon for graphite as a fuel-to-cladding barrier in eutectic-diffusion-bonded Zircaloy-clad UO_2 plate fuel elements at Bettis[34] has eliminated the fuel-cladding interaction problem and simplified application of the barrier. Reduction and control of the surface roughness of fuel receptacle plates have reduced bond-line porosity in diffusion-bonded oxide plates to a low acceptable level.

Fifteen fuel-element blankets of Zircaloy-clad UO_2 were fabricated by the pack-assembly bonding technique for evaluation studies at Bettis.[34] This bonding method has attractive potentialities in the realm of process improvement by eliminating edge seal welding and product improvement by providing smooth heat-transfer surfaces and close dimensional control of fuel-element thickness.

(M. A. Gedwill, Jr.)

Coextrusion

A process is being developed by Hanford[36] for the casting of fuel-bearing aluminum alloys directly into aluminum containers for the purpose of making coextruded aluminum-clad fuel rods. The cap material is directly cast over the solidifying fuel alloy so that it fuses to the cladding, thus completely sealing the fuel material from the atmosphere and excluding air from the container. This process eliminates several steps in the billet preparation and makes the coextrusion process more economical and more adaptable to remote processing of highly radioactive fuel. Of five billets cast, in which aluminum-nickel alloys were substituted for the fuel material, only one was sound. It was extruded into a $^{9}/_{16}$-in.-diameter rod with a reduction ratio of 20 to 1. The rod had no blisters over the entire length of the 10-ft extrusion, and sectioning indicated complete bonding between the core and cladding.

The fabrication of clad UO_2 rods by coextrusion is also being studied by Nuclear Metals.[37]

A program aimed at developing power tubes with uranium-rich alloy cores other than uranium–2 wt.% zirconium is being conducted by Nuclear Metals for Du Pont.[38–40] They will produce as many as 10 different alloys of uranium and determine their amenability to fabrication. Sound castings have been made of four experimental alloys of the following systems: uranium–0.2 wt.% aluminum, uranium–0.5 wt.% aluminum, uranium–1 wt.% silicon, and uranium–1.5 wt.% molybdenum. Extrusions of copper-clad rod of the four alloys and a standard unalloyed uranium, cast and triple beta treated, have been produced in order to obtain information on extrusion constants (Fig. 12) and on grain size as it affects the uranium-copper interface. Three of these alloys were further processed and extruded as Zircaloy-clad model-scale tubes. The uranium–0.5 wt.% aluminum alloy cracked in beta treatment and was not coextruded. The alloys extruded into tubes presented fabrication difficulties of the same nature as those encountered with unalloyed uranium.

The feasibility of extruding Zircaloy-2-clad tubes directly to size by using an automatic roll-cooling device, but without employing a cold-drawing step, has been demonstrated[38,39] with favorable results. Three tubes containing fully enriched uranium alloy cores were satis-

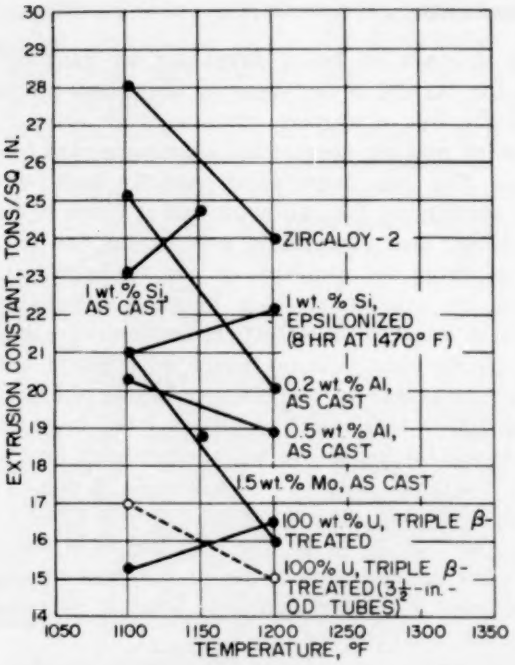
EXTRUSION CONSTANT, TONS/SQ IN.
TEMPERATURE, °F
ZIRCALOY-2
1 wt % Si, AS CAST
1 wt. % Si, EPSILONIZED (8 HR AT 1470° F)
0.2 wt % Al, AS CAST
0.5 wt % Al, AS CAST
1.5 wt % Mo, AS CAST
100 wt % U, TRIPLE β-TREATED
100% U, TRIPLE β-TREATED (3½-in.-OD TUBES)

Figure 12 — Extrusion constants vs. temperature of Zircaloy-2 and uranium alloys.[39]

factorily extruded except for outside surface scoring on two tubes.

Hanford[36] has essentially completed the investigation of controlled additions of zirconium and carbon to uranium in the as-cast and heat-treated conditions. Preliminary results indicated that the grain size of unalloyed uranium has little effect on the extrusion coefficient of coextruded rods in either the as-cast or heat-treated condition. Both zirconium and carbon additions cause a definite increase in the extrusion constant. Extrusion coefficients for zirconium additions varied from 32,800 psi at 200 ppm zirconium to 40,000 psi at 2 wt.% zirconium in the as-cast condition. Carbon alloys, at the same conditions, varied from 30,000 psi at 200 ppm carbon to 36,600 psi at 1 wt.% carbon. An excessive variation in wall thickness was observed in alloys that were not heat-treated, whereas a very uniform Zircaloy-2 wall thickness was obtained in all heat-treated zirconium alloys above 0.25 wt.% zirconium and in carbon alloys above 0.5 wt.% carbon.

(C. B. Boyer)

Extrusion Cladding

Savannah River workers[35,41,42] have developed the tool design and techniques for the external and internal extrusion cladding of uranium tubes with aluminum. Recent work involved the extrusion cladding of the inside and outside of 4- and 10.5-ft-long uranium tubes. The shorter tubes contained mild steel end plugs to which were attached aluminum extensions to position the uranium in the high-flux area of the reactor for irradiation experiments.

Mechanical difficulties encountered in initial work have been overcome, and 11 tubes have been clad successfully with the present design of tools and equipment. (H. J. Wagner)

Canning

A method of fabricating segmented-core aluminum-clad fuel elements by hot pressing has been developed at Hanford.[43] Techniques for edge electroplating of uranium washers with nickel, assembly procedures, furnace design for hot pressing of core and can components, design of pressing dies, and optimum firing cycles have been worked out.

Alloy fuel slugs of U^{235}-aluminum have been hot-press bonded in 1245 aluminum alloy cans.[44] Du Pont has experimented with various component cleaning and lubricating processes, die components and assembly, and bonding methods.

The United Kingdom[45] reports that a uranium body may be enclosed in a metallic sheath by surrounding the solid body with a metal powder and then compacting the powder, above the β-α transition point of uranium, by pressure.

(P. H. Bonnell)

Electroplating

Oak Ridge investigated the feasibility of removing oxygen from yttrium by solid-state electrolysis at 1250°C. Chemical analysis showed a higher percentage of oxygen at the anode than at the cathode, but even the purest portions of the specimen retained not less than 1000 ppm oxygen. Single crystals about ½ in. long and of a diameter equivalent to that of the specimen were grown during electrolysis.

Lombardo and Dazen[46] are setting up specifications for reactor control-rod material and control-rod design. Nickel electroplates were satisfactorily diffusion bonded to silver-indium-cadmium control rods by holding for 4 hr at 600°C in vacuum. Grain growth and depth of diffusion bond were essentially complete at the end of 4 hr. A slow furnace cool eliminated

thermal microcracking at the interface. The heat-treatment produced a ductile coating.

A patented process[47] for electroplating on uranium features an anodic pickling in an aqueous solution of 50 wt.% trichloroacetic acid. Another patented treatment[48] of uranium surfaces features, as a pretreatment for electroplating, a 20-min anodizing in 20 to 60 wt.% phosphoric acid which contains 20 cm^3 of concentrated HCl per liter. Temperature is 35 to 45°C, and 0.5 amp/sq in. is used.

Huddle and Flint[49] have patented an anodic treatment of uranium metal. A clean, bright, and passive surface is produced by anodic treatment in concentrated sulfuric acid, to which 5 wt.% chromium trioxide may be added. A potential of 12 volts with a lead cathode and a separating porous diaphragm is said to give a bright surface that persists for periods up to 12 months on exposure to air.

A patent[50] has also been granted for a method for electronickel plating tungsten carbide. The novel feature appears to be an anodic etching in $Na_4P_2O_7$ solution (200 g/liter) at 2 amp/sq in. for 10 min, using lead cathodes. This pretreatment allows nickel to be electrodeposited in an adherent coating that is weldable.

(J. McCallum)

Nonelectrolytic Chemical-plating Techniques

Well-bonded thin coatings of copper, iron, tin, and nickel on Zircaloy-2 were obtained by Armour[51] by immersion in solutions containing hydrofluoric acid and a salt of the metal. The effects of temperature and solution composition on the rate of plating were studied.

Hiler and Jenkin[52] deposited pure ductile aluminum on copper plates by decomposing triisobutyl aluminum in argon (equimolar) at 500°F. The adherence of the coating varied from poor to excellent, depending upon conditions. The addition of 0.1 per cent oxygen acted as a hydrogen scavenger and increased the rate of deposition.

In a study of the kinetics of deposition of pyrolytic carbon, Murphy et al.[53] measured the conductivity of a growing film of carbon deposited on a porcelain tube by pyrolysis of benzene, toluene, and methane.

Wright Field[54] deposited thin (1 mil) coatings of silicon nitride on molybdenum by the reaction of nitrogen with silicon tetrabromide in an atmosphere of hydrogen at 960°C.

Zirconium diboride powder particles were coated[27,55] with 5 μ of niobium by hydrogen reduction of the chloride at 900°C without indication of interaction. The coated powder will be evaluated for the prevention of boron loss on sintering compacts containing 26 wt.% UO_2 and 1 wt.% ZrB_2 in type 347 prealloyed stainless-steel powder. (J. M. Blocher, Jr.)

Ceramic Coatings

Georgia Institute of Technology[56] is investigating the arc spraying of refractory powders to form shapes. Shapes of zirconia or alumina had densities of 80 to 90 per cent or 70 to 80 per cent of theoretical and tensile strengths of 2020 to 3370 psi or 457 to 1155 psi, respectively. Rods of hafnia had tensile strengths of 1450 to 3500 psi. (Burnham W. King)

Welding and Brazing

Methods of joining beryllium and graphite to metals are described in two recent British publications.[57,58] An improved technique for producing lap joints in beryllium parts involves the following procedure: Magnesium is melted on the beryllium surfaces that will form the joint at a temperature of 750°C for 30 min. The parts are then cooled, and an aluminum foil is placed between the mating surfaces that have been coated with magnesium. The assembly is then reheated to a temperature of 750°C in argon for 10 min to form a joint.

The technique for joining graphite to an alloy called Nilo-K involved brazing with a foil consisting of the silver-copper eutectic alloy and a core layer of titanium which comprises 12 per cent of the thickness. This foil is used to produce brazed joints at a temperature of 950°C in high vacuum. Another brazing alloy being used for joining graphite to metal at Oak Ridge[59] consists of 48 wt.% titanium–48 wt.% zirconium–4 wt.% beryllium.

A technique for arc cutting of zirconium and similar materials is described in the same Oak Ridge report.[59] In this technique a special torch, similar to commercial tungsten-arc cutting torches, is operated under water. A supply of positive gas pressure is provided to prevent water from filling the torch. The operation under water prevents burning of the cut metal and the spread of contaminated particles, if radioactive material is involved.

Bettis[60] is continuing research on the development of brazing alloys for Zircaloy-2. Six experimental alloys have been evaluated in recent work. The compositions of these alloys are given in Table V-1. Typical brazing cycles for the alloys are given in Table V-2, along with comments on alloy penetration and joint strength. The zirconium–5 wt.% beryllium–15 wt.% copper brazing alloy has been used to braze complex parts with what appears to be good success.

Table V-1 COMPOSITION OF EXPERIMENTAL BRAZING ALLOYS[60] GIVEN IN WT.%

Zirconium	Beryllium	Iron
95.5	5.22	
95.4	5.07	
84.3	4.0	12.2
80.6	5.72	13.6
84.8	3.76	12.8
79.9	4.57	15.1

Table V-2 ZIRCALOY-2 BRAZING CYCLES[60]

Brazing alloy (balance Zr), wt.%	Brazing temp., °C	Brazing time, min	Heat-treatment	Average fracture load, lb	Maximum alloy penetration, in.
5 Be	1000	5	Fast cool (100°C/min)	330	0.004
5 Be	1035	30	Fast cool (100°C/min)	300	0.015
5 Be	1035	60	Fast cool (100°C/min)	345	0.025
5 Be	1035	5	1 hr at 800°C	360	0.007
4 Be–15 Fe	875	10	1 hr at 800°C	125	0.008
4 Be–15 Fe	900	5	1 hr at 800°C	320	0.010
4 Be–15 Fe	950	15	Fast cool (100°C/min)	335	0.012
4 Be–15 Fe	950	30	Fast cool (100°C/min)	365	0.014
4 Be–15 Fe	1000	15	Fast cool (100°C/min)	310	0.015
4 Be–15 Cu	850	5	1 hr at 800°C	200	0.002
4 Be–15 Cu	875	10	1 hr at 800°C	270	0.008
4 Be–15 Cu	900	5	1 hr at 800°C	445	0.010
4 Be–15 Cu	950	15	Fast cool (100°C/min)	375	0.012
4 Be–15 Cu	1000	15	Fast cool (100°C/min)	335	0.017

Another Bettis study has been made of the problem of backup contamination in Zircaloy-2 welds. The corrosion resistance of the weld area in Zircaloy-2 parts is reduced whenever contamination occurs from the conventional copper weld backups. Studies were made of various alternate backup materials, the use of modified joint designs, and the possibility of completely eliminating weld backups. The most satisfactory substitute for copper was found to be Zircaloy-2. Copper backups can be readily replaced with Zircaloy-2 backups of essentially the same design. In some joint configurations, it is possible to eliminate entirely any backup. However, in most instances, the use of a backup is still required.

Battelle investigators have made a survey[61] of end-capping methods for Zircaloy-2-clad uranium-metal fuel elements. The survey consisted of a literature search on sealing coextruded elements and a limited amount of experimental work. No new or novel joining techniques were found in the literature search. A novel method of end sealing, resistance sintering of a powdered-metal end cap, was explored in the experimental work. This technique shows promise as a method of improving end-seal reliability.

Welding studies were conducted[62] on thin sheet components made of an iron–24 wt.% chromium–1 wt.% yttrium alloy. In one phase of this work, techniques were developed for making end seals on thin flat fuel sheets clad with the iron-chromium-yttrium alloy. Fuel material was recessed at the seal location by electrolytic etching. The recess was then filled with an insert of cladding stock, and an edge weld was made by tungsten-arc welding to complete the seal. Another phase of this work consisted of attaching hardware such as spacers to fuel sheet. Both resistance and ultrasonic welding techniques were employed with some success. (R. E. Monroe)

Explosion Forming

The use of explosive forming as a method of fabricating superalloys,[63] such as René 41, Hastelloy, cobalt-base alloys,[64] and titanium-base alloys,[65] into intricate geometries, primarily for aircraft or missile components, has been investigated by several industrial firms.[66] Research has also been initiated on the use of the shock waves generated by the detonation of a high-explosive charge for surface hardening,[67] cutting,[68] powder compaction,[69] forging,[70] and welding.[70,71]

A study of the behavior of powdered materials under impulsive loads[6] has been conducted by the U. S. Naval Ordnance Test Station at China Lake, California. Both single- and double-acting presses were employed during this experimentation. The double-acting press used was of the sandwich type construction, in which two simultaneously detonated explosive charges drive two opposed pistons together into a central steel cylinder containing the specimen. Since the press does not impart a completely hydrostatic loading condition on the specimen, the specimen is free to undergo plastic deformation. An expendable press was used during this study to increase specimen recovery. Practice has shown that the positioning and detonation of the charges are critical factors relating to the effectiveness of the double-piston press. If detonations are not simultaneous, the specimen is usually lost; and, if the charges are not accurately aligned, asymmetrical loading results which jams the pistons. It is estimated that the double-acting press can produce peak pressures of several million pounds per square inch. Both single- and double-acting presses have been used to transform high-purity sponge cobalt from the metastable cubic beta phase to the more stable hexagonal alpha phase. Although this transition in cobalt after cold working is well known, the process indicates that the time for transformation is extremely short.

Iron oxide powders with additions of aluminum powder or with additions of titanium filings have been compacted in the double-acting press to 80 and 95 per cent of theoretical density, respectively. Results of testing have indicated that the final density is closely related to the ductility of the material being compacted. The faces of the pistons were machined for these tests to produce various successfully compacted shapes.

The thermal effects of the high strain rates and the short time intervals involved in explosive compacting were studied qualitatively by compacting a disk of yellow sulfur which, under normal conditions, melts at 120°C. An examination of the resulting disk revealed that traces of melting of the yellow sulfur had occurred around the edges only, indicating a lower equilibrium temperature of the sulfur and press assembly than that reported by Riabinin[72] in other types of high-pressure investigations. The experiment helped to substantiate the theory that, despite high frictional temperatures, the heating effect is extremely localized, and the integrated heating is unimportant.

A study of the metallographic structures and hardnesses induced in copper, iron, and brass by subjecting them to an explosive shock was conducted by the University of Chicago with the cooperation of Los Alamos.[73] Both copper and iron are hardened more by about a 400-kb shock (see footnote in Table V-3) than by cold

Table V-3 HARDNESS[73] OF EXPLOSIVELY SHOCKED COPPER AND IRON

Condition	Hardness*	
	OFHC copper	Armco iron
Annealed	54	95
After 225-kb shock†	105	
250-kb shock		250
350-kb shock	109	
425-kb shock	132	
600-kb shock		284
Cold rolled, 60% reduction	109	212
Cold rolled, 95% reduction	129	259

*100-g load. Vickers 136-deg diamond pyramid indentor.
†1 kb is equal to approximately 1000 atm. The kilobar values given are estimates but are believed to be good to about ±20 kb.

rolling to 95 per cent reduction, although the dimensions of the sample remain virtually unchanged. Copper also forms numerous mechanical twins, which have been previously observed in copper only at very low temperatures and after large deformation or irradiation. Photomicrographs of this twinning are shown in Fig. 13. The amount of work hardening resulting from various explosive shocks is shown in Table V-3. The author[73] points out,

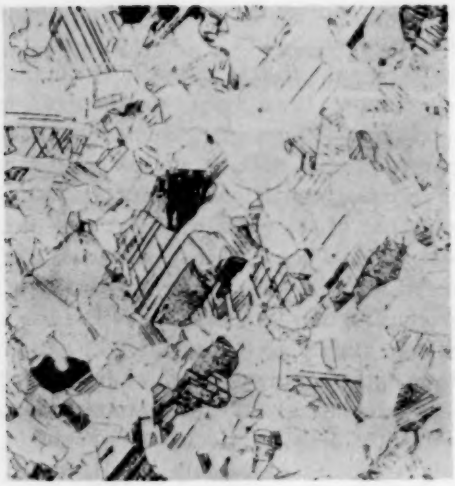

(a)

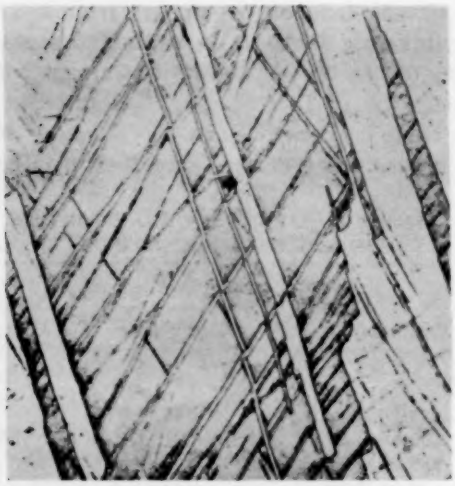

(b)

Figure 13—Microstructures of OFHC copper subjected to 425-kb explosive shock.[73] (a) Annealed and shocked OFHC copper (note the excessive twinning). (b) Cold-drawn and shocked OFHC copper (note the uniform shear evident where two sets of twins cross each other). (Reprinted by permission from *Transactions of the American Institute of Mining, Metallurgical, and Petroleum Engineers.)*

however, that, despite this hardening, neither the specimens themselves nor the grains that compose them have suffered significant distortion.

Iron develops Neumann bands when explosively shocked. When shocked at pressures above 130 kb, iron undergoes a transition to a different phase which, upon returning to atmospheric pressure, leaves a complex microstructure reminiscent of carbon-free martensite, as seen in Fig. 14. The resulting intense residual hardening could not occur by simple translation of a dislocation interface, but it probably results from the movement of dislocation complexes. The appearance of twins in copper suggests that the principal mechanism is on a scale inaccessible to the optical microscope.

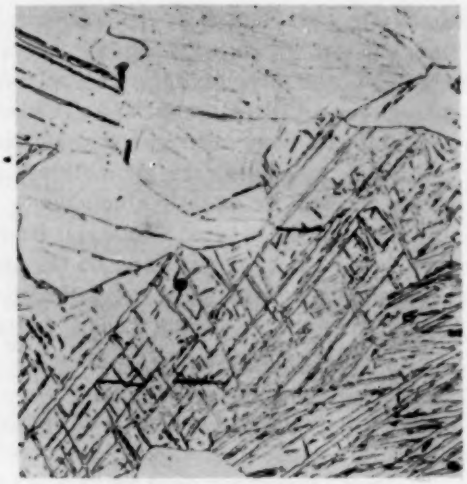

Figure 14—Microstructure[73] of Armco iron after 190-kb shock (note martensitic-appearing structure). (Reprinted by permission from *Transactions of the American Institute of Mining, Metallurgical, and Petroleum Engineers.)*

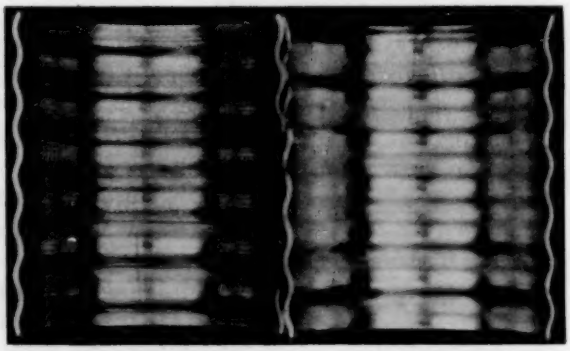

SPECIMEN 10 SPECIMEN 11

Figure 15—Surfaces obtained on Nichrome specimens explosion formed in one step and in two steps without an intermediate anneal.[74] Specimen 10 was formed in two steps without an intermediate anneal, whereas specimen 11 was formed in one step. Notice the orange-peel effect on specimen 10.

A feasibility study has recently been conducted by Battelle[74] concerning the application of explosive forming for producing cylinders

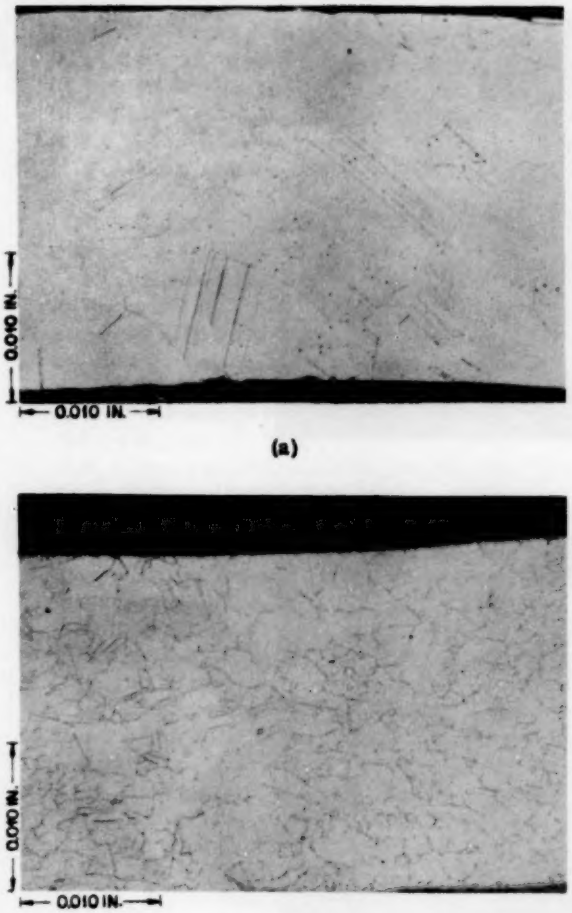

Figure 16—Microstructures of Nichrome cylinders explosion formed in one step and in two steps without an intermediate anneal.[74] (a) Specimen 10, formed by the two-step method without an intermediate anneal. (b) Specimen 11, formed in one step. The initial grain size of specimen 11 was smaller than that of specimen 10. These photomicrographs are of typical areas.

having circumferential corrugations and a welded seam. They were approximately 2½ in. in diameter in 3- and 4-in. lengths and were formed from 0.030-in.-thick Nichrome sheet. The weight, type, and placement of charge used were varied. In forming the specimens, it was found that the only critical factor was whether a one-step or two-step process was used. Good specimens were obtained in all cases when using the one-step full-draw process, whereas an "orange-peel" appearance was developed on the inside-diameter surfaces of the specimens formed by a two-step process without an intermediate anneal. Figure 15 shows the inside-diameter surfaces produced by these forming processes, whereas Fig. 16 depicts the resulting microstructures. The effect of the explosion forming on the welded seam is shown in Fig. 17.

Battelle has also been investigating[74] explosive compacting. Dispersions of 75 wt.% nickel–25 wt.% UO_2 and 70 wt.% type 347 stainless steel–30 wt.% UO_2 have been successfully compacted. The nickel-UO_2 dispersion has been compacted in the form of platelets and tubes clad with stainless steel. The stainless steel–UO_2 dispersion has been compacted to a very high theoretical green density in the form of a tubular fuel element 12 in. long, containing a 0.030-in.-thick dispersion core, and clad with type 321 stainless steel 0.010 in. thick. The compacting of powdered tungsten in the form of tubes and the sizing of Zircaloy-2 module boxes have also been investigated with very promising results. (C. C. Simons)

Nondestructive Testing

Completely reliable, fast, and sensitive means of inspecting completed fuel elements and fuel-element assemblies are being sought. In addition to the problems of inspecting elements for flaws in the clad or bond areas are those associated with fissionable-element geometry and location. Residual material remaining from the processing of elements must also be detected, and the thickness of cladding on the finished element has proved to be important. Extension of the work on the common techniques is noted in references 5, 59, and 75 to 77, and brief descriptions of more novel techniques or applications are given here.

Residual ferromagnetic spacer material is being detected by magnetic means at Bettis.[78] Small particles remaining after the pickling operation are being magnetized in a strong field and then located with a high-sensitivity magnetic-field-strength metering system. Particles weighing less than 1 mg can be found under favorable conditions by this technique.

The distribution and total load of U^{235} in fuel elements have been determined at Knolls by a gamma-scanning technique.[79,80] The detection system is designed to be sensitive to the 0.19-Mev photo gamma intensity emitted by the U^{235}. The specimen is examined through a slit that is moved stepwise along the fuel element, stopping at each increment to count the gammas.

(a)

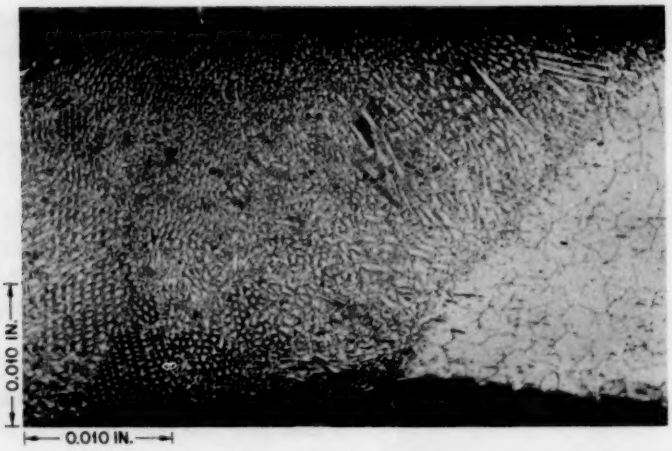

(b)

Figure 17—Microstructures of the welded seam on a Nichrome cylinder explosion formed in one step. (a) Welded area before forming. (b) Welded area after forming. The photomicrographs show that no rupturing of the weld has occurred during forming.[74]

Total load determinations of ±1 per cent accuracy with high reliability have been obtained using $\frac{1}{8}$-in. steps at a rate of one step per minute.

An instrument operating on the eddy-current principle which can be used to measure the thickness of a zirconium cladding on uranium metal base has been developed at Savannah River.[81] The hand-held sensing element allows the measurement of cladding thickness of between 5 and 25 mils with a sensitivity of $\pm\frac{1}{4}$ mil, and the measurements are only slightly affected by temperature changes and input power variations. The probe is tuned to resonance by a shunt capacitance. A change in cladding resistance because of the resistivity difference between uranium and zirconium changes the inductance of the probe, unbalancing a bridge circuit. Operating one end of the probe coil at ground potential reduces stray capacitance effects. (D. R. Grieser)

References

1. J. W. Simmons (Ed.), Summary Technical Report, January 1 to March 31, 1959, USAEC Report NLCO-785, Apr. 15, 1959. (Classified)
2. John W. Simmons (Ed.), Summary Technical Report for the Period July 1 to September 30, 1959, USAEC Report NLCO-795, Oct. 20, 1959. (Classified)
3. Ellis Foster, Jr., et al., Experimental and Theoretical Studies of the Solidification of Uranium Castings, USAEC Report BMI-1390, Oct. 28, 1959.
4. E. M. Avallone et al., Cast Hollow Fuel Rods, USAEC Report NMI-1224, July 31, 1959.

5. Bettis Technical Review: Reactor Metallurgy, USAEC Report WAPD-BT-15, September 1959.
6. R. F. Decker et al., Boron and Zirconium from Crucible Refractories in a Complex Heat-resistant Alloy, Report NACA-1392.
7. R. F. Decker et al., Vacuum-induction, Vacuum-arc, and Air-induction Melting of a Complex Heat-resistant Alloy, Report NASA-TN-D-6, August 1959.
8. J. F. Collins et al., "Application of Rare Earths to Ferrous and Nonferrous Alloys," paper presented at ASM-AEC Symposium on Rare Earths and Related Metals, Chicago, Ill., Nov. 2, 1959.
9. R. W. Endebrock et al., The Effect of Impurities on Iron-Chromium-Yttrium Alloys, USAEC Report BMI-1338, Apr. 27, 1959.
10. C. B. Dittmar and Stanley Abkowitz, The Electron Beam Melting of Beryllium, Boron, Boron Carbide, Tantalum Carbide, Titanium Carbide, Tungsten, and Zirconium Diboride, Quarterly Progress Report No. 1, Report NP-7928, Mallory-Sharon Metals Corp., Niles, Ohio, July 1958.
11. C. B. Dittmar and Stanley Abkowitz, The Electron Beam Melting of Beryllium, Boron, Boron Carbide, Tantalum Carbide, Titanium Carbide, Tungsten, and Zirconium Diboride, Quarterly Progress Report No. 2, Report NP-7927, Mallory-Sharon Metals Corp., Niles, Ohio, November 1958.
12. S. R. Seagle and Stanley Abkowitz, The Electron Beam Melting of Beryllium, Boron, Boron Carbide, Tantalum Carbide, Titanium Carbide, Tungsten, and Zirconium Diboride, Quarterly Progress Report No. 4, Report NP-7925, Mallory-Sharon Metals Corp., Niles, Ohio, May 1959.
13. S. R. Seagle and Stanley Abkowitz, The Electron Beam Melting of Beryllium, Boron, Boron Carbide, Tantalum Carbide, Titanium Carbide, Tungsten, and Zirconium Diboride, Report NP-7929, Mallory-Sharon Metals Corp., Niles, Ohio, August 1959.
14. J. L. Klein et al., Fabrication and Properties of Extruded Uranium Tubes, USAEC Report NMI-4313(Pt. 1), Sept. 30, 1959. (Classified)
15. G. W. Riedeman, Uranium Cold Extrusion, USAEC Report HW-60059, Apr. 21, 1959. (Classified)
16. J. U. Shepardson and J. A. Nelson (Eds.), Process Development Quarterly Report, USAEC Report MCW-1433, Nov. 2, 1959.
17. John W. Simmons (Ed.), Summary Technical Report for the Period October 1 to December 31, 1959, USAEC Report NLCO-800, Jan. 22, 1960. (Classified)
18. Process Development Quarterly Report for October to December 1958, USAEC Report BRB-50, Oct. 19, 1959. (Classified)
19. J. T. Lamartine and W. C. Thurber, Development of Swaged Stainless-steel Fuel Rods Containing UO_2, USAEC Report CF-59-10-8, Oct. 12, 1959.
20. L. Isakoff, comp., Heavy-water-moderated Power Reactors, Quarterly Progress Report for February, March, and April 1959, USAEC Report DP-385, July 1959.
21. R. Cole and T. Ferrara, "Swaged UO_2 Fuel Elements," in US/UK Research Newsletter No. 6 on UO_2, June 1959.
22. R. J. Anicetti, "Uranium Oxide Fuel-element Fabrication," in US/UK Research Newsletter No. 7 on UO_2, November 1959.
23. L. Sundquist, "Swaged Metal Fiber-UO_2 Element," in US/UK Research Newsletter No. 6 on UO_2, June 1959.
24. M. D'Amore, Investigation of Stretch-forming Process for Fabrication of Reactor Fuel Elements, USAEC Report YAEC-146, September 1959.
25. R. W. Dayton and C. R. Tipton, Jr., Progress Relating to Civilian Applications During September 1959, USAEC Report BMI-1381, Oct. 1, 1959.
26. R. W. Dayton and C. R. Tipton, Jr., Progress Relating to Civilian Applications During October 1959, USAEC Report BMI-1391, Nov. 1, 1959. (Classified)
27. R. W. Dayton and C. R. Tipton, Jr., Progress Relating to Civilian Applications During November 1959, USAEC Report BMI-1398, Dec. 1, 1959. (Classified)
28. F. W. Albaugh, Reactor and Fuels Research and Development Operation Monthly Report for August 1959, USAEC Report HW-61702A, Sept. 15, 1959. (Classified)
29. G. V. Alm et al., Hot-pressure Bonding of OMR Fuel Plates, USAEC Report NAA-SR-3583, Nov. 15, 1959.
30. J. L. Zambrow, Quarterly Technical Progress Report for the Period Ending September 30, 1959, USAEC Report SCNC-303, November 1959. (Classified)
31. F. W. Albaugh, Reactor and Fuels Research and Development Operation Monthly Report for October 1959, USAEC Report HW-62587A, Nov. 15, 1959. (Classified)
32. Quarterly Progress Report for the Period April 1 to June 30, 1959, USAEC Report CVNA-30, July 20, 1959.
33. W. Feduska, An Evaluation of Diffusion-bonding Characteristics of Zircaloy-2, *The Welding Journal (New York)*, 38: 289s–295s (July 1959).
34. Pressurized Water Reactor (PWR) Project Technical Progress Report for the Period June 24 to August 23, 1959, USAEC Report WAPD-MRP-81.
35. M. G. Buck, comp., Semiannual "Confidential" Technical Progress Report for January to June 1959, USAEC Report DP-414, September 1959. (Classified)
36. F. W. Albaugh, Reactor and Fuels Research and Development Operation Monthly Report for September 1959, USAEC Report HW-62012A, Oct. 15, 1959. (Classified)
37. F. S. Gardner et al., The Fabrication of Clad Massive UO_2 Fuel Elements by Coextrusion,

Quarterly Report No. 1, USAEC Report NMI-2502, Sept. 15, 1959.

38. S. Isserow et al., Power Reactor Program, Progress Report to E. I. du Pont de Nemours & Company for the Period June 1 to June 30, 1959, USAEC Report NMI-4395, Sept. 16, 1959.
39. S. Isserow et al., Power Reactor Program, Progress Report to E. I. du Pont de Nemours & Company for the Period July 1 to July 31, 1959, USAEC Report NMI-4396, Oct. 21, 1959.
40. L. Isakoff, comp., Heavy-water-moderated Power Reactors Progress Report for August 1959, USAEC Report DP-415, October 1959.
41. M. G. Buck, comp., Semiannual "Confidential" Technical Progress Report for January to June 1958, USAEC Report DP-350, December 1958. (Classified)
42. M. G. Buck, comp., Semiannual "Confidential" Technical Progress Report for July to December 1958, USAEC Report DP-366, February 1959. (Classified)
43. J. C. Tverberg and G. S. Allison, Fabrication of NPR Segmented Fuel Elements by Hot Pressing, USAEC Report HW-59130, Apr. 15, 1959. (Classified)
44. D. T. Kauer, Canning of U^{235}-Al Alloy Fuel Slugs, USAEC Report DP-390, August 1959. (Classified)
45. Improvements in or Relating to a Method for Enclosing a Uranium Body in a Metallic Sheath, British Patent 799,771, Aug. 13, 1958.
46. H. E. Walchli, Quarterly Progress Report for the Period April 1 to June 30, 1959, USAEC Report YAEC-161, Aug. 15, 1959.
47. E. W. Rebol and R. F. Wehrmann, Method of Electroplating on Uranium, U. S. Patent 2,884,364, Apr. 28, 1959.
48. C. J. Slunder, Treatment of Uranium Surfaces, U. S. Patent 2,872,389, Feb. 3, 1959.
49. R. A. U. Huddle and O. Flint, Anodic Treatment of Uranium Metal, British Patent 803,990, 1959.
50. Harvey L. Slatin, Method for Electro-Nickel Plating Wolfram Carbide, U. S. Patent 2,885,329, May 5, 1959.
51. L. R. Kohan, Immersion Plating on Zircaloy-2, *Metal Finishing*, 57(11): 68 (November 1959).
52. M. J. Hiler and W. C. Jenkin, Development of a Method To Accomplish Aluminum Deposition by Gas Plating, U. S. Air Force Report WADC-TR-59-88, June 1959.
53. D. B. Murphy et al., "A Kinetic Study of the Deposition of Pyrolytic Carbon Films," in *Industrial Carbon and Graphite*, Society of Chemical Industry, London, 1959.
54. C. R. Barnes and C. R. Geesner, Silicon Nitride Thin Film Dielectric, *Journal of the Electrochemical Society*, 107: 98 (1960).
55. R. W. Dayton and C. R. Tipton, Jr., Progress Relating to Civilian Applications During December 1959, USAEC Report BMI-1403, Jan. 1, 1960. (Classified)
56. C. R. Mason et al., Investigation of High-temperature Resistant Materials; Quarterly Report No. 15 for May 1 to July 31, 1959, Report NP-7842, Georgia Institute of Technology.
57. J. Williams and J. W. S. Jones, Improvements in or Relating to the Brazing of Beryllium, British Patent 814,270, June 3, 1959.
58. B. Stapleton, Brazing Graphite to Nilo-K Tubes, British Report IGR-140(RD/CA), Apr. 28, 1959.
59. Metallurgy Division Annual Progress Report for the Period Ending September 1, 1959, USAEC Report ORNL-2839, Dec. 16, 1959.
60. Research and Development Program Quarterly Progress Report for the Period July 1 to September 30, 1959, USAEC Report CVNA-36, Nov. 20, 1959.
61. J. J. Vagi et al., Survey of End-capping Methods for Zircaloy-2-clad Uranium Fuel Elements, USAEC Report BMI-1389, Oct. 27, 1959. (Classified)
62. J. J. Vagi et al., Fuel-sheet End-seal and Hardware-attachment Studies, USAEC Report BMI-1385, Oct. 15, 1959.
63. Paul J. Wolf, Super Alloys Formed with Explosives, *Tool Engineer*, 41(6): 78 (December 1958).
64. Explosive Forming Blasts Complex Shapes in Fraction of Time by Conventional Methods, *Western Metalworking*, 17(4): 52–53 (April 1959).
65. Thomas A. Dickinson, Explosives Form Titanium Too, *American Machinist*, 103(11): 138 (June 15, 1959).
66. High-energy Rate Metal Forming, Interim Engineering Report No. 1 for Period October 18, 1957 to February 28, 1958, Reports LR-12970, (AD-156722), Lockheed Aircraft Corporation, Burbank, Calif.
67. W. A. Harper, Controlled Explosive Blasts Hardness into Steel, *Product Engineering*, 30(15): 62–63 (Apr. 13, 1959).
68. Do It Yourself Explosive Cutting, *Steel*, 144(12): 104 (Mar. 23, 1959).
69. Edward W. LaRocca and John Pearson, The Explosive Press as a Research Tool in Material Behavior and Forming, Report NAVORD-5880, May 12, 1958.
70. D. Freiday, Briefing the Record, *Mechanical Engineering*, 81(12): 78–79 (December 1959).
71. H. P. Tardiff, Explosive Forming in Canada, *Metal Progress*, 77(1): 128–130 (January 1960).
72. I. N. Riabinin, Certain Experiments on Dynamic Compression of Substances, *Soviet Physics—Technical Physics*, 1(12): 2575–2579 (1956).
73. Cyril Stanley Smith, Metallographic Studies of Metals After Explosive Shock, *Transactions of the American Institute of Mining, Metallurgical, and Petroleum Engineers*, 212(5): 574–588 (October 1958).
74. C. C. Simons, unpublished data obtained at Battelle Memorial Institute through January 1960.
75. Solid State Division Annual Progress Report for

Period Ending August 31, 1959, USAEC Report ORNL-2829, Dec. 11, 1959.

76. G. Lancellotti and M. Robba, Nondestructive Testing of MTR Fuel Elements Through Autoradiography, *Metallurgia italiana*, 51(11): 504 (November 1959).
77. John M. Fouts, The Use of Ultrasonics in the Testing of Irradiated Fuel Elements, *ASTM Bulletin*, No. 242, pp. 60–62 (December 1959).
78. R. A. Betz, Location of Residual Spacer Material in Subassemblies, Inspection Development Report, USAEC Report WAPD-NCQ(DR)-7, May 18, 1959.
79. D. G. Miller, The Nondestructive Determination of UO_2 Distribution in UO_2–Zr Dispersion Type Fuel Plates, USAEC Report KAPL-M-DGM-2, Jan. 29, 1959.
80. D. G. Miller, The Nondestructive Determination of U^{235} Distribution and Total U^{235} Load in Uranium–Zircaloy-2 Alloy Type Irradiation Specimens, USAEC Report KAPL-M-DGM-3, Sept. 10, 1959.
81. A. P. Holt, A Cladding Thickness Tester for Zirconium over Uranium, USAEC Report DP-408, September 1959.

LEGAL NOTICE

This document was prepared under the sponsorship of the U. S. Atomic Energy Commission. Neither the United States, nor the Commission, nor any person acting on behalf of the Commission:

A. Makes any warranty or representation, expressed or implied, with respect to the accuracy, completeness, or usefulness of the information contained in this report, or that the use of any information, apparatus, method, or process disclosed in this report may not infringe privately owned rights; or

B. Assumes any liabilities with respect to the use of, or for damages resulting from the use of any information, apparatus, method, or process disclosed in this report.

As used in the above, "person acting on behalf of the Commission" includes any employee or contractor of the Commission, or employee of such contractor, to the extent that such employee or contractor of the Commission, or employee of such contractor prepares, disseminates, or provides access to, any information pursuant to his employment or contract with the Commission, or his employment with such contractor.

NUCLEAR SCIENCE ABSTRACTS

The U. S. Atomic Energy Commission, Technical Information Service, publishes *Nuclear Science Abstracts (NSA)*, a semimonthly journal containing abstracts of the literature of nuclear science and engineering.

NSA covers (1) research reports of the U. S. Atomic Energy Commission and its contractors; (2) research reports of government agencies, universities, and industrial research organizations on a world-wide basis; and (3) translations, patents, books, and articles appearing in technical and scientific journals.

Complete indexes covering subject, author, source, and report number are included in each issue. These are cumulated quarterly, semiannually, and annually providing a detailed and convenient key to the literature.

Availability of *NSA*

SALE *NSA* is available on subscription from the Superintendent of Documents, U. S. Government Printing Office, Washington 25, D. C., at $18.00 per year for the semimonthly abstract issues and $15.00 per year for the four cumulated-index issues. Subscriptions are postpaid within the United States, Canada, Mexico, and all Central and South American countries, except Argentina, Brazil, British and French Guiana, Surinam, and British Honduras. Subscribers in these Central and South American countries, and in all other countries throughout the world, should remit $22.50 per year for subscriptions to semimonthly abstract issues and $17.50 per year for the four cumulated-index issues.

EXCHANGE *NSA* is also available on an exchange basis to universities, research institutions, industrial firms, and publishers of scientific information. Inquiries should be directed to the Technical Information Service Extension, U. S. Atomic Energy Commission, P. O. Box 62, Oak Ridge, Tennessee.